

This is to certify that the dissertation entitled

PARAMETRIC IDENTIFICATION OF CHAOTIC/NONLINEAR SYSTEMS AND REDUCED ORDER MODELS BASED ON PROPER ORTHOGONAL DECOMPOSITION

presented by

Yang Liang

has been accepted towards fulfillment of the requirements for the

Ph.D. degree in Mechanical Engineering

Major Professor's Signature

12/1/2/005

MSU is an Affirmative Action/Equal Opportunity Institution

Date

LIBRARY Michigan State University PLACE IN RETURN BOX to remove this checkout from your record.

TO AVOID FINES return on or before date due.

MAY BE RECALLED with earlier due date if requested.

DATE DUE	DATE DUE	DATE DUE
JAN 1 2 2009		
-		

2/05 p⁻/CIRC/DateDue.indd-p.1

PARAMETRIC IDENTIFICATION OF CHAOTIC/NONLINEAR SYSTEMS AND REDUCED ORDER MODELS BASED ON PROPER ORTHOGONAL DECOMPOSITION

By

Yang Liang

A DISSERTATION

Submitted to
Michigan State University
in partial fulfillment of the requirements
for the degree of

DOCTOR OF PHILOSOPHY

Department of Mechanical Engineering

2005

ABSTRACT

PARAMETRIC IDENTIFICATION OF CHAOTIC/NONLINEAR SYSTEMS AND REDUCED ORDER MODELS BASED ON PROPER ORTHOGONAL DECOMPOSITION

By

Yang Liang

In the dissertation, the parametric identification and proper orthogonal modes (POMs) were investigated on chaotic/nonlinear systems such that a reliable and general-purpose process can be developed to reconstruct the mathematical models of nonlinear and/or chaotic systems.

First, a parametric identification method was examined for different chaotic systems, e. g. whirling, multi-degree-of-freedom, and strong nonlinearity, and by simulation and experiments. The original parametric identification method of chaotic systems is a hybrid time and frequency domain method based upon the harmonic balance method applied to unstable periodic orbits (UPOs), and solved by least mean squares. A chaotic base-excited single pendulum system was simulated. The identification method was modified for the whirling system with measured data of angular displacement. The nonlinearity was also approximated by two types of function series: linear interpolation functions and harmonic functions. Poincaré sections showed that the identified system and the original simulation system had similar chaotic behavior. Then, the identification method was applied to an experimental chaotic

double pendulum under vertical base excitation. Several noise reduction techniques were applied to reduce the identification errors due to the noise contamination in the experimental data and the strong nonlinearity. Meanwhile, an error optimization process, based on the linear regression and statistics, was proposed to improve the identified parameters by selecting sub-harmonics of the unstable periodic orbits. An energy balance method, as a second-step identification after the harmonic balance method, was applied to give a more accurate estimation of the small damping coefficients.

It was also found that any chaotic orbit can be an approximated representation of some UPO, and the longer the orbit the better the approximation. Thus, there is an option between collecting UPOs for the extraction, and using longer arbitrary data segments. The identification process can be simplified to a frequency domain method. Examples were examined to show the success of the simplification.

The study then goes to parametric identification and the POM for building reduced order models of unknown systems. The special interest here is systems with strong nonlinearity, where the reduced order models from experimental POM was limited in simulating the unknown systems other than the neighborhood set plane where the POM data is in the phase space. An added-constraint method was proposed and examined by two simple systems: a two-mass system with nonlinear spring and a mass-pendulum system. It showed that the added constraint can improve applicability of the POM reduced order model as well as increasing the accuracy of the simulation result. Nevertheless, the method is to be tested by high dimensional nonlinear systems, to which the proposed added constraint method can really make a big difference in applications.

Copyright © by
Yang Liang
2005

To Xiaobei.

ACKNOWLEDGMENTS

I wish to acknowledge the National Science Foundation (CMS-0099603) and NASA (NAG-1-01048 with Dr. Walt Silva) for their finaicial support for this research.

I would like to express my gratitude to my advisor Professor Brian Feeny for the guidance, help and encouragement provided during the course of my research.

I am please to acknowledge my colleagues at the Dynamics Lab who created a pleasant working atmosphere. I would like to thank particularly Brian Olson for helpful discussions.

I would also like to acknowledge the help of Professor Steven Shaw on discussions of nonlinear normal modes, and Professor Michael Frazier on talks of the wavelet analysis.

Finally, I would like to express my love and gratitude to my wife Xiaobei, my mom, dad and my brother for their enormous support and understanding during my study at Michigan State University.

TABLE OF CONTENTS

L	ST (OF TABLES	ix
Ll	ST (OF FIGURES	x
1	Intr	roduction	1
	1.1	Motivation	1
	1.2	Literature review	4
	1.3	Outline of the dissertation	6
2	Sim	ulation Study of a Base-Excited Single Pendulum	10
	2.1	Introduction	10
	2.2 2.3	Horizontally excited single pendulum & identification algorithm Introduction to phase plane reconstruction and extraction of unstable	11
		periodic orbits	17
		2.3.1 Choosing the time delay and embedding dimension	18
		2.3.2 Extracting unstable periodic orbits (UPOs)	18
	2.4	Numerical simulation of the horizontally excited pendulum	19
		2.4.1 Phase space reconstruction	19
		2.4.2 Parametric identification	20
	2.5	Discussion and validation	27
	2.6	Concluding remarks	28
3	Exp	perimental Study of a Base-Excited Double Pendulum	29
	3.1	Description of the double pendulum system	29
	3.2	Method	32
	3.3	Experiment description	37
	3.4	Results and validation	39
		3.4.1 Phase space reconstruction & UPO extraction	39
		3.4.2 Identified parameters	45
		3.4.3 Friction issue	46
		3.4.4 High frequency noise in unstable periodic orbits	48
		3.4.5 Digital differentiation and error reduction	54
		3.4.6 Validation methods	62
	3.5	The energy balance method for identification of the damping coefficients	65
	3.6	Concluding remarks	68

4	Sim	plification to Frequency Domain Method	70
	4.1	System identification by frequency method	70
	4.2	More chaotic properties and the improved frequency domain method	72
	4.3	Calculation examples	76
		4.3.1 Base-excited single pendulum	77
		4.3.2 Experimental double pendulum	79
	4.4		80
5	The	e Reduced Order Models of Nonlinear Systems Based on Proper	r
	Ort	hogonal Modes	85
	5.1	Need for reduced order models	85
	5.2	Proper orthogonal decomposition introduction	86
	5.3	Improving POD for strong nonlinear systems	90
		5.3.1 Limitation of the POD	90
		5.3.2 The example of a two-mass system with nonlinear spring	92
		5.3.3 The example of a mass-pendulum system	99
	5.4	Concluding remarks	112
6	Cor	nclusions and Future Work	114
	6.1	Main contributions	114
	6.2	Directions for future work	
\mathbf{B}	IBLI	OGRAPHY	120

LIST OF TABLES

2.1	The n_k , p_k and q_k values when harmonic basis is applied	23
3.1	Physical properties of the double pendulum	38
3.2	Experimental settings	38
3.3	Identified parameters by applying low-pass filter, FFT convolution, Fourier series expansion of UPO, harmonic balance method with sub-harmonics whose frequencies are \leq excitation frequency f_e =5 Hz, and	
	sub-harmonics optimization	45
3.4	Identified non-dimensional parameters by optimized identification pro-	
	cess and noise reduction provided that the friction coefficients are known.	48
3.5	Comparison of $\mathcal{F}(y)$ with and without filter added	52
3.6	Optimized identification with no digital filter applied	54
3.7	Comparison of calculated values by Fourier Series (FS) method and	
	Digital Differentiation (DD) method when error tolerance is set as 8%	
	with filtering and optimization process applied	55
3.8	Identified parameters with the Fourier series method and low-pass fil-	
	tering, but without optimization to sub-harmonics set	60
3.9	Comparison of the identified values and the true parametric settings of	
	the simulated system with low-pass filtering and optimization applied.	64
	Natural frequencies	65
3.11	Identified damping coefficients by the energy balance method	67
4.1	Comparison of the true values and the identified parameters by new	
	frequency method	83
5.1	Identified parameters of the POM-constraint model (5.16) under the	
	first three conditions	96
5.2	·	101
5.3	Estimated polynomial coefficients of the constraint equation	103

LIST OF FIGURES

2.1	A period-4 orbit (a) sampled signal; (b) actual continuous signal x_c ; (c) \cdots constant rotation part $\omega_{ck}t$, – oscillatory part x_{var}
2.2	Reconstructed phase plane (a) and Poincaré section plot (b); $\theta(t)$ is
2.2	represented by theta(t) in the plots
2.3	Mutual information of the data; the first minimum is at $dt=5$
2.4	(a) A period-1 orbit; (b) A period-2 orbit; (c) A period-2 orbit; (d) A
	period-2 orbit
2.5	The n_k curve for linear interpolation basis; (*) identified values, (—)
	true function
2.6	The p_k curve for linear interpolation basis; (*) identified values, (—)
	true function
2.7	The q_k curve for linear interpolation basis; (o) identified values, (—)
	true function
2.8	Poincaré section plots of identified systems: (a) by linear interpolation
	basis, (b) by Harmonic basis
3.1	A sketch of the double pendulum
3.2	Mutual information $I(dt)$
3.3	Phase portrait of experimental data with $dt=24$, (a) $\theta_1(t)-\theta_1(t+dt)$,
	(b) $\theta_1(t) - \theta_2(t)$, (c) $\theta_2(t) - \theta_2(t + dt)$; θ is represented by theta in the
	figure
3.4	A period 4 UPO; theta1 and theta2 in the plot represent θ_1 and θ_2 ;
	dt=24; same for the following figures
3.5	A period 9 UPO.
3.6	A period 12 UPO
3.7	A period 12 UPO
3.8	A period 15 UPO
3.9	A period 15 UPO
3.10	Phase portrait of the simulated system with $C_{11} = 1.02 \times 10^{-3}$, $C_{11} = 0.0366$ and $C_2 = 0.0485$; $dt = 24$
2 11	
J.11	FFT amplitude of the θ_1 and θ_1 with and without low pass filter applied; the continuous line is FFT of signals with filter of $1/5f_8$ cut-off
	frequency; the dotted line is FFT of signals without filter; k is the
	order of sub-harmonics
	Uluci di Sud-naimonics

3.12	Signals without and with low pass filter applied; (a) and (b) are θ_1 without and with filter; (c) and (d) are y without and with filter applied	- 0
3.13	to each convolution components; k is the k th sampled point of the orbit. Obtained $\dot{\theta}_1$ and $\ddot{\theta}_1$ orbits by Fourier series method (a) and (b) by digital differentiation method (c) and (d); the recurrence impulses occur	
3.14	at $k=800$ in (a) and (b)	57
3.15	harmonic set whose frequency \leq the excitation frequency Identification residual $\vec{e_2}$ after optimization with each dot representing a subharmonic	59 62
4.1	The left shift one dimensional map	73
4.2	Identified functions by interpolation functions on noise-free data, (a)	
4.3	n_k , (b) p_k , (c) q_k	79 80
4.4	Identified functions by interpolation functions on 10% noise contami-	
4 5	nated data, (a) n_k , (b) p_k , (c) q_k	81
4.5	The residual plot of the first matrix equation of the double pendulum system	82
5.1	Phase portraits of the original system ('+'), the POD only model (the dashed line), and the POD-constraint model (the dotted line) under	Or
5.2	the 5th initial condition	92
	correspond to the five initial conditions.	93
5.3	Comparison of the invariant manifold: (a) under small amplitude (the first three conditions), (b) under all five conditions; Surf 1 is the empirical surface from POD, Surf 2 is Shaw's surface, the continuous lines	
	are the orbits under five conditions; x axis is y_2 , y axis is y_2 , z axis is y_1 .	97
5.4	·	100
5.5	The shapes of the 1st NNM of the mass-pendulum system under 5 i. c. : 1. (0.125, 0.385), 2. (0.250, 0.733), 3. (0.375, 1.10), 4. (0.500, 1.54),	100
5.6	5. (0.575, 1.892)	102
0.0	pendulum system (the continuous lines) simulated under 1st initial	
		105
5.7	Comparison of Model I (the dotted lines) to the original mass-	
	pendulum system (the continuous lines) simulated under 3rd initial condition, (a) phase plane, (b) mode shape.	106

5.8	Comparison of Model I (the dotted lines) to the original mass-	
	pendulum system (the continuous lines) simulated under 5th initial	
	condition, (a) phase plane, (b) mode shape	106
5.9	Comparison of Model II (the dotted lines) to the original mass-	
	pendulum system (the continuous lines) simulated under 1st initial	
	condition, (a) phase plane, (b) mode shape	107
5.10	Comparison of Model II (the dotted lines) to the original mass-	
	pendulum system (the continuous lines) simulated under 3rd initial	
	condition, (a) phase plane, (b) mode shape	108
5.11	Comparison of Model II (the dotted lines) to the original mass-	
	pendulum system (the continuous lines) simulated under 5th initial	
	condition, (a) phase plane, (b) mode shape	108
5.12	A time domain comparison between the original system (continuous	
	line), the Model-I (dashed line), the Model-II (dotted line) under the	
	3rd initial condition.	110
5.13	Natural frequency comparison under different initial conditions (rep-	
	resented by the maximum potential energy) between the original sys-	
	tem (continuous line), the Model-I (dashed line), the Model-II (dotted	
	line); the '*' and 'o' mark the five initial conditions for Model-I and	
	Model-II.	111

CHAPTER 1

Introduction

1.1 Motivation

System identification, as an inverse question of dynamical systems analysis and quite often a prerequisite of dynamics analysis, has been widely used and investigated in industry, such as for the control and modeling of complex structures. There are basically two classifications of system identification:

- 1. Non-parametric identification requires no actual governing dynamical equations of a system, but rather an approximated model by a series of approximation functions. Thus, no physical paremeters are identified, but coefficients of the approximation functions. Some of the non-parametric identification methods are based upon differential equations, which share many common features with the parametric identification that we are going to discuss. On the other hand, many more are based upon time-delay models, which are to be used in control applications to approximate short-term behaviors of systems. The time-delay models are also quite easy for instant, real time approximation of the dynamical behavior.
- 2. Parametric identification is based upon governing differential equations, or re-

duced order models of the systems. Therefore, the identified parametric systems can be better representations of the original unknown systems, and are often used for dynamics analysis of the systems.

Our focus here is to use parametric identification to reconstruct a model which can simulate an original unknown system. The advantages of a nonlinear mathematical model over a linear one are quite obvious: more accurate description of the real physical systems and thus, more precise prediction of dynamical behavior, which satisfies the requirements of modern technologies. For the nonlinear systems, chaotic systems are among the most mysterious. Due to their random-like responses, they were once considered stochastic systems, until "chaos theory" and chaotic data observation techniques were developed. Chaos is generally considered as aperiodic time-asymptotic behavior in a deterministic system which exhibits sensitive dependence on initial conditions [1]. The phase-space trajectories of chaotic systems do not settle down to fixed points or periodic orbits. Many developed identification methods are not suitable for systems with chaotic responses. Therefore, this study here is aimed at developing and perfecting an identification process which can be applied to general chaotic (also nonlinear) systems. The systems in our scope include strongly nonlinear systems, whirling systems, and high dimensional systems, because of their special features and difficulty in accurate identification.

A general expression of a class of nonlinear oscillation systems is

$$M\ddot{\vec{x}}(t) + C\dot{\vec{x}}(t) + K\vec{x}(t) + f_{NL}(\vec{x}, \dot{\vec{x}}) + f_{NP}(\vec{x}, \dot{\vec{x}})f_p(t) = f(t),$$
 (1.1)

where \vec{x} is a vector variable, matrices M, K, C are mass, spring and damping matrices, vectors f_{NL} and f_{NP} are nonlinear functions of displacement and velocity, and $f_p(t)$ is the parametric excitation term. For simple systems, we can derive the mathematical model, and identify the actual physical parameters. However, for many high

dimensional systems, such as fluids and continuous structures, we tend to avoid the exact differential equation of the original system, but use a simplified reduced order model based upon modal analysis. The benefits of reduced order models (ROMs) are:

- 1. ROMs are simple and require much fewer parameters to identify.
- Generally, only a few of the low order normal modes of that system show up in the dynamics of an actual system.
- 3. Identification of partial differential equations (PDEs) of continuous systems is much more complex than ordinary differential equations (ODEs) and also restricted by experimental data.
- 4. The ODEs are handier in simulation than the PDE, and thus, easier for analysis.

We can simplify nonlinear continuous or high dimensional systems by using either assumed modes, linear normal modes (LNMs), nonlinear normal modes (NNMs) [2] or proper orthogonal modes (POMs) [3] to project the PDEs into the form of a series of ordinary differential equations in modal coordinates. Then, since usually only few of the normal modes (or orthogonal modes if POMs are used) are typically active with some level of significance in the dynamical behavior of a system, a truncated series of equations can be used to approximate the original system.

For linear systems, both NNMs and the weighted POMs [4] become the linear normal modes (LNMs). But, it should be noticed that the NNM method is more fit to theoretical analysis which assumes known systems' structures, and governing equations. On the other hand, POM method is more of an experimental method, which deals with orthogonal modes obtained from experimental or testing data, by which the governing differential equations can be reconstructed.

Hence, the scheme of the dissertation involves two parts: parametric identification and reconstruction of reduced order models by POD.

1.2 Literature review

Till now, most of the methods of parametric identification of nonlinear systems focused mainly on free vibration, random excitation or periodically forced steady state vibration behavior. Mohammad [5] introduced a direct identification method by using time-domain displacement, velocity and acceleration signals. The method is simple, but also requires all of the displacement, velocity and acceleration information, and is not noise-resistant. In [6], nonlinear resonances by random excitations were utilized and part of the parameters were identified. Chen and Tomlinson [7] proposed a time series acceleration, velocity and displacement model (AVD model) with a narrowed investigation scope: dry Coulomb friction, viscous damping and nonlinear stiffness. Also, many other methods are effective within limited dynamical systems [8, 9, 10, 11, 12, 13, 14, 15]: weak non-linearity, complex algorithm and time-consuming, non-chaotic behavior, single or two degree-of-freedom systems.

Some of the identification methods, though not originally proposed or examined under chaotic systems, have potential application to be applied to chaotic nonlinear systems. Plakhtienko [16, 17] introduced a special weight method for parametric identification, which is derived from orthogonal basis functions. If Fourier series functions are applied as the orthonormal basis, the method then becomes the harmonic balance method. The inverse harmonic balance method has been applied to various nonlinear systems identification [18, 19, 20, 21] which are under forced excitation and have steady-state periodic responses. Thothadri [22] also developed a similar harmonic balance identification on multi-degree-of-freedom nonlinear systems. A wavelet-based approach was discussed by Ghanem and Romeo [23]. Both the discrete wavelet transform and Fourier transform are based upon signal reconstruction by an orthonormal basis, except that the wavelet transform is a localized time-frequency reconstruction. Meanwhile, the harmonic balance method is, in essence, a frequency domain method,

and much easier to apply than the wavelet method. Due to this property, Feeny and Yuan [24, 25] proposed a method for chaotic systems, which exploits the harmonic balance of extracted unstable periodic orbits (UPOs), because one of the fundamental properties of deterministic chaos is that the chaotic set of a dynamical system contains infinite number of unstable periodic orbits. It is the primary method used in this the dissertation. There are several reasons for choosing this method:

- The identification process can be theoretically applied to any dynamical system. For linear systems, it becomes the frequency response function method if multiple excitation frequencies are tested. For non-chaotic nonlinear systems, there have been successful applications of the harmonic balance method.
- The method exploits the existence of unstable periodic orbits, and has generated satisfying identification results.
- Some possible developments exist for further improvement, including the friction issue, experiments, and error reduction.

Parametric identification of large order systems is greatly facilitated in reduced order models. A popular tool for reduced order modeling is proper orthogonal decomposition. Proper orthogonal decomposition (POD), or Karhunen-Loève decomposition, has been widely used for empirical modal analysis. As a statistical method utilizing the correlation matrix derived from a set of measurement histories, POD produces the empirical modes, which are known as proper orthogonal modes (POMs), from the eigenvectors of the correlation matrix, and the corresponding energy levels of the modes, known as proper orthogonal values (POVs), from the matrix eigenvalues.

For linear systems with evenly distributed mass, POMs are actually the linear normal modes [26]. Therefore, it can be used as modal analysis tool [27, 28, 29, 4, 30, 31]. Meanwhile, since its introduction, POD has been widely used in fluid, turbulence

areas as modal reduction tool [3, 32, 33], and recently in structural dynamics [34, 35, 36, 37, 38, 39, 40, 41, 42, 43]. Some used it to estimate the active dimension of a dynamical system [33, 37, 38].

For reduced order models, combining POD with system identification is a very promising area in the analysis of systems dynamics. For chaotic and nonlinear systems, the POM based reduced order models can approximate the systems' behavior by fewer modes than the models based upon linear normal modes [41], which implies that the POM models are more efficient than the LNM models for reducing nonlinear systems. POD's applications in system identification and reduced order modeling for nonlinear/chaotic systems has also gained some improvements in applications of systems with simple nonlinearity [39, 44, 40, 42, 43]. In [39] the POM itself is also part of the system identification process.

1.3 Outline of the dissertation

The purpose of this dissertation is to generate accurate and robust models of non-linear and/or chaotic vibration systems. We can either do it by direct parametric identification provided that the governing equations of the systems are handy, or for large-order systems, by obtaining approximated reduced order models based upon POMs or NNMs of the systems, and identifying parameters of the reduced order models. Consequently, the dissertation consists of two major parts. The first part focuses on parametric identification of single and two degree-of-freedom (d. o. f.) systems. The systems studied are whirling pendulum systems. The second part is on the parametric identification of ROMs. POD is used for the reduced-order modeling, and we focused attention on broadening the applicability of identified models to conditions beyond those for which the POD was performed. Details are outlined below.

First, we will concentrate the focus on parametric identification method, c. g.

a harmonic balance based identification process for chaotic and nonlinear systems [24]. Since the method has been tested on simple single d. o. f. systems, the goal of this study is to test it on systems with more complicated nonlinearity and multiple d. o. f. systems. The pendulums, due to their whirling nature and trigonometric nonlinearity, are distinctive from ordinary oscillatory systems, and thus are chosen for the investigation. The pendulums are also easily examined by experiments due to their simple structures. A simulated single pendulum was first examined. Then, a base-excited double pendulum was selected for experimental application to whirling and multi-degree-of-freedom systems. Once successfully tested, the follow-up goal is to simplify and improve the current method. Hence, the identification investigation will be divided into three separate chapters, and each with a different focus.

Chapter 2 deals with a simulation study of a chaotic single pendulum system. The main contribution of this chapter is to apply the identification method to whirling chaotic systems. A brief introduction will be given to explain special features, dynamical behaviors and tools for analysis of chaotic systems. The purpose is to examine the method on a whirling, chaotic and parametrically excited single degree-of-freedom system. It is assumed that the system is unknown to us except that the pendulum is parametrically excited with some known frequency. Meanwhile, to make the simulation resemble an experiment setup, only the angular displacement signal was used. An embedding technique was then applied to obtain the reconstructed phase space, which is essential to extract the UPOs from the chaotic data. The extracted orbits are actually not the true unstable periodic orbits, but their approximations, whose accuracy can be measured by the tolerance error during the extraction. It is also hoped that many UPOs can be obtained so as to increase the reliability of the identified results. Based upon the UPO, the harmonic balance method can be applied to build the identification matrix equation, and the parameters can be identified simultaneously. Another aspect of the identification study is the use of function series to approximate the unknown nonlinear functions. Two sets of function series were used: the Fourier series and the linear interpolation functions. Both approximations showed good matches with the true values.

Chapter 3 upgrades the study to a experimental double pendulum system. This investigation was to examine the identification method by a experimental multi-degree-of-freedom system, to develop noise reduction, optimization techniques to improve the identification results, and to estimate damping terms more accurately by energy balance method. Again, the system is chaotic, whirling and parametrically excited. Since the collected angular displacements were noise contaminated, noise reduction techniques were applied. The strong nonlinearity of the double pendulum was also found to contribute to the errors in the identified parameters, especially those nonlinear terms with velocity and/or acceleration signals. To quantify and reduce error in the identification results, an identification error was defined to indicate quantitatively how 'good' the identification is, and based upon it, an optimization process was developed. The core of the optimization process is to obtain a smart choice of sub-harmonics of the UPOs for harmonic balancing. Based upon the results of the harmonic balance method, the energy method was developed as a follow-up to give more accurate estimation of the damping parameters.

Chapter 4 describes a simplified identification process. The underlying reason for the improvement is because UPOs become less available for extraction, as the degrees of freedom of a system goes up. As a result, the identification result can deteriorate with fewer UPOs. The idea comes from the unstable periodic orbits inside the chaotic data. Since the UPOs are the 'skeleton' of the chaotic set, every chaotic orbit is considered to be an approximated periodic orbit of large period. Thus, the extraction step can be skipped, making the whole identification process look quite like a frequency domain method for linear systems. The importance of the simplification can not be underestimated. It actually makes it possible to identify all kinds of

systems in the frequency domain.

Ultimately, as the d. o. f. of systems increases, the need for reduced-order modeling becomes mandatory. Thus, the second part of the dissertation is to combine POD and parametric identification to build reduced order models for nonlinear systems. For high dimensional systems, reduced order models are effective replacements of the original governing equations. POD provides a simple and theoretically applicable vehicle for reduced order modeling through experimental data. Our focus is on systems with strong nonlinearity, where the POM based models are limited to a small neighborhood of the initial conditions where the POM comes from due to the nonlinearity. A new added-constraint method was developed and tested to improve the reconstructed reduced order models. Due to the complexity of this topic, the study was only a beginning of a series of future studies.

Chapter 5 poses the problem of reduced-order modeling with strongly nonlinear systems. By borrowing ideas from NNM analysis, a geometric constraint method was proposed to accompany the POM models. The idea was tested on two simple systems: a two-mass system with nonlinear spring and a mass-pendulum system. The analysis was based upon simulation. It turned out that the added constraint method can not only increase the accuracy of the POM models, but extend the applicability of those models. Although it is not clear if this method will be as effective on high d. o. f. systems as it is to the analyzed low d. o. f. examples., it gives us a possible direction to improve the accuracy of the reduced order models.

Finally, Chapter 6 will conclude the dissertation with possible future research on this topic. The improvements could be real-time identification of chaotic systems, further identification of small parameters (i. e. frictions terms), POD for whirling systems, and experiments or simulations of reduced order models of nonlinear high dimensional systems.

CHAPTER 2

Simulation Study of a

Base-Excited Single Pendulum

2.1 Introduction

A simulated, horizontally base-excited pendulum is investigated as a first step for whirling, chaotic system identification. A harmonic balance parametric identification method is examined here, because of its simplicity and capacity for handling chaotic data.

Pendulum systems are among the most thoroughly investigated dynamic systems in chaotic, nonlinear system research [45, 46, 47, 48, 49, 50, 51] for their simplicity in both theoretical expression and experimental validation. Water [45] studied the unstable periodic orbits of a vertically excited system. Jeong and Kim [46] investigated the bifurcation phenomena and routes to chaos of a horizontally excited system. Furthermore, Bishop [47] and Dooren [48] studied the regions of chaos of a parametrically excited pendulum in parametric space. These works provide the general relationship between chaotic behavior and the influence of parameters on the system, and facilitate our investigation of the pendulum with horizontal base-excitation.

Meanwhile, based upon the harmonic balance method [18, 19, 20, 21], Feeny and

Yuan [24, 25] proposed a method for chaotic systems which exploits the extracted unstable periodic orbits. This method was successfully applied to single degree of freedom systems, and is theoretically applicable to chaotic or non-chaotic, strongly nonlinear multi-degree-of-freedom systems.

Our purpose here is to apply the harmonic balance algorithm to the horizontally excited pendulum system such that we can examine the algorithm's applicability on systems with chaotic whirling behavior and parametric excitation. The identification method has been examined on smooth excitation single d. o. f. systems [24]. However, the pendulum is a more complicated case. Since the single pendulum is both whirling and under parametric excitation, the algorithm must be modified and can now be improved partially. In the following sections, the single pendulum system and the modified method will be introduced first. Pre-requisites for applying this method will be discussed, primarily regarding the phase plane reconstruction. Then, the simulation results will be presented and discussed.

2.2 Horizontally excited single pendulum & identification algorithm

Single pendulum systems have simple structures, but strong non-linearity due to their whirling property. The governing differential equations can be simulated easily, and the experimental verification is also feasible. Based upon these advantages, horizontally base excited single pendulums are chosen for investigation here. The non-dimensional form of the differential equation is

$$\ddot{\theta} + 2\xi/r\dot{\theta} + 1/r^2\sin\theta - f\sin t\cos\theta = 0, \tag{2.1}$$

where $t=\omega \tau$, ω is the angular excitation velocity, and τ is the actual time; ξ is the viscous damping coefficient; $r=\omega/\omega_N$, $\omega_N=\sqrt{mge/J}$ is the natural frequency of the linearized system, m is the pendulum mass, e is the the centroid offset from the pendulum hinge, J is the moment of inertia about the joint point. Meanwhile coefficient f=mea/J is the non-dimensional excitation amplitude, and a is the excitation amplitude. For simplicity, we denote $c_T=2\xi/r$ as the new non-dimensional damping coefficient. The function $f\sin t\cos\theta$ is the nonlinear parametric excitation term, and $1/r^2\sin\theta$ is the autonomous nonlinear part. The angular displacement θ is in S^1 space (one dimensional sphere space), whereas the angular velocity and acceleration are in R^1 space.

In the simulation study, it is assumed that we know little of the system except for the parametric identification. To apply the identification algorithm [24] to the pendulum system, the following more general expression of a single d. o. f. system can be assumed:

$$c_r \dot{x} + kx + f_{anl}(x, \dot{x}) + \{d_1 + f_{pnl}(x, \dot{x})\}p(t) = -\ddot{x},$$
 (2.2)

where k is the linear stiffness parameter, $f_{anl}(x,\dot{x})$ is the autonomous nonlinear part, $f_{pnl}(x,\dot{x})$ is the time-independent part of the parametric excitation term, and coefficient d_1 is the amplitude of external excitation force. If d_1 is non-zero and f_{pnl} equal to zero, the system becomes a nonlinear system with external excitation force. On the contrary, if d_1 is zero and f_{pnl} is non-trivial, it is then a parametrically excited system. For the examined single pendulum, parameter k=0 and $d_1=0$. Meanwhile, since the non-linearity of the pendulum is caused by geometry, it is convenient to assume f_{anl} and f_{pnl} in equation (2.2) as functions of only displacement, such that it becomes

$$c_r \dot{x} + f_{anl}(x) + f_{pnl}(x)p(t) = -\ddot{x}.$$
 (2.3)

Based on equation (2.3), the harmonic excitation term $p(t) = \alpha_1 \cos \omega t + \beta_1 \sin \omega t$ with excitation frequency ω . Unknown functions f_{pnl} and f_{anl} can be approximated by

$$f_{pnl} \approx \sum_{i=1}^{N} P_i \phi_i(x), \tag{2.4}$$

$$f_{anl} \approx \sum_{i=1}^{N} q_i \phi_i(x), \tag{2.5}$$

where $\{\phi_i(x)\}$ is a set of orthogonal basis functions, and P_i , q_i are unknown parameters. Since the choice of basis functions can affect accuracy of the identified functions, two sets of basis functions were tested in the simulation: linear interpolation functions and Fourier series functions.

Substituting (2.4), (2.5) and the harmonic excitation into (2.3), we have

$$c_{\tau}\dot{x} + \sum_{i=1}^{N} q_{i}\phi_{i}(x) + \sum_{i=1}^{N} n_{i}\phi_{i}(x)\cos t + \sum_{i=1}^{N} p_{i}\phi_{i}(x)\sin t = -\ddot{x},$$
 (2.6)

where $n_i = P_i \alpha_1$ and $p_i = P_i \beta_1$. With equation (2.6), harmonic balance identification [24] can be applied after extracting unstable or stable periodic orbits from the collected displacement data. For a period k orbit, if displacement x is in R^1 (one dimensional real space), the displacement, velocity and acceleration signals can be approximated by the following truncated Fourier series expansions:

$$x_k(t) \approx \frac{1}{2}a_{0,k} + \sum_{j=1}^{M} (a_{j,k}\cos\frac{j\omega t}{k} + b_{j,k}\sin\frac{j\omega t}{k}),$$
 (2.7)

$$\dot{x}_k(t) \approx \sum_{j=1}^M \frac{j\omega}{k} (-a_{j,k} \sin \frac{j\omega t}{k} + b_{j,k} \cos \frac{j\omega t}{k}), \tag{2.8}$$

$$\ddot{x}_k(t) \approx \sum_{j=1}^M -j^2 \omega^2 / k^2 \left(a_{j,k} \cos \frac{j\omega t}{k} + b_{j,k} \sin \frac{j\omega t}{k} \right), \tag{2.9}$$

where, for non-dimensional equation (2.6), $\omega=1$. However, for x in S^1 (one di-

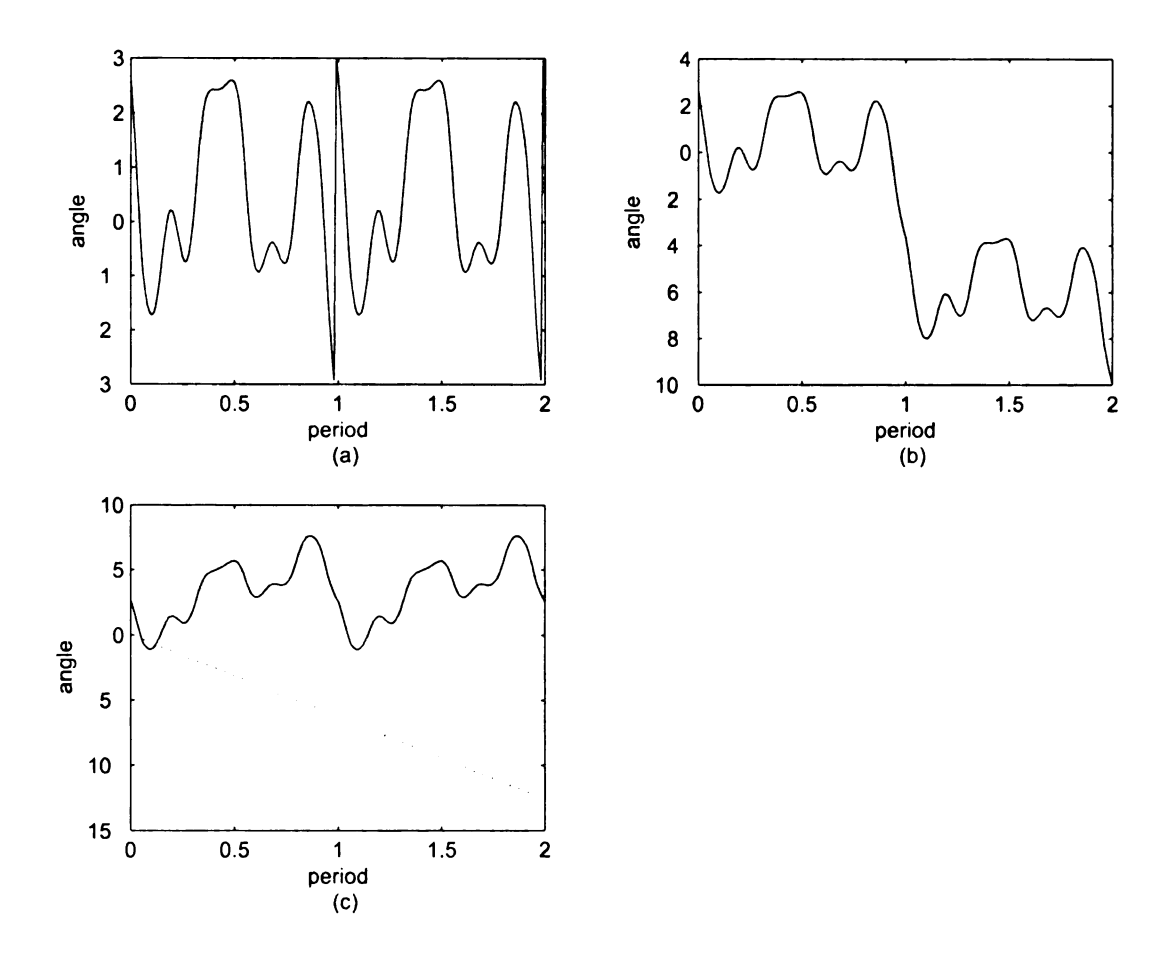


Figure 2.1. A period-4 orbit (a) sampled signal; (b) actual continuous signal x_c ; (c) \cdots constant rotation part $\omega_{ck}t$, – oscillatory part x_{var} .

mensional sphere space, e. g. the angular displacement θ in the single pendulum), Equations (2.7) – (2.9) are not applicable for whirling. The harmonic balance method can still be applied here, but with proper modification. The issue is that the velocity and acceleration are R^1 signals, and cannot be derived directly from the sampled S^1 displacement signal.

Consider an experiment in which whirling angle θ signal is collected with an encoder such that the output x has values in the interval $[-\pi, \pi)$. Thus, x is discontinuous. According to the illustration in Figure 2.1 of a period four orbit of the single

pendulum system, the sampled data $\{x\}$ should be converted to a continuous signal $\{x_c\}$ in \mathbb{R}^1 , and then decomposed as

$$x_{ck} = \omega_{ck}t + x_{var,k},$$

where $\omega_{ck}t$ represents the constant rotating part of a whirling periodic orbit, and $x_{var,k}$ is the oscillatory part of the orbit signal, which can be approximated by the truncated Fourier series expansion

$$x_{var,k}(t) \approx \frac{1}{2}u_{0,k} + \sum_{j=1}^{M} (u_{j,k}\cos\frac{j\omega t}{k} + v_{j,k}\sin\frac{j\omega t}{k}).$$

Based upon x_{ck} , the corresponding velocity and acceleration can be expressed as

$$\dot{x}_k(t) \approx \omega_{ck} + \sum_{j=1}^M \frac{j\omega}{k} \left(-u_{j,k} \sin \frac{j\omega t}{k} + v_{j,k} \cos \frac{j\omega t}{k}\right), \tag{2.10}$$

$$\ddot{x}_k(t) \approx \sum_{j=1}^M -j^2 \omega^2 / k^2 \left(u_{j,k} \cos \frac{j\omega t}{k} + v_{j,k} \sin \frac{j\omega t}{k} \right). \tag{2.11}$$

Meanwhile, for a period-k orbit, if $\phi_i(x): S^1 \to C[-1,1]$, as in the case of the pendulum, the continuous functions $\phi_i(x_k)$, $\phi_i(x_k)\cos\omega t$ and $\phi_i(x_k)\sin\omega t$ can also be approximated by

$$\phi_i(x_k) \approx c_{i0,k}/2 + \sum_{j=1}^{M} (c_{ij,k} \cos \frac{j\omega t}{k} + d_{ij,k} \sin \frac{j\omega t}{k}),$$
 (2.12)

$$\phi_i(x_k)\cos t \approx e_{i0,k}/2 + \sum_{j=1}^M (e_{ij,k}\cos\frac{j\omega t}{k} + f_{ij,k}\sin\frac{j\omega t}{k}), \qquad (2.13)$$

$$\phi_i(x_k)\sin t \approx g_{i0,k}/2 + \sum_{j=1}^{M} (g_{ij,k}\cos\frac{j\omega t}{k} + h_{ij,k}\sin\frac{j\omega t}{k}).$$
 (2.14)

Substituting (2.10)–(2.14) into (2.6), the differential equation can be transformed into the following matrix equation for a period-k orbit

$$\begin{pmatrix} \omega_{ck} & e_{10,k}/2 & g_{10,k}/2 & c_{10,k}/2 & \cdots & e_{N0,k}/2 & g_{N0,k}/2 & c_{N0,k}/2 \\ \frac{\omega}{k}v_{1,k} & e_{11,k} & g_{11,k} & c_{11,k} & \cdots & e_{N1,k} & g_{N1,k} & c_{N1,k} \\ -\frac{\omega}{k}u_{1,k} & f_{11,k} & h_{11,k} & d_{11,k} & \cdots & f_{N1,k} & h_{N1,k} & d_{N1,k} \\ \vdots & \vdots & \vdots & \vdots & \ddots & \vdots & \vdots & \vdots \\ \frac{M\omega}{k}v_{M,k} & e_{1M,k} & g_{1M,k} & c_{1M,k} & \cdots & e_{NM,k} & g_{NM,k} & c_{NM,k} \\ -\frac{M\omega}{k}u_{M,k} & f_{1M,k} & h_{1M,k} & d_{1M,k} & \cdots & f_{NM,k} & h_{NM,k} & d_{NM,k} \end{pmatrix}$$

$$\begin{pmatrix} c_r \\ n_1 \\ p_1 \\ \vdots \\ n_N \\ p_N \\ q_N \end{pmatrix} = \begin{pmatrix} 0 \\ \omega^2 u_{1,k}/k^2 \\ \vdots \\ M^2 \omega^2 u_{M,k}/k^2 \\ \vdots \\ M^2 \omega^2 v_{M,k}/k^2 \end{pmatrix}$$

$$(2.15)$$

For simplicity, $A_{\pmb{k}}$ is denoted as the left-hand side matrix,

and

$$\beta_k = (0 \ \omega^2 u_{1,k}/k^2 \ \omega^2 v_{1,k}/k^2 \ \cdots \ M^2 \omega^2 u_{M,k}/k^2 \ M^2 \omega^2 v_{M,k}/k^2)^T$$

Equation (2.15) can then be expressed as $A_k \lambda = \beta_k$.

For multiple periodic orbits, by combining the single periodic orbit matrices to-

gether, we can obtain the following matrix equation

$$A\lambda = \beta, \tag{2.16}$$

where

$$A = (A_1^T \cdots A_k^T \cdots A_K^T)^T,$$

$$\beta = (\beta_1^T \dots \beta_k^T \dots \beta_K^T)^T,$$

and A is a $K(2M+1) \times (3N+1)$ identification matrix. When K(2M+1) > 3N+1, the matrix can be solved by least mean square method. The least squares solution of (2.16) is

$$\lambda = (A^T A)^{-1} A^T \beta. \tag{2.17}$$

The error of the identification algorithm can be affected by several factors, including accuracy of unstable periodic orbits, noise contamination, system nonlinearity and the choice of basis functions of approximation.

2.3 Introduction to phase plane reconstruction and extraction of unstable periodic orbits

Usually in an experiment, only limited signals can be acquired accurately, e. g. the angular displacement signal in this simulation. However, for the extraction of unstable periodic orbits, phase plane information is necessary. It is then that the phase plane reconstruction technique [52] is applied. Suppose that s(k) is the sampled smooth signal from dynamical systems. Smooth dynamics in an n dimensional phase space could be approximately represented by an embedding dimension space

$$S(k) = \{s(k), s(k+T_d), \dots, s(k+(d-1)T_d)\},\$$

where d is the dimension of the reconstructed phase space and T_d is the time delay of the embedding dimension. Although the reconstructed phase space is a distorted appearance of the real phase plane, it provides us information of phase orbits, attractors, periodic orbits and other chaotic characteristics. To the pendulum system, $s(k) = \theta(k), \ \theta \in [-\pi, \pi)$ is actually a non-smooth observable. But the method can also be applied here since the functions of angular displacement, speed and acceleration are all smooth.

2.3.1 Choosing the time delay and embedding dimension

The time delay value T_d can be obtained from average mutual information function [52], which is expressed as

$$I_{AB}(t) = \sum_{a,b} P_{AB}(a,b) \log_2 \frac{P_{AB}(a,b)}{P_{A}(a)P_{B}(b)},$$
(2.18)

where t is the time lag, a is the sampled data s(i), A is the set of $\{s(i)\}$, k = i + T, b is thus s(i + t), and B is considered as the set of $\{s(i + t)\}$. Meanwhile, $P_A(x)$ is the probability function of observing x out of a set A, $P_B(y)$ is the probability of observing y out of a set B, and $P_{AB}(x,y)$ is defined as the probability of observing function of (x,y) out of the set of $A \cap B$. After calculating I(t), the 'best' time delay T_d is chosen when I(t) reaches its first minimum.

To determine the value of d_E for minimum required delay dimensions, the false nearest neighbors method was applied [52]. The false nearest neighbors method identifies the embedding dimension for which false trajectory crossings do not occur.

2.3.2 Extracting unstable periodic orbits (UPOs)

There are numerous unstable periodic orbits in a chaotic signal. The UPO set is a dense set within the chaotic orbits. The reconstructed phase space can be used to ex-

tract the hidden UPOs. Since the horizontally excited single pendulum is excited by a harmonic signal with period T, the UPOs will have the periodicities of integral multiples of the excitation period T. Though theoretically, no exact UPO can be found through the collected data, the theory proved that some very close approximation of the UPO exists provided that the data is long enough. With the error tolerance e set for UPO extraction, we say that an approximated UPO of period k is extracted if |S(n-kT)-S(n)| < e, where S(n-kT) is the starting point of the extracted orbit, and S(n) is the end point. Usually e is set as 1–5% of the span of the data [24], and the smaller e value is always desirable if possible, since the corresponding UPO will be closer to the real periodic orbits.

Meanwhile, a recurrence error between the starting and end points will occur in the extracted UPO by the choice of e, which is an exhibition of the accumulated error compared to the 'true' periodic orbit. Generally, to acquire more accurate UPOs, smaller e is used.

2.4 Numerical simulation of the horizontally excited pendulum

2.4.1 Phase space reconstruction

The simulation was based upon the non-dimensional differential equation (2.1). A data set of 30000 points was gathered with a sampling rate $f_s = 25/T$. Displayed in Figure 2.2 (a) is the 2-D reconstructed phase space. The coefficients were chosen as f = 1.52, c = 0.03, r = 0.8333. The actual minimum embedding dimension needed for a complete phase space reconstruction was found to be four. However, since our purpose of reconstructing phase space is to extract UPOs, which compare points with kT time interval (implying the addition of the S^1 dimension of time), the possibility

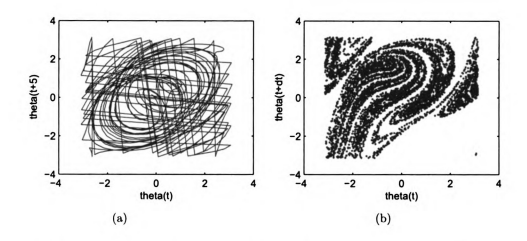


Figure 2.2. Reconstructed phase plane (a) and Poincaré section plot (b); $\theta(t)$ is represented by theta(t) in the plots.

of encountering a false nearest neighbor is greatly reduced. Hence, two embedding coordinates are adequate for this case, and are also simpler for display purposes.

According to Figure 2.3 of the average mutual information, the calculated best time delay was $T_d=5$. The phase portrait and the Poincaré section are displayed in Figure 2.2 (a) and (b). The Poincaré section plot, obtained by plotting the cross-section of the phase flow at a fixed periodic time position $\tau=t\mod 2\pi$ since the system is under periodic excitation, provides us a handy tool for visually comparing chaotic properties of different systems. Similar Poincaré section plots give evidence of similar dynamical behaviors of the systems.

2.4.2 Parametric identification

For simplicity, the data used in the identification process was noise-free, thus excluding the noise-generated error in the identified parameters. The UPOs were extracted before applying the identification algorithm. An error tolerance of e = 3% was

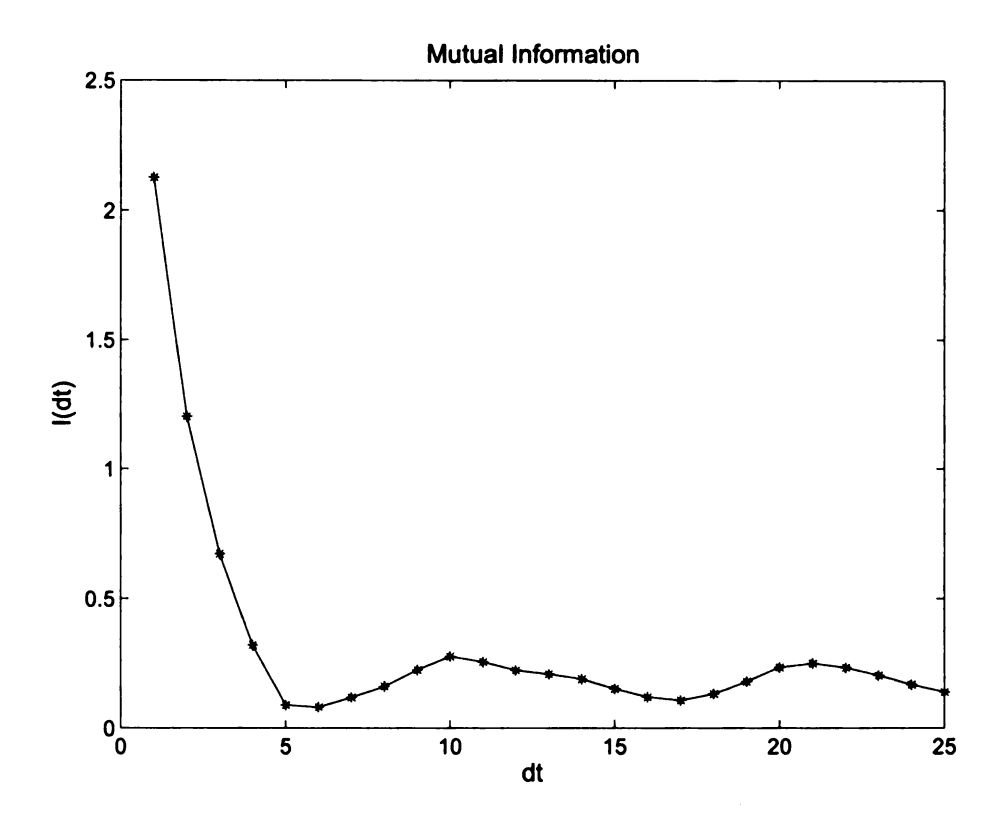


Figure 2.3. Mutual information of the data; the first minimum is at dt=5.

applied in the extraction. The error tolerance can be made smaller if longer sampled data is available. Consequently, around 25 UPOs were extracted from period 1 to period 16. Figure 2.4 shows a example of periodic orbits of period one and two. Some are whirling orbits, whereas others are oscillating orbits. With the UPOs extracted, in the identification process, two sets of basis functions were tested to approximate the unknown nonlinear functions in the governing equation.

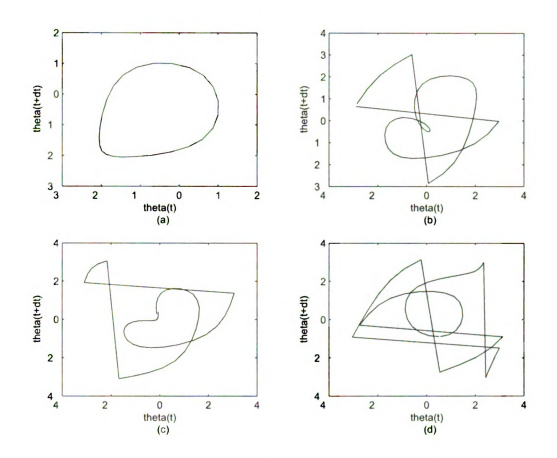


Figure 2.4. (a)A period-1 orbit; (b) A period-2 orbit; (c) A period-2 orbit; (d) A period-2 orbit.

Harmonic basis functions

If basis functions are set as $\phi_{2k-1}(x)=\cos kx$, $\phi_{2k}(x)=\sin kx$, $k=1,\ 2,\ 3,\ \ldots$, the differential equation (4.12) is then converted to

$$\begin{split} c_r \dot{x} + \sum_{k=1}^K (n_{2k-1}\cos kx + n_{2k}\sin kx)\cos t + \sum_{k=1}^K (p_{2k-1}\cos kx + p_{2k}\sin kx)\sin t \\ + \sum_{k=1}^K (q_{2k-1}\cos kx + q_{2k}\sin kx) = -\ddot{x}. \end{split} \tag{2.19}$$

Table 2.1. The n_k , p_k and q_k values when harmonic basis is applied.

	$\hat{n}_{m{k}}$	n_k	$ n_k - \hat{n}_k $	$\hat{p}_{m{k}}$	p_k	$ p_k - \hat{p}_k $	$\hat{p}_{m{k}}$	q_k	$ q_k - \hat{q}_k $
$\cos k\theta$	0.009	0.0	0.009	-1.526	-1.52	0.006	-0.004	0.0	0.004
$\sin k\theta$	0.003	0.0	0.003	-0.0	0.0	0.0	1.434	1.44	0.006

For the investigated pendulum, it is convenient to set K=1, i. e. include only the first harmonics, since the differential equation is simple and consists of harmonic type non-linearity.

For systems like the single pendulum, where the non-linearity comes from angular rotation and the displacement variables belonging to the sphere space, a harmonic basis can be a very good choice due to its capability of representing rotation and periodic behaviors. Displayed in Table 2.1 are the identified coefficients of (2.19) with \hat{n}_k , \hat{p}_k , \hat{q}_k representing the estimated values, and n_k , p_k , q_k representing the true values. The estimated c_r value is 0.0339. Compared to the real values, all of the parameters are quite accurate with minor errors less than 0.01.

Linear interpolation basis functions

Linear interpolation functions can be expressed as

$$\phi_k(x) = \begin{cases} \frac{x - (k-1)d}{d}, & (k-1)d < x < kd \\ \frac{(k+1)d - x}{d}, & kd \le x < (k+1)d \\ 0, & otherwise \end{cases}$$

where d is the distance interval. Had we not known the appropriate basis functions, e. g. harmonics in this case, interpolation functions are good alternatives [21]. For better expression of the nonlinear functions, generally more interpolation points (functions) are needed [25]. However, that implies more unknown parameters and

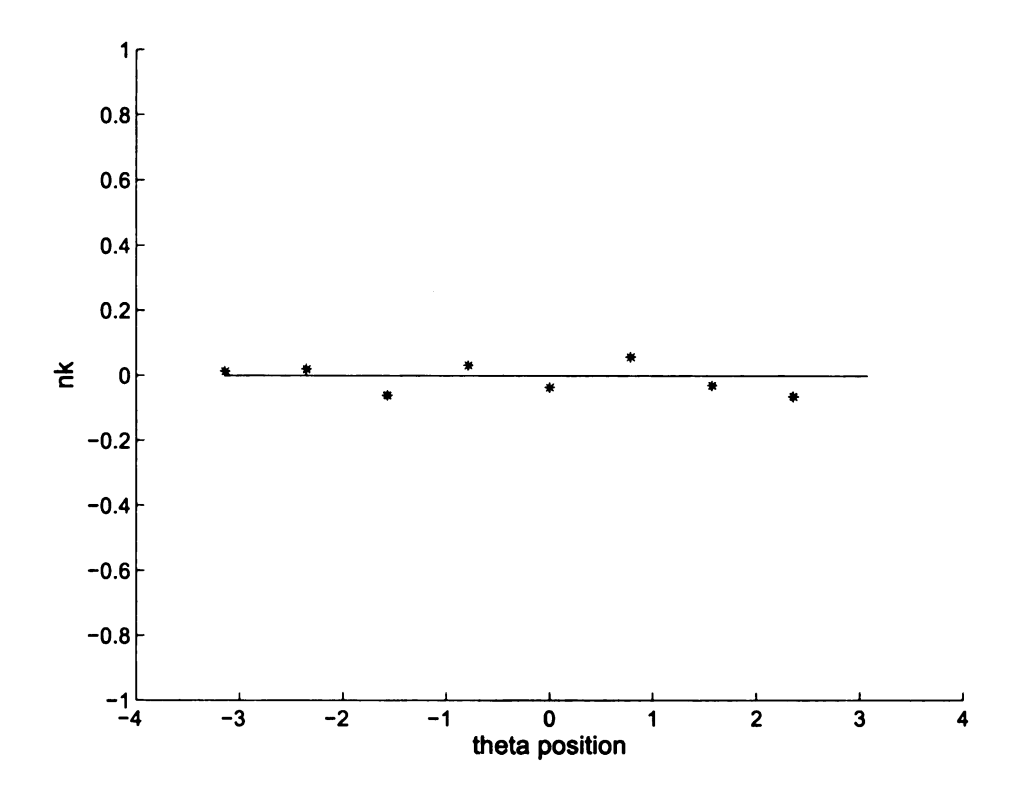


Figure 2.5. The n_k curve for linear interpolation basis; (*) identified values, (—) true function.

requires more periodic orbits for the least mean square method. Eight points were utilized in this identification. The interval $[-\pi,\pi)$ was divided evenly into eight equal sub-intervals. The unknown curves can be represented by the piece-wise linear curve connected between sub-interval nodes.

Figures 2.5, 2.6, and 2.7 show the piece-wise curves of $\{n_k\}$, $\{p_k\}$, $\{q_k\}$. Meanwhile, the identified friction coefficient $c_r = 0.0348$. It can be seen that $\{n_k\}$ curve is nearly zero, $\{p_k\}$ curve is a cosine curve, and the $\{q_k\}$ curve is a sine curve, which are consistent with the differential equation (2.1). The eight-point approximation is still a rough representation of the real curve, and consequently introduces more error than the harmonic basis case. In the next section, we will discuss the error's influence on the dynamic characteristics of the system.

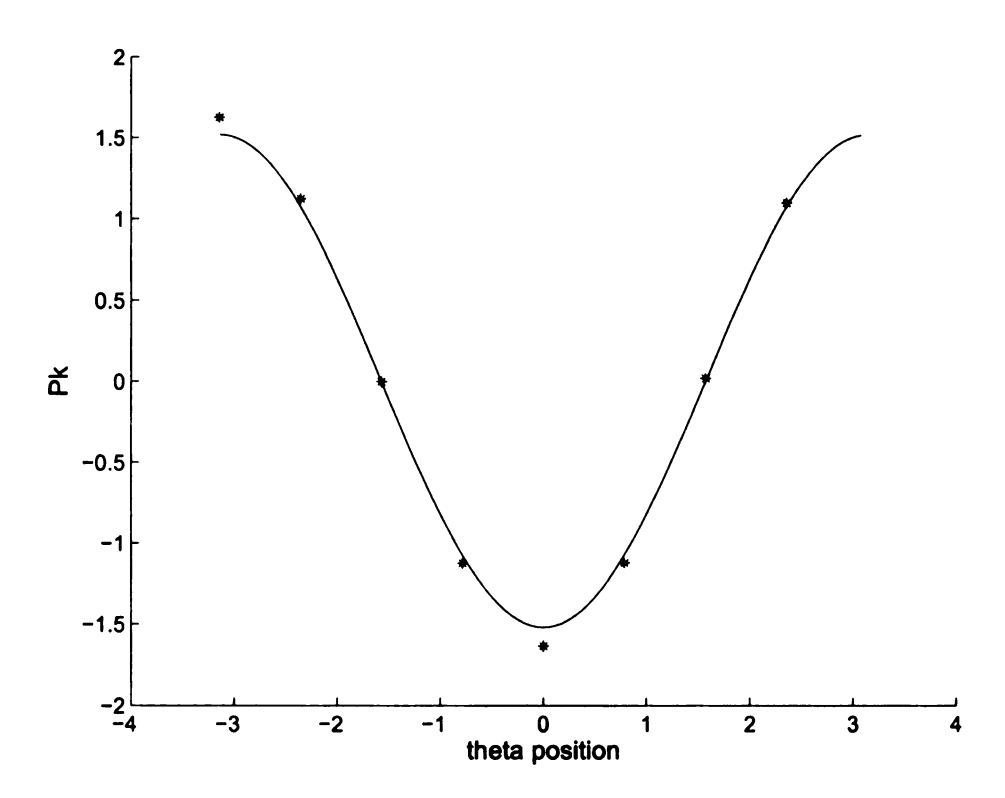


Figure 2.6. The p_k curve for linear interpolation basis; (*) identified values, (—) true function.

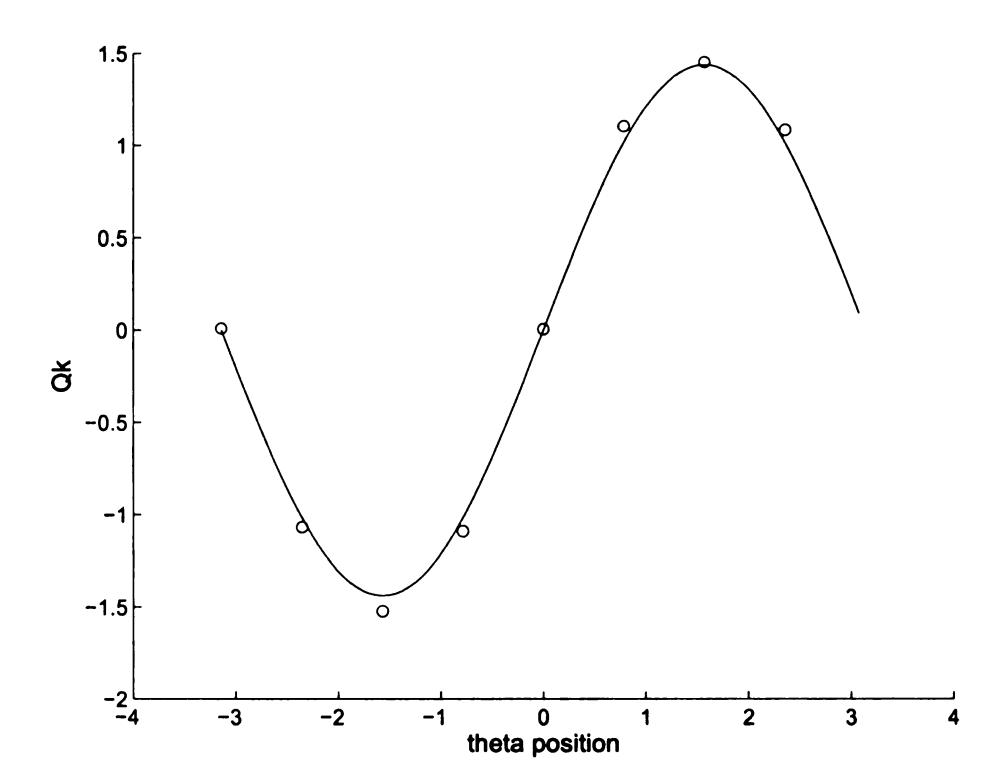


Figure 2.7. The q_k curve for linear interpolation basis; (o) identified values, (—) true function.

2.5 Discussion and validation

Direct comparison showed that the identification algorithm was satisfying for the single degree of freedom system. Furthermore, it was the harmonic basis that generated the more precise identification result, due to the fact that the unknown nonlinear functions consist of harmonics. However, when investigating unknown systems, direct comparison is unavailable. In this case, it is then natural to examine the dynamical behavior, e. g. chaotic characteristics, of the identified system for validation purposes.

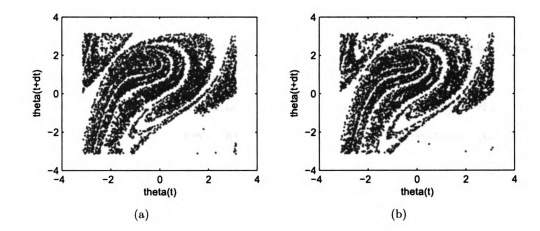


Figure 2.8. Poincaré section plots of identified systems: (a) by linear interpolation basis, (b) by Harmonic basis.

Displayed in Figure 2.8 (a) and (b) are Poincaré sections of the identified systems with harmonic basis and linear interpolation basis. The Poincaré sections look similar to the original pendulum, which implies the dynamical similarity of these three chaotic systems. Thus, for the purpose of chaotic characteristics, the linear interpolation approximation, though a coarse representation, is still acceptable.

For more validation methods of the unknown systems, we can also refer to the linearized model method, comparison of fractal dimensions, bifurcation diagrams, and Lyapunov exponents. But for this simulation case, where the parameters are known, direction comparison is the best tool.

2.6 Concluding remarks

In this chapter, the simulated parametric identification procedure was investigated for a chaotic horizontally base-excited pendulum. The identification was assumed to apply to a single-degree-of-freedom system with a known parametric excitation frequency and unknown nonlinearity. The identification algorithm [24, 25] was modified for application to the whirling pendulum system. Two types of basis functions were applied to approximate the unknown functions. Then, the simulations of the identified models were presented to verify the effectiveness of the algorithm. Both the direct comparison and the validation methods showed the accuracy of the identified parameters and the similarity between the original and the identified systems. Although both of the methods gave similar results, the harmonic basis functions matched the form of the true nonlinearity, and therefore in this case, gave a more precise result. On the other hand, the linear interpolation was also valuable since it is a good choice for a general unknown type of non-linearity in a single variable. According to the simulation result, the modified parametric identification process was successful in the single degree of freedom whirling system. However, the simulation was limited to single degree of freedom systems with no noise contamination. For more general applications, multi-degree of freedom systems and experimental verifications are needed for full investigation of the proposed method.

CHAPTER 3

Experimental Study of a

Base-Excited Double Pendulum

The approximated periodic orbits can be extracted by phase space reconstruction techniques [53, 54, 52] with a certain tolerance of error for extraction. The approximated UPOs made little influence on the identification of the single pendulum system. However, it is not clear whether it is so for multi-degree-of-freedom systems, or systems with strong nonlinearity. Also, it is necessary to examine the harmonic balance based identification method in experimental systems in which the collected signals are noise contaminated. These are the reasons for the continued research on an experimental multi-degree-of-freedom system: the double-pendulum system. Another reason that the double-pendulum system was chosen for experiment is that it is easier to adjust parameters of the double pendulum system to exhibit chaotic behavior than the single pendulum system.

3.1 Description of the double pendulum system

A schematic diagram of the double pendulum is shown in Figure 3.1. The first arm has mass m_1 , centroid offset e_1 , arm length l_1 , and angular inertia J_{c1} based upon

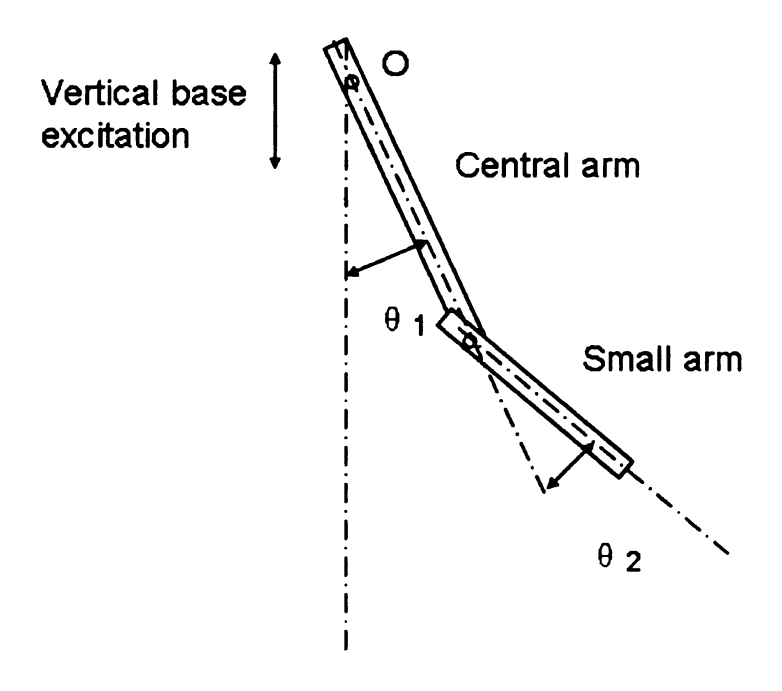


Figure 3.1. A sketch of the double pendulum.

the arm centroid point. The second arm has mass m_2 , centroid offset e_2 , arm length l_2 , and angular inertia J_{c2} . θ_1 is the absolute angular displacement of the first arm and θ_2 is relative angular displacement of the second arm.

The two arms of the pendulum are supported and connected by low friction bearings. The bearings are assumed to have two types of friction: dry Coulomb friction and viscous damping. To the specific double pendulum that was used in the experiment, tests indicated that the first arm bearings had dominantly Coulomb friction because of no oil lubrication, and the second arm bearings had dominantly viscous friction due to full oil lubrication. With these known properties, we can then obtain

the non-dimensional governing differential equations of this system:

$$\begin{cases} \ddot{\phi_{1}} + b_{11}\ddot{\phi_{2}}\cos(\phi_{2} - \phi_{1}) - b_{11}\dot{\phi_{2}}^{2}\sin(\phi_{2} - \phi_{1}) + b_{12}\sin\phi_{1} \\ + b_{13}\sin\phi_{1}\ddot{y} + c_{11}sign(\dot{\phi_{1}}) - c_{12}(\dot{\phi_{2}} - \dot{\phi_{1}}) = 0 \\ \ddot{\phi_{2}} + b_{21}\ddot{\phi_{1}}\cos(\phi_{2} - \phi_{1}) + b_{21}\dot{\phi_{1}}^{2}\sin(\phi_{2} - \phi_{1}) + b_{22}\sin\phi_{2} \\ + b_{23}\sin\phi_{2}\ddot{y} + c_{2}(\dot{\phi_{2}} - \dot{\phi_{1}}) = 0 \end{cases}$$

$$(3.1)$$

where $\phi_1=\theta_1$ and $\phi_2=\theta_1+\theta_2$ are absolute angular deflections, $B_{11}=m_2e_2l_1/J_{o1}$, $b_{12}=g(m_1e_1+m_2l_1)/J_{o1}$, $b_{13}=(m_1e_1+m_2l_1)/J_{o1}$, $B_{21}=m_2e_2l_1/J_{o2}$, $b_{22}=gm_2e_2/J_{o2}$, $b_{23}=m_2e_2/J_{o2}$, $c_{12}=c_{r2}/J_{o1}$, $c_2=c_{r2}/J_{o2}$, $J_{o1}=J_{c1}+m_1e_1^2+m_2l_1^2$, and $J_{o2}=J_{c2}+m_2e_2^2$; y is the excitation displacement of the support with known

frequency
$$f_e$$
; and $f(x) = sign(x) = \begin{cases} 1, & x > 0 \\ 0, & x = 0 \end{cases}$ is a sign function representing $-1, x < 0$

Coulomb friction. Function f(x) is valid if there are no sticks. For convenience of the analysis, a non-dimensional form of the governing differential equation is desired. By letting $\tau = 2\pi f_e t$ and $\Omega = 2\pi f_e$, then, $\frac{d}{dt} = \frac{d}{d\tau} \cdot \frac{d\tau}{dt} = 2\pi f_e \frac{d}{d\tau} = \Omega \frac{d}{d\tau}$. Under a sinusoidal excitation $y = a \cos \tau$, where a is the excitation amplitude, equation (3.1) can be expressed as

$$\begin{cases} \phi_{1}'' + B_{11}\phi_{2}''\cos(\phi_{2} - \phi_{1}) - B_{11}\phi_{2}'^{2}\sin(\phi_{2} - \phi_{1}) + B_{12}\sin\phi_{1} \\ + B_{13}\sin\phi_{1}y'' + C_{11}sign(\phi_{1}') - C_{12}(\phi_{2}' - \phi_{1}') = 0 \\ \phi_{2}'' + B_{21}\phi_{1}''\cos(\phi_{2} - \phi_{1}) + B_{21}\phi_{1}'^{2}\sin(\phi_{2} - \phi_{1}) + B_{22}\sin\phi_{2} \\ + B_{23}\sin\phi_{2}y'' + C_{2}(\phi_{2}' - \phi_{1}') = 0 \end{cases}$$
(3.2)

where ${\phi_i}'=\frac{d}{d\tau}\phi_i$, $B_{i1}=b_{i1}$, $B_{i2}=b_{i2}/\Omega^2$ for $i=1, 2, B_{i3}=-b_{i3}a$, $C_{11}=c_{11}/\Omega^2$, $C_{12}=c_{12}/\Omega$ and $C_2=c_2/\omega$. The differential equation is non-autonomous because of the time dependence of $y(\tau)$.

For identification purposes, the excitation signal y can be approximated by the

Fourier series expansion of

$$y(\tau) = \sum_{j=1}^{J} (E_j \cos j\tau + F_j \sin j\tau), \tag{3.3}$$

where the coefficients E_j and F_j are unknown. For the present system with harmonic excitation, $y = E_1 \cos \tau + F_1 \sin \tau$ is adequate for identification. Since all the parameters are unknown with the only exception of the excitation frequency, equation (3.2) can then be transformed into

$$\begin{cases} B_{11}\phi_{2}''\cos(\phi_{2}-\phi_{1}) - B_{11}\phi_{2}'^{2}\sin(\phi_{2}-\phi_{1}) + B_{12}\sin\phi_{1} \\ + B'_{13}\sin\phi_{1}\cos\tau + B'_{14}\sin\phi_{1}\sin\tau + C_{11}sign(\phi_{1}') - C_{12}(\phi_{2}'-\phi_{1}') = -\phi_{1}'' \\ B_{21}\phi_{1}''\cos(\phi_{2}-\phi_{1}) + B_{21}\phi_{1}'^{2}\sin(\phi_{2}-\phi_{1}) + B_{22}\sin\phi_{2} \\ + B'_{23}\sin\phi_{2}\cos\tau + B'_{24}\sin\phi_{1}\sin\tau + C_{2}(\phi_{2}'-\phi_{1}') = -\phi_{2}'' \end{cases}$$

$$(3.4)$$

where $B'_{i3} = B_{i3}E_1$ and $B'_{i4} = B_{i3}F_1$ for i=1, 2. For simplicity, we will use B_{i3} and B_{i4} to replace B'_{i3} and B'_{i4} in the later parts of this report. Equation (3.4) is then the desired form for identification.

3.2 Method

The identification process is similar to the one used in the simulated parametrically excited single pendulum (Chapter 2), which contains data acquisition/post-processing, phase plane reconstruction/extracting unstable periodic orbits, formation of the identification matrix and the solution by the least mean square method. Due to apparatus limitations, some signal noise occurred during digitization. Therefore certain digital filtering techniques were applied to the acquired signals. Details of the post-processing will be introduced in next section. Other modifications are also applied to the double pendulum system for improvement of the identification.

Due to the complexity of the non-linearity of the double pendulum equation (3.4), our unknown parameters contain only those coefficients of terms of the differential equations, which will greatly simplify the identification matrix. There are totally 11 unknown parameters in the two differential equations, namely, B_{11} , B_{12} , ..., B_{24} , C_{11} , C_{12} and C_{2} . Similar to the case in the single pendulum simulation, the angular displacements θ_{1} and θ_{2} are both variables in S^{1} (one dimensional sphere space). However the angular speeds, accelerations and $\sin \phi_{i}$ (i = 1,2) belong to R^{1} (one dimensional continuous real space). Hence, for any period-k orbit (there may be multiple orbits of same periodicity k, the Fourier series expression of the periodic orbits is

$$\phi_{1,k,l}(t) \approx \Omega_{1,k,l}t + a_{0,k,l}/2 + \sum_{j=1}^{m} (a_{j,k,l}\cos\frac{j\omega t}{k} + b_{j,k,l}\sin\frac{j\omega t}{k})$$
 (3.5)

and

$$\phi_{2,k,l}(t) \approx \Omega_{2,k,l}t + c_{0,k,l}/2 + \sum_{j=1}^{m} (c_{j,k,l}\cos\frac{j\omega t}{k} + d_{j,k,l}\sin\frac{j\omega t}{k}), \quad (3.6)$$

where $\Omega_{i,k,l}$, is the average rotation speed per cycle for the lth orbit of period k. By doing so, the following equations can be obtained through the Fourier expansion of periodic orbits:

$$\dot{\phi}_{1,k,l}(t) \approx \Omega_{1,k,l} + \sum_{j=1}^{m} \frac{j\omega}{k} \left(-a_{j,k,l} \cos \frac{j\omega t}{k} + b_{j,k,l} \sin \frac{j\omega t}{k} \right), \tag{3.7}$$

$$\dot{\phi}_{2,k,l}(t) \approx \Omega_{2,k,l} + \sum_{j=1}^{m} \frac{j\omega}{k} \left(-c_{j,k,l} \cos \frac{j\omega t}{k} + d_{j,k,l} \sin \frac{j\omega t}{k} \right), \tag{3.8}$$

$$\ddot{\phi}_{1,k,l}(t) \approx \sum_{j=1}^{m} -\frac{j^2 \omega^2}{k^2} \left(a_{j,k,l} \cos \frac{j\omega t}{k} + b_{j,k,l} \sin \frac{j\omega t}{k}\right),\tag{3.9}$$

$$\ddot{\phi}_{2,k,l}(t) \approx \sum_{j=1}^{m} -\frac{j^2 \omega^2}{k^2} (c_{j,kl} \cos \frac{j\omega t}{k} + d_{j,k,l} \sin \frac{j\omega t}{k}), \tag{3.10}$$

$$\ddot{\phi}_{i,k,l}(t)\cos(\phi_{2,k,l}-\phi_{1,k,l}) \approx \frac{e_{1,0,k,l}}{2} + \sum_{j=1}^{m} (e_{i,j,k,l}\cos\frac{j\omega t}{k} + f_{i,j,k,l}\sin\frac{j\omega t}{k}), \quad (3.11)$$

$$\dot{\phi}_{i,k,l}^2(t)\sin\left(\phi_{2,k,l} - \phi_{1,kl}\right) \approx \frac{g_{1,0,k,l}}{2} + \sum_{j=1}^m (g_{i,j,k,l}\cos\frac{j\omega t}{k} + h_{i,j,l,k}\sin\frac{j\omega t}{k}), \quad (3.12)$$

$$sign(\dot{\phi}_{i,k,l}(t)) \approx \frac{p_{1,0,k,l}}{2} + \sum_{j=1}^{m} (p_{i,j,k,l} \cos \frac{j\omega t}{k} + q_{i,j,k,l} \sin \frac{j\omega t}{k}),$$
 (3.13)

$$\sin \phi_{i,kl} \approx \frac{r_{1,0,k,l}}{2} + \sum_{j=1}^{m} (r_{i,j,k,l} \cos \frac{j\omega t}{k} + s_{i,j,k,l} \sin \frac{j\omega t}{k}), \tag{3.14}$$

$$\sin \phi_{i,k,l} \cos t \approx \frac{u_{1,0,k,l}}{2} + \sum_{j=1}^{m} (u_{i,j,k,l} \cos \frac{j\omega t}{k} + v_{i,j,k,l} \sin \frac{j\omega t}{k}), \tag{3.15}$$

$$\sin \phi_{i,k,l} \sin t \approx \frac{w_{1,0,k,l}}{2} + \sum_{j=1}^{m} (w_{i,j,k,l} \cos \frac{j\omega t}{k} + z_{i,j,k,l} \sin \frac{j\omega t}{k}), \tag{3.16}$$

where k=1, 2, ..., K, and i=1, 2, is the corresponding period of the orbit; K is the maximum periodicity. Meanwhile, for the non-dimensional differential equations, time t here is actually τ in equation (3.4), and fundamental frequency is 1. If incremental encoders are used to sense the angular displacements, then velocity and acceleration are not directly measured. Their Fourier transforms can be handily generated by the displacement's Fourier transform for periodic response. However, for noise contaminated displacement signals, noisy errors may be amplified in the obtained Fourier spectrum of velocity and acceleration.

Also, Fourier series expansions of some terms in the differential equations, such as $\dot{\phi}_{i,k}^2 \sin(\phi_{2,k} - \phi_{1,k})$, are not obtained by direct Fourier series expansion of their time domain signal, but by convolution of known Fourier expansion components with a low pass filter applied. The purpose of applying a low pass filter to each signal component before convolution is to avoid noise amplification. Reasons will be explained in the following sections. Substituting (3.5–3.16) into (3.4), and equating the coefficients of

terms with identical harmonic order, we obtain two matrix equations:

or

$$A_1 \vec{x}_1 = \vec{q}_1 \tag{3.18}$$

and

$$\begin{pmatrix} (e-g)_{1,0,1,1} & r_{2,0,1,1} & u_{2,0,1,1} & w_{2,0,1,1} & -\Omega_{1,1,1} + \Omega_{2,1,1} \\ (e-g)_{1,1,1,1} & r_{2,1,1,1} & u_{2,1,1,1} & w_{2,1,1,1} & d_{1,1,1} - b_{1,1,1} \\ (f-h)_{1,1,1,1} & s_{2,1,1,1} & v_{2,1,1,1} & z_{2,1,1,1} & -(c_{1,1,1} - a_{1,1,1}) \\ \vdots & \vdots & \vdots & \vdots & \vdots \\ (e-g)_{1,0,k,l} & r_{2,0,k,l} & u_{2,0,k,l} & w_{2,0,k,l} & \Omega_{1,k,l} - \Omega_{2,k,l} \\ (e-g)_{1,1,k,l} & r_{2,1,k,l} & u_{2,1,k,l} & w_{2,1,k,l} & d_{1,k,l} - b_{1,k,l} \\ (f-h)_{1,1,k,l} & s_{2,1,k,l} & v_{2,1,k,l} & z_{2,1,k,l} & -(c_{1,k,l} - a_{1,k,l}) \\ \vdots & \vdots & \vdots & \vdots & \vdots \end{pmatrix} \begin{pmatrix} 0 \\ c_{1,1,1} \\ d_{1,1,1} \\ \vdots \\ 0 \\ c_{1,k,l}k^{-2} \\ d_{1,k,l}k^{-2} \\ \vdots \end{pmatrix},$$

$$(3.19)$$

or

$$A_2 \vec{x}_2 = \vec{q}_2, \tag{3.20}$$

where \vec{x}_1 and \vec{x}_2 are vectors of unknown parameters. Given a set of periodic orbits, it is adequate to equate the coefficients of the first several orders of sub-harmonics since they are usually the major components of the periodic orbits and less contaminated by noise. We then truncate the Fourier series expansion, and take the first M harmonics, such that $(2M+1) \cdot K > N_c$, where $(2M+1) \cdot K$ is the total number of rows in the matrix A_i , and N_c is the number of unknown coefficients in \vec{x}_1 or \vec{x}_2 . With

these conditions satisfied, the two equations can be solved by the least mean square method:

$$\vec{\hat{x}}_1 = (A_1^T A_1)^{-1} A_1^T \vec{q}_1 \tag{3.21}$$

and

$$\vec{\hat{x}}_2 = (A_2^T A_2)^{-1} A_2^T \vec{q}_2. \tag{3.22}$$

After the non-dimensional parameters are identified, the physical properties can then be restored according to non-dimensional parameters' definition if part of the physical parameters are known prior to identification. In the experiment, m_2 , e_2 , l_1 were treated as known since these physical properties were easily evaluated. Also, by defining $B_{i5} = \sqrt{B_{i3}^2 + B_{i4}^2}$, i=1, 2, we can obtain

$$p_b = |B_{i2}/B_{i5}| = \frac{g}{(2\pi f_e)^2 a}. (3.23)$$

Hence p_b is a constant for a constant excitation amplitude a and can be used as an indicator of the accuracy of the identified results.

3.3 Experiment description

Figure 3.1 shows a sketch of the double-pendulum that was used in the experiment. Two optical encoders (US Digital) were separately attached to the central arm (US Digital H5S-1024-157H) and the second arm (US Digital H5S-1024) to measure the relative angular displacements θ_1 and θ_2 . Both of the encoders had a resolution of 1024, and were therefore capable of detecting a minimum angular difference of 0.3516°. The two encoders sent out TTL square waves, which are noise-resistant, to two EDAC (Encoder Digital to Analogue Converter) converters, which transformed the TTL waves into analogue signals. After that, a data acquisition terminal trans-

lated all the signals into computer-acceptable digital signals.

Table 3.1. Physical properties of the double pendulum.

$m_1 ext{ (kg)}$	0.1362	$m_2~(\mathrm{kg})$	0.040
e_1 (m)	0.0127	e_2 (m)	0.0267
l_1 (m)	0.0635	l_2 (m)	0.0534
$J_1 (\text{kg} \times \text{m}^2)^*$	5.99×10^{-4}	$J_2 (\text{kg} \times \text{m}^2)^*$	4.033×10^{-5}
1 (0)	0.00 / 10	02 (6/)	1.000 × 10
C ₁₁ *	1.01×10^{-3}	C_1 *	0.0485

For validation purposes, Table 3.1 lists all the physical properties of the double pendulum. The asterisks in the table denote that some properties are not directly measured, but estimated from other dynamic methods, which implies that those parameters could have small errors. To estimate the mass moment of inertia, a small-amplitude free vibration was tested on the double pendulum. By evaluating the two natural frequencies of the system through the FFT, the mass moment of inertia values were calculated. Some parameters related to sampling and experimental settings are listed in Table 3.2.

Table 3.2. Experimental settings.

Sampling rate (f_s)	500 Hz	Excitation freq. (f_e)	5 Hz
Cut-off freq. (f_c)	80 KHz	Excitation amplitude (a)	1.15 cm

With all these settings, data were obtained during a three-hour-long chaotic vibration. The data record lasted 22 minutes.

3.4 Results and validation

3.4.1 Phase space reconstruction & UPO extraction

The embedding dimension was chosen to be eight by the false nearest neighbors method. Mutual information [52] of the signal was used for choosing adequate time delay T_d .

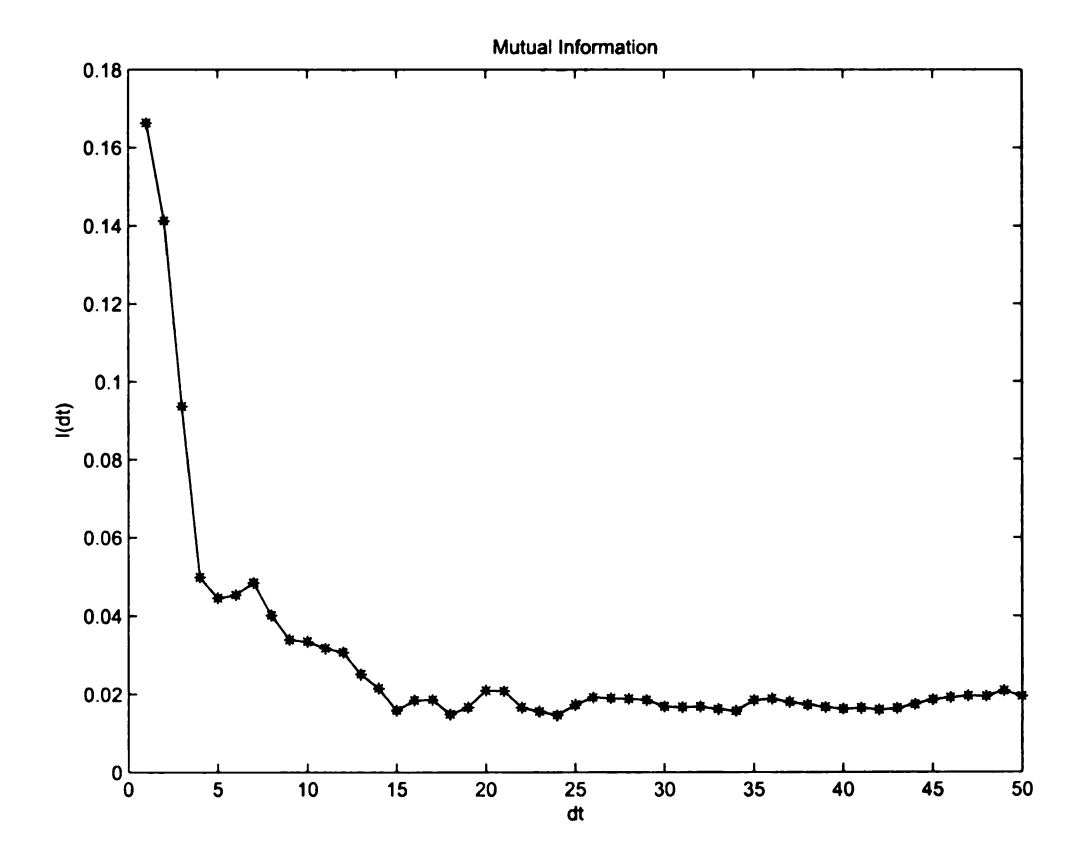


Figure 3.2. Mutual information I(dt).

It can be seen from Figure 3.2 that there are weak minima of I(dt) at dt = 5, 15, 18 and 24. But, $T_d = 24$ in a driving period of 100 samples is somewhat close to a quarter period, the ideal delay for a sinusoidal signal. The reconstructed phase

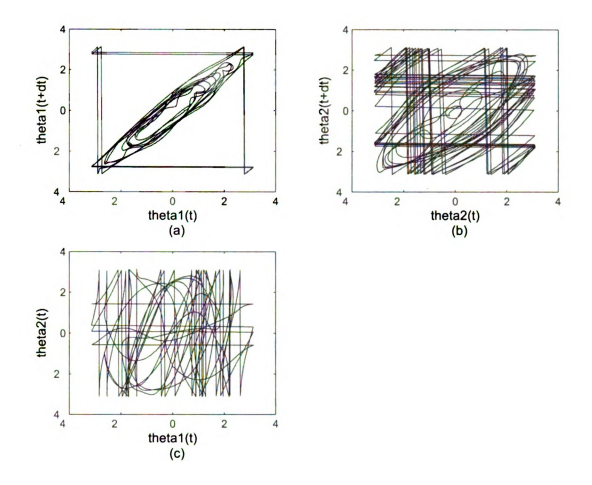


Figure 3.3. Phase portrait of experimental data with dt=24, (a) $\theta_1(t)$ - $\theta_1(t+dt)$, (b) $\theta_1(t)$ - $\theta_2(t)$, (c) $\theta_2(t)$ - $\theta_2(t+dt)$; θ is represented by theta in the figure.

portrait is plotted in Figure 3.3 with $T_d=24$. The portrait shows that the central arm, represented by θ_1 , oscillated in small angles most of the time with occasional large-angle whirling, which implies relatively larger noise in the θ_1 signal due to the limitation of the optical encoders. The second arm displacement, represented by θ_2 , consisted mainly of whirling vibration.

After choosing the embedding dimension and time delay, we used the reconstructed phase plane to extract unstable periodic orbits (UPOs). The error tolerance of extraction e was set at 5%. Supposing that the sampled signal is $s_i(t) = [\theta_i(t) \quad \theta_i(t + T_d)]$

for i=1, 2, an approximated UPO with error tolerance e is extracted if

$$||s_i(t) - s_i(t + kT)|| < e_i, i = 1, 2,$$
 (3.24)

where T is the excitation period and k is periodicity of the recurrence. For the given experimental settings, $f_s=500$ Hz, $f_e=5$ Hz, $T=f_s/f_e=100$. Then, for example, for a given k=4, if inequality (3.24) is satisfied, a period 4 orbit is then said to be extracted. One data set of 670,000 points was used in the analysis. For a 5% tolerance, 6 distinct orbits were extracted.

Figures 3.4–3.9 show all of the distinct extracted UPOs. In all cases, the small arm whirled. In Figures 3.5 and 3.7, the central arm whirled, whereas in other figures, the central arm oscillated without whirling. Compared to [24, 25], there were much fewer extracted UPOs in this double pendulum system than those in the single d. o. f. systems, which even had tolerance error much smaller than 5%. This is because recurrences are less frequent in higher dimensional spaces for small periodicity k. Suppose the number of boxes of size r needed to cover an attractor of dimension α is $N_1 \sim A_1 r^{\alpha}$, where A_1 some constant determined by the chaotic attractor. Roughly assuming even distance of data over an chaotic attractor, the probability of recurrently hitting a given box p_1 is $p_1 \sim 1/N_1 \sim 1/A_1 r^{-\alpha}$. Comparing this with another chaotic attractor of dimension β , we have

$$\frac{p_1}{p_2} \sim \frac{A_2}{A_1} r^{\beta - \alpha},$$

which implies that the higher the dimension of a chaotic attractor, the smaller the probability of finding a UPO with tolerance of error r.

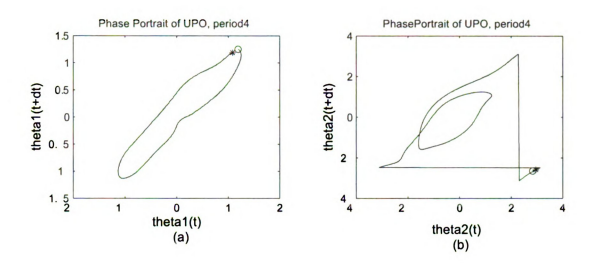


Figure 3.4. A period 4 UPO; theta1 and theta2 in the plot represent θ_1 and θ_2 ; dt=24; same for the following figures.

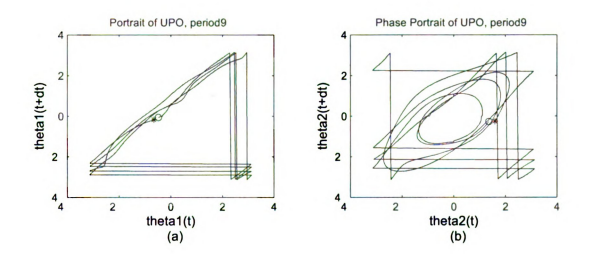


Figure 3.5. A period 9 UPO.

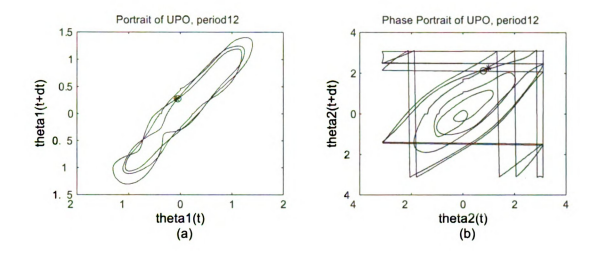


Figure 3.6. A period 12 UPO.

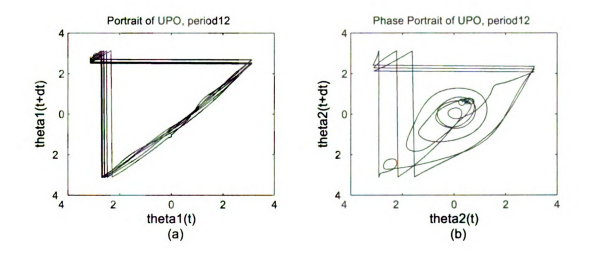


Figure 3.7. A period 12 UPO.

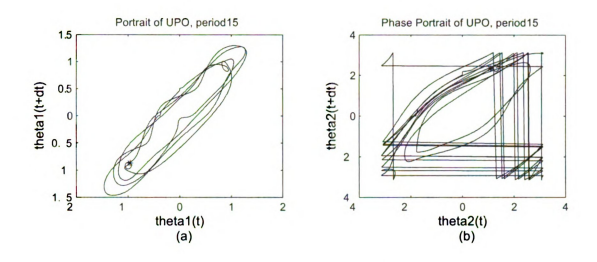


Figure 3.8. A period 15 UPO.

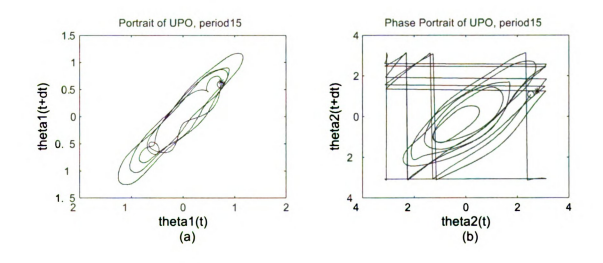


Figure 3.9. A period 15 UPO.

3.4.2 Identified parameters

Table 3.3 lists all of the identified parameters by Fourier series expansion of UPOs with these enhancements: a low-pass filtering, FFT convolution of nonlinear terms involving angular velocity and acceleration, the harmonic balance method and the optimization. The reasons for the modifications will be explained in the following sections.

Table 3.3. Identified parameters by applying low-pass filter, FFT convolution, Fourier series expansion of UPO, harmonic balance method with sub-harmonics whose frequencies are \leq excitation frequency f_e =5 Hz, and sub-harmonics optimization.

_	Identified values	True values	Error×100%
B_{11}	0.1167	0.1131	3.2%
B_{12}	0.0781	0.0711	9.8%
B_{13}	0.0809	_	_
B_{14}	0.0264	_	_
$B_{15} = \sqrt{B_{13}^2 + B_{14}^2}$	0.0849	0.0820	3.6%
B_{21}	1.6149	1.6816	4.0%
B_{22}	0.2562	0.2630	3.6%
B_{23}	0.2777	_	_
B_{24}	0.0715	-	-
$B_{25} = \sqrt{B_{23}^2 + B_{24}^2}$	0.2868	0.2913	1.6%
C ₁₁ *	0.0001	1.02×10^{-3}	-
C ₁₂ *	0.0007	0.00366	_
C_2 *	0.0106	0.0485	_
$J_{o1} (\text{kg·m}^2)^*$	5.8113×10^{-4}	5.99×10^{-4}	2.0%
$J_{o2}~(\mathrm{kg}\cdot\mathrm{m}^2)^*$	4.1995×10^{-5}	4.033×10^{-5}	3.9%
a (cm)	1.18	1.15	2.6%
$m_1e_1 \; (\mathrm{kg\cdot m})$	1.73×10^{-3}	1.60×10^{-3}	8.5%

The sub-harmonic terms whose frequencies were smaller than (or equal to) the excitation frequency were selectively included by an optimization method discussed later in the identification procedure, because the noise is actually reduced in this

frequency interval. The optimization process utilizes linear regression techniques and will be introduced later. The friction coefficients have relatively much larger error comparing to the errors of other identified values. Part of the reason for this inaccuracy is due to the fact that both of the Coulomb friction and viscous damping factors are much smaller than other factors in the same matrix equations. So an error deemed small for a stiffness/mass parameter may cause large errors of the damping parameters. As such, the damping coefficients will be estimated later by other means. However, despite the friction factors inaccuracy, most of other parameters match with the actual values within an error range of 10%, which is generally satisfying for experimental data.

Meanwhile, as we have mentioned before, some of the 'true' values (marked with '*') listed in Table 3.3 were obtained by an indirect dynamical method, e. g. small angle free vibration, and thus those 'true' physical parameters and related non-dimensional parameters may also have some error. Thus, more verification methods were examined (see Section 3.4.6).

3.4.3 Friction issue

Our first result has shown that friction coefficients may not be precisely identified due to their small values. Previous researches [24, 25] also indicate that friction parameters were more difficult to identify accurately than other parameters in experiments for a single degree of freedom system. The inaccuracy can result from mainly several reasons:

- 1. experimental noise in the sampled data;
- inadequate sensor sensitivity (the resulting error can also be treated as a noise component);

- inaccurate model of friction, e. g. viscous friction, dry friction, or their combination;
- 4. recurrence errors of the extracted UPOs;
- 5. strong nonlinearity of the investigated system.

Meanwhile, since the damping factors are much smaller than others, and the method of least mean squares is used for solving, an error deemed small for other parameters can cause relatively large errors for the damping terms. Inadequate sensor sensitivity can actually be considered as one of the noise sources during data acquisition process. The noise decreases the accuracy of the extracted UPOs. As a result of the above reasons, the identified friction coefficients are erroneous, whereas other estimated parameters show only small discrepancies from the real values. On the other hand, if the friction coefficients can be determined prior to identification, the identification could likely be improved. Here, one would like to know the roles of friction parameters in the identification process, and whether the friction errors have influence on other identified parameters in the two-degree-of-freedom double pendulum system, which is lightly damped.

We can assume that friction parameters are already known, and we want to identify the other parameters in our harmonic balance method. In this work, we determined the friction in each pendulum bearing by a small amplitude free vibration method. The free vibration test indicated that in the central arm, solely Coulomb friction was involved, and in the second arm, solely viscous friction was involved. The non-dimensional form of the friction parameters are listed in Table 3.1. As such, the friction parameters were estimated by using free vibration decrements. Hence, we applied the identification algorithm with known friction coefficients.

The result in Table 3.4 shows that the friction parameters, due to their much smaller values compared to other parameters (less than 1/5 of other parameters),

Table 3.4. Identified non-dimensional parameters by optimized identification process and noise reduction provided that the friction coefficients are known.

_	Identified values	True values	Error×100%
B_{11}	0.1178	0.1131	4.2%
B_{12}	0.0774	0.0711	8.8%
B_{13}	0.0829	-	_
B_{14}	0.0185		
$B_{15} = \sqrt{B_{13}^2 + B_{14}^2}$	0.0852	0.0820	3.9%
B_{21}	1.6040	1.6816	4.6%
B_{22}	0.2646	0.2630	0.6%
B_{23}	0.2840	_	-
B_{24}	0.0483	_	_
$B_{25} = \sqrt{B_{23}^2 + B_{24}^2}$	0.2880	0.2913	1.2%

have little influence on the overall result. This was also shown in [25]. It implies that the small errors in other parameters can cause a large percent error in the friction terms. Hence, the first result in Table 3.3 is believed to be reliable for the coefficients of conservative and parametric excitation terms.

For further verification, a simulation of the double pendulum system based on equation (3.2) and the identified parameters was examined. However, the simulated double pendulum system is extremely sensitive to parameter settings, e. g. friction parameter values. The simulation was done in Matlab by digital integration. The simulation result was obtained (shown in Figure 3.10) under $C_{11} = 1.02 \times 10^{-3}$, $C_{11} = 0.00366$ and $C_2 = 0.0485$ and other parameters set as the identified values in Table 3.3.

3.4.4 High frequency noise in unstable periodic orbits

In the previous application of the chaotic system identification process ([24, 25], the single pendulum simulation) in which single d. o. f. systems were examined, the

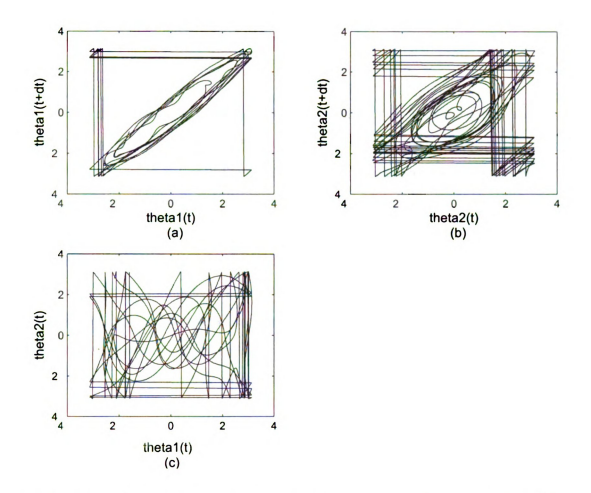


Figure 3.10. Phase portrait of the simulated system with $C_{11}=1.02\times 10^{-3},$ $C_{11}{=}0.0366$ and $C_2=0.0485;$ $dt{=}24.$

identification algorithm was noise resistant. However, a similar hypothesis could not be applied to the present two d. o. f. system. The reason is simply due to the strong non-linearity of the double pendulum, and it can be explained by the difference in the governing differential equations of the investigated single and double pendulums.

The governing equation of the horizontally excited single pendulum in Chapter 2 is

$$\ddot{\theta} + c/r\dot{\theta} + 1/r^2 \sin \theta - f \sin t \cos \theta = 0. \tag{3.25}$$

Although the parametric excitation term is nonlinear, the $\dot{\theta}$ and $\ddot{\theta}$ terms are, on the other hand, linear. The $\sin\theta$ term in (3.25) can also be regarded as linear in terms of harmonic functions. Suppose the contaminated signal is composed of the real signal and noise n(t): $\theta(t) = \theta_t(t) + n(t)$. The angular velocity and acceleration of periodic orbits can be obtained by equations similar to (3.7)–(3.10). Hence, by equations (2.8) and (2.9), the noise in the obtained velocity and acceleration jth subharmonic is actually amplified by $j\omega/k$ and $j^2\omega^2/k^2$, though n(t) is rather small in the displacement signal. The overall signals of speed and acceleration are then considered to be contaminated mainly by high frequency noise. Apparently, to the system (3.25), where speed and acceleration terms are all linear, since in the identification matrix, only the first K terms of harmonic order are used, the high frequency noise whose frequency larger than K+1th harmonic term will be automatically filtered out, which explains why the identification process is noise resistant for systems like (3.25).

However, in the double pendulum system (3.4), the identification process appears to be less noise resistant than the previous examples since velocities and accelerations do not appear linearly in differential equations. Specifically, it is the $(\phi_i')^2 \sin(\phi_2 - \phi_1)$ and $\phi_i'' \cos(\phi_2 - \phi_1)$ terms that contribute most to the noise inaccuracy of the result. Other high order terms also have similar problems of noise

amplification. It can be explained, for example, by the following FFT equation

$$\mathcal{F}[\dot{\phi}_i^2 \sin(\phi_2 - \phi_1)] = \mathcal{F}(\dot{\phi}_i)^2 \otimes \mathcal{F}[\sin(\phi_2 - \phi_1)], \tag{3.26}$$

where $\mathcal{F}(x)$ represents the Fourier transform of x, and operator \otimes represents convolution. The convolution operation can be expressed by

$$F(\omega) \otimes G(\omega) = \int_{-\infty}^{+\infty} F(\sigma)G(\sigma - \omega)d\sigma, \qquad (3.27)$$

where $F(\sigma)$ and $G(\sigma)$ are two integrable functions. By convolution, the high frequency noise in each component is, therefore, mixed into the lower-frequency components of the nonlinear terms. Furthermore, it actually amplifies the noisy influence of the angular displacement, e. g. high frequency noise, since in the algorithm, the frequency components of $\dot{\theta}_i$ and $\ddot{\theta}_i$ are obtained by equations (3.7–3.10). Hence, the truncation of the first K harmonic terms could not reduce the disturbance of the noise.

One way to avoid noise contamination is to filter out the high frequency noise of the displacement signals after UPO extraction and before convolution. By doing so, the noise component can be effectively controlled. The algorithm was incorporated in the identification process, and it turned out to be effective. For $y = (\phi_i')^2 \sin(\phi_2 - \phi_1)$, Table 3.5 compares the difference of the first four orders of Fourier series coefficients of y with low-pass filtering before convolution and without filtering. The discrepancy between the two methods is quite obvious and intolerable. It shows the necessity of applying an adequate low-pass filter. On the other hand, we may also refer to some optimization method such that only sub-harmonics with less noise contamination can be selected into the identification process. The cut-off frequency was set to be $1/5f_8$ Hz. Figure 3.11 shows the velocity and acceleration frequency spectra of θ_1 . It can be seen that the acceleration's high frequency noise is quite intolerable, and even

with the low pass filter of $1/5f_s$ cut-off frequency, there is still considerable noise remaining.

Table 3.5. Comparison of $\mathcal{F}(y)$ with and without filter added.

i	Coefficients	of $\cos(ix)$	Coefficients of $\sin(ix)$		
	without filter	with filter	without filter	with filter	
1	-3.2486	-0.3087	0.0328	0.0000	
2	-34.0713	-27.1330	17.7370	17.7403	
3	-15.6946	-8.6732	-23.6908	-23.2652	
4	-31.2079	-24.1696	-10.2571	-10.6034	

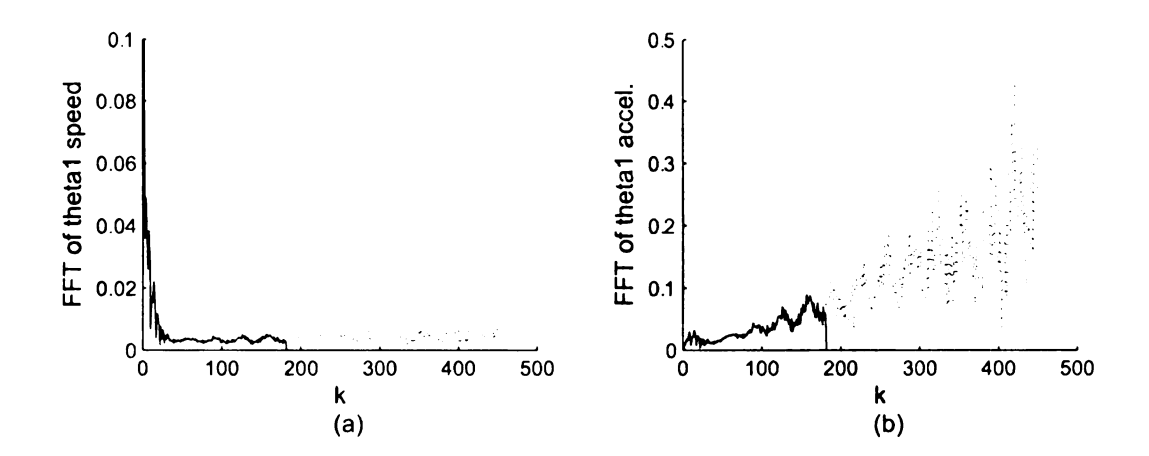


Figure 3.11. FFT amplitude of the θ_1 and θ_1 with and without low pass filter applied; the continuous line is FFT of signals with filter of $1/5f_s$ cut-off frequency; the dotted line is FFT of signals without filter; k is the order of sub-harmonics.

Displayed in Figure 3.12 are also signals with and without the low pass filter for the period-9 UPO. The low pass filtered signals are more smooth and assumed to be closer to real signals. Meanwhile, an identification process without any filtering was

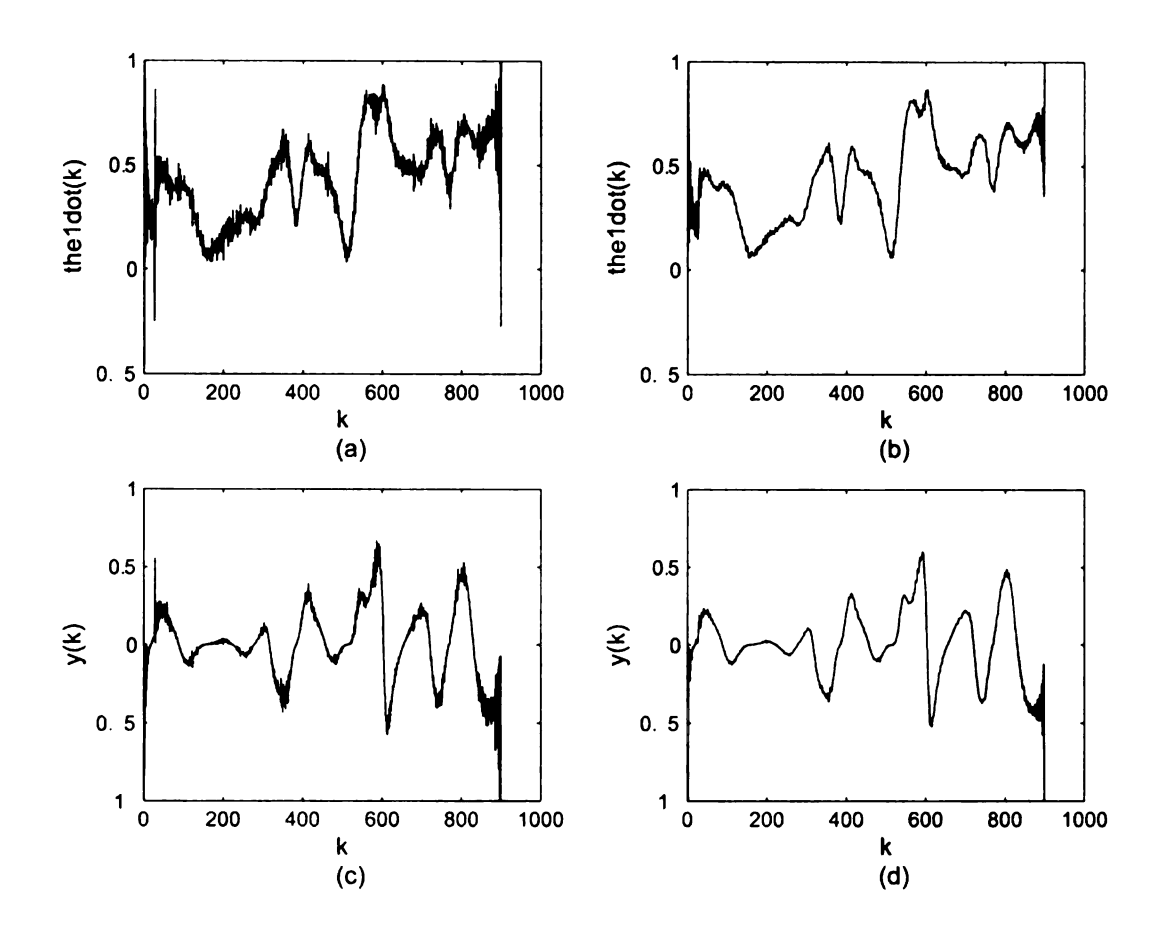


Figure 3.12. Signals without and with low pass filter applied; (a) and (b) are $\dot{\theta_1}$ without and with filter; (c) and (d) are y without and with filter applied to each convolution components; k is the kth sampled point of the orbit.

examined by utilizing the same periodic orbits displayed in Figures 3.4–3.9. Listed in Table 3.6 are the identified parameters. Coefficient B_{21} displays a larger error because of the strong non-linearity of the related term and the relatively larger noise contamination level (due to θ_1 's small oscillation amplitude and the sensitivity of optical encoders).

Table 3.6. Optimized identification with no digital filter applied.

Parameters	Identified values	True values	Error×100%
B_{11}	0.1125	0.1131	0.5%
B_{12}	0.0790	0.0711	11.1%
B_{15}	0.0825	0.0820	0.6%
B_{21}	1.1611	1.6816	31.0%
B_{22}	0.2553	0.2630	3.0%
B_{25}	0.2564	0.2913	12.0%
C_{11}	0.0003	1.02×10^{-3}	_
C_{12}	-0.0002	0.00366	-
C_{2}	0.0164	0.0485	

3.4.5 Digital differentiation and error reduction

Recurrence tolerance

Due to the limited length of the experimental data, not many periodic orbits were extracted by setting the extraction error tolerance small, e. g. less than 5% in the present experiment. Thus, one would naturally tend to increase the error tolerance such that more periodic orbits can be extracted. However, with the increased error tolerance and hence more, but less accurate, periodic orbits, the identification results turned out to get worse for the double pendulum system. The observation is consistent with [55]. Table 3.7 lists the identified parameters (Fourier series method) with 8%

error tolerance of extraction (in this case, 58 different orbits extracted), and showed large errors. For the present system, the coefficients B_{11} and B_{21} are parameters of strong nonlinear terms, and therefore, identification of these two parameters are usually less stable and more prone to error due to the fact that the strong nonlinear terms can magnify high frequency noise and the recurrence error is a major source of high frequency noise.

Table 3.7. Comparison of calculated values by Fourier Series (FS) method and Digital Differentiation (DD) method when error tolerance is set as 8% with filtering and optimization process applied.

Parameters	FS ID	FS Error×100%	DD ID	DD Error×100%
B_{11}	0.0126	88.5%	0.1224	8.2%
B_{12}	0.0730	2.7%	0.0760	6.9%
B_{15}	0.0908	10.7%	0.0908	10.7%
B_{21}	1.4703	12.6%	1.6103	4.3%
B_{22}	0.2607	0.9%	0.2559	3.7%
B_{25}	0.2851	2.1%	0.2772	4.8%
C_{11}	0.0014	_	-0.0003	-
C_{12}	0.0005	_	0.0016	_
C_2	0.0053	_	0.0093	-

The large recurrence error resulted from the error tolerance of the UPO extraction. Figure 3.13 (a) and (b) display the calculated angular velocity and acceleration curves of a period-9 (Figure 3.5) orbit by means of the Fourier series expansion method. An impulse caused by the recurrence error occurs in the periodic velocity and acceleration curves, which is not true for the real periodic orbits. If we look at the velocity curve, it can be expressed as

$$\dot{\hat{\theta}}(t) = \dot{\theta}(t) + \alpha \delta(t - t_c) + \eta(t), \tag{3.28}$$

where $\dot{\hat{ heta}}(t)$ is the calculated velocity, $\dot{ heta}(t)$ is the real velocity, $lpha\delta(t-t_c)$ is the impulse

with amplitude α proportional to the recurrence error, t_c is time delay, and $\eta(t)$ is noise other than recurrence, which is considered to be small due to low-pass filtering. Thus, after digital filtering, and applying the Fourier transform, we obtain

$$\mathcal{F}(\dot{\theta}) \cong \mathcal{F}(\dot{\hat{\theta}}) + \alpha exp(-jt_c\omega),$$

where α is the expression of the impulse function in frequency domain and is a white noise. Furthermore, this noise contaminates all sub-harmonics of the velocity curve, which could not be eliminated by the low pass digital filter and could hence generate large error in the identification result.

Digital differentiation

Through the previous analysis, for a large recurrence error, one would naturally consider that a similar scenario would happen to other dynamic systems with strong non-linearity. In this case, digital differentiation could be applied given adequate sampling points per cycle, e. g. a high sampling rate f_s . In this experiment, there were 100 points per excitation period. Hence, a five-point differentiation algorithm was applied to obtain the derivatives and double derivatives of angular displacements:

$$\dot{f}(x) = \frac{8[f(x+h) - f(x-h)] - f(x+2h) + f(x-2h)}{12h} + o(h^4)$$
 (3.29)

and

$$\ddot{f}(x) = \frac{16[f(x+h) + f(x-h) - 2f(x)] - f(x+2h) - f(x-2h) + 2f(x)}{12h^2} + o(h^4).$$
(3.30)

The errors of these algorithms can be reduced with a smaller time interval h. The five-point algorithm can also reduce the influence of high frequency noise since it involves the neighboring four points. The obtained curves are in Figure 3.13 (c) and

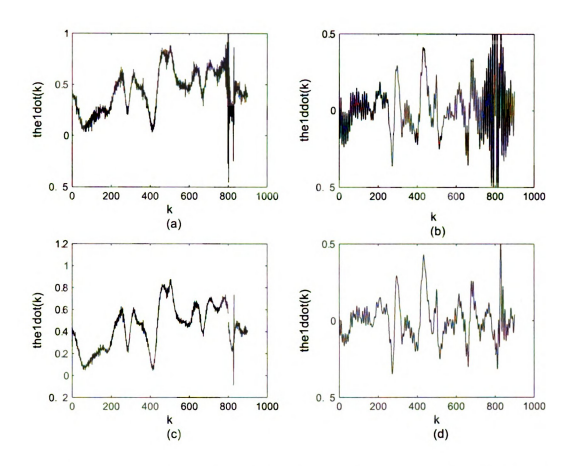


Figure 3.13. Obtained θ_1 and θ_1 orbits by Fourier series method (a) and (b) by digital differentiation method (c) and (d); the recurrence impulses occur at k=800 in (a) and (b).

(d) for the extracted period-9 orbit. It is apparent that the recurrence impulses are eliminated for both of the cases, and much less high frequency noise is displayed in the velocity and acceleration curves. The corresponding identified parameters are listed in Table 3.7, which is more precise compared to the result of Fourier series method.

However, the algorithm for digital differentiation itself introduces calculation errors in equation (3.29) and (3.30). It could not predict precisely the small value parameters, e. g. friction parameters, according to an identification test based on the simulated noise-free double pendulum system. On the other hand, the Fourier series method can identify all of the parameters with satisfying accuracy if error tolerance of extraction is small enough (2% in this case). It shows that the digital differentiation method is more stable, but not more accurate compared to the Fourier series expansion algorithm.

Choice of sub-harmonics or harmonics

The identification result varied when a different choice of sub-harmonics was applied. The problem was not so troublesome in previous applications of the harmonic balance method [24, 25] where nonlinearity was simple and not as strong as the double pendulum case. However, in the present experiment, different sub-harmonic sets led to quite different estimated parameters. It is then necessary for us to seek some general rules for judging the result.

In equation (3.18) and (3.20), the first M sub-harmonics of each UPO (sub-harmonics are functions of $\sin{(ix/k)}$ or $\cos{(ix/k)}$ where i and k represent the ith term in Fourier series of a period k orbit. Here, we denote M_k as the truncated sub-harmonics for a period-k orbit. The choice of M_k remains an issue. For a periodic orbit whose period is a multiple k of the excitation period, if $M_k \leq k$, i. e. including only sub-harmonic frequencies less than or equal to the driving frequency, the result was tested to be the best for the examined pendulum system. One reason is that these sub-harmonics consisted of a large part of the energy of the displacement signal, and hence, contained a relatively small portion of the noise contamination (see Figure 3.11). Also, the noise components in the velocity and acceleration signals were reduced according to equations (3.7–3.10).

The remaining question is whether it is possible to measure the identification error and use it as an indicator of how 'true' the identification is. To quantify the identification error, we refer to linear regression techniques, borrow some concepts in

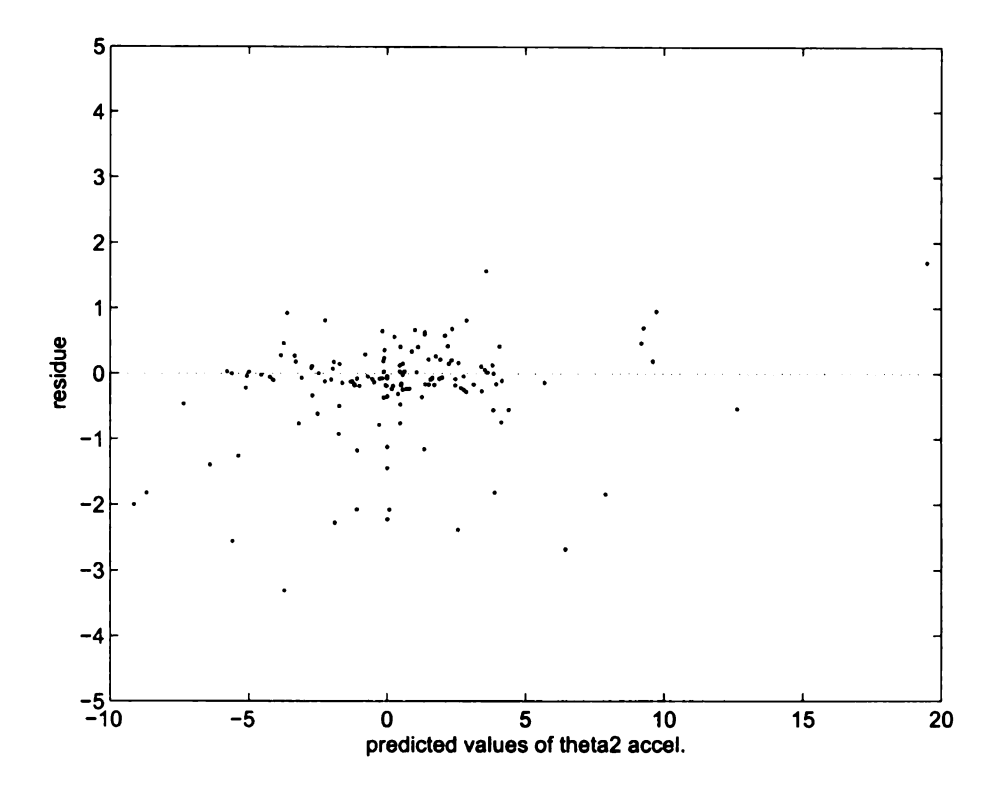


Figure 3.14. Identification residual \vec{e}_2 with each dot representing a subharmonic; the horizontal position of each dot is the predicted value of \vec{q}_2 , the vertical position of each point is the identification residual; identification was done with low-pass filtering, the Fourier series expansion and the sub-harmonic set whose frequency \leq the excitation frequency.

statistics, and transform (3.18)-(3.22) into

$$\vec{e_i} = A_i \vec{x}_i - \vec{q}_i, i = 1, 2, \tag{3.31}$$

where $\vec{e_i}$ is the residual vector. Then, we can define the identification error ε_i as

$$\varepsilon_i = \frac{\|\vec{e_i}\|_{\infty}}{\|\hat{q}_i\|_{\infty}},$$

where $\vec{q}_i = A_i \vec{x}_i$ is the predicted vector of \vec{q}_i . With the identification error defined, the rule of thumb for judging a good identification is $\varepsilon_i < \epsilon_c$, where ϵ_c is a positive

critical value. $\epsilon_c = 10\%$ was used in the experiment. Figure 3.14 displays the residuals \vec{e}_2 and the corresponding identification error ϵ_2 is 18.4% when all 140 sub-harmonics were included in the identification, whose frequencies were less than or equal to the driving frequency. Apparently, the results for B_{2j} for j=1, 2, 5, are not satisfying, and the comparison in Table 3.8 and Table 3.3 also corroborates the rule of thumb since B_{21} has a 11.2% error. On the other hand, the B_{1j} parameters have $\epsilon_1 = 8.8\%$, and are quite consistent with the result after optimization in Table 3.3.

Table 3.8. Identified parameters with the Fourier series method and low-pass filtering, but without optimization to sub-harmonics set.

Parameters	Identified	True values	Error×100%
B_{11}	0.1178	0.1131	4.2%
B_{12}	0.0782	0.0711	10.0%
B_{15}	0.0861	0.0820	5.0%
B_{21}	1.4935	1.6816	11.2%
B_{22}	0.2562	0.2630	0.5%
B_{25}	0.2828	0.2913	3.4%
C_{11}	0.0001	1.02×10^{-3}	_
C_{12}	0.0007	0.00366	_
C_2	0.0147	0.0485	_

Our problem is now how to optimize the identification process so as to improve the accuracy, i. e. minimize the identification error. From the statistics point of view, we have a good linear regression curve if the resulting residuals are distributed evenly and randomly around the predicted values. For this purpose, an optimization algorithm was developed to exclude the sub-harmonics terms which result in large residuals, and retain the terms which consist of most of the sub-harmonics and should have small residuals. The sub-harmonics having large residuals are very likely contaminated heavily by noise. The optimization process involves the following steps:

- 1. Given the set of sub-harmonics, do the identification process and find the maximum absolute residual value e_{max} .
- 2. For a level of significance β , which is a small value, remove from the sub-harmonic set those sub-harmonics whose corresponding residual $e > (1 \beta)e_{max}$.
- 3. Repeat the first step by using the remaining sub-harmonics, and compute the identification error ε_i .
- 4. If ε_i < 10%, then stop the optimization process and assume that the desired result has been obtained; if not, go back to step 1 with the remaining subharmonics set and repeat the optimization process.

For the investigated system, after three optimization processes with $\beta=5\%$ (by excluding 10 erroneous sub-harmonics), the identification errors were reduced to $\varepsilon_1=8.1\%$ and $\varepsilon_2=9.4\%$. The corresponding results are listed in Table 3.3. Displayed in Figure 3.15 is the residual distribution of $\vec{e_2}$ after optimization. Compared to the identified values without optimization in Table 3.8 and Figure 3.14, the optimized ones have smaller errors, smaller residuals, and are more accurate. However, the proposed optimization can not work well for all cases. After a few cycles of optimization, if the identification errors are still undesirable, we should either use more precise UPOs, or re-select the set of sub-harmonics before optimization such that the noise contamination can be minimized. In order to obtain more precise UPOs, besides the UPO extraction with smaller tolerance of error, we can also refine the extracted UPOs [55]. But the refinement process may generate erroneous results for quasi-periodic orbits and may not be adequate for limited data sets. For better selection of sub-harmonics, one may choose only those sub-harmonics that have the largest amplitude in the UPO acceleration FFT spectrum (also avoid those noise contaminated high

frequency harmonics, since it could only be noise). Furthermore, the selection could be simplified by choosing the harmonics instead of sub-harmonics if most of the orbits are composed mainly of the harmonics of the driving frequency f_e .

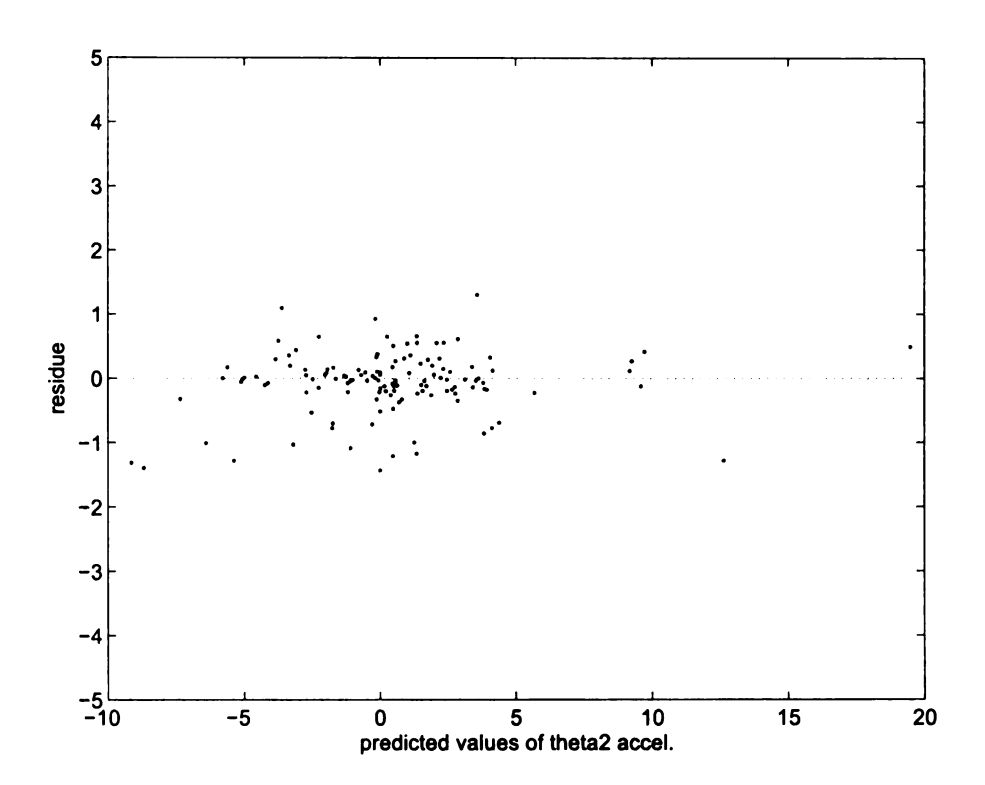


Figure 3.15. Identification residual \vec{e}_2 after optimization with each dot representing a subharmonic.

3.4.6 Validation methods

Generally, most of the parameters of a nonlinear system are unknown to us. The direct comparison discussed in previous sections is not available for most applications. Besides, lots of the 'true' parameters in Table 3.1 were also estimated. Hence, we do not know the exact errors for the identified values. Two other methods were applied

here to verify the identified parameters and the effectiveness of the identification algorithm. The first one is to verify our method by identifying the simulated double pendulum system such that comparisons can be made based on identification results and the phase portraits of the experimental and simulated systems. The second method involves the linearized system properties, e. g. natural frequencies.

Identification of the simulated double pendulum system

To verify the effectiveness of the identification process, a simulated system was also examined with parameters set as the identified values listed in Table 3.3 except for the friction terms (see Section 3.4.3). The error tolerance of extracted unstable periodic orbits is 5%. The phase portrait has been shown in Figure 3.10. Some similarity observed in the simulated system compared to the experimental phase portrait (displayed in Figure 3.3), e. g. chaotic behavior. Many detailed chaotic characteristics were not available due to the inadequate experiment data. However, it turned out that more and different UPOs could be extracted from the equally large, sampled data of the simulated system, than from the experimental data set. The difference can be explained by the sensitivity of the chaotic systems to parameter settings and initial conditions. Meanwhile, for the simulated system, the comparison in Table 3.9 between the identified values and the parameter settings shows that all the parameters including the friction coefficients are identified correctly, which confirms the effectiveness of this algorithm. The friction coefficients, probably due to their much smaller values and the weakness of the least mean square method, are still hard to calculate very accurately, and thus, have larger error percentages. With little noise in the simulated data, the error can only come from the recurrence error of the extracted periodic orbits. Also, it confirms the difficulty of identifying small friction parameters in the experiment, since more noise contamination occurred in the experimental data.

Table 3.9. Comparison of the identified values and the true parametric settings of the simulated system with low-pass filtering and optimization applied.

	Identified	Parameters setting	Error×100%
J_{o1} (kg.m ²	5.767×10^{-4}	5.757×10^{-4}	0.2%
$J_{o2}~(\mathrm{kg.m^2})$	4.310×10^{-5}	4.228×10^{-5}	1.0%
B_{11}	0.1166	0.1167	0.1%
B_{12}	0.0787	0.0781	0.8%
B_{15}	0.0848	0.0849	0.1%
C_{11}	0.0005	0.0	_
C_{12}	0.0038	0.00366	3.8%
B_{21}	1.5943	1.6149	1.3%
B_{22}	0.2568	0.2562	0.2%
B_{25}	0.2866	0.2868	0.1%
C_2	0.0429	0.0485	11.5%

Linear properties

The linearized pendulum can also be applied to validate the identification results, e. g. by comparing the natural frequencies of the linearized system. Suppose the pendulum has only small-angle oscillations without an excitation force. By discarding the higher order terms and neglecting dry friction, equation (3.4) can be simplified as

$$\begin{cases} \phi_1'' + B_{11}\phi_2'' + B_{12}\phi_1 - C_{12}(\phi_2' - \phi_1') = 0\\ \phi_2'' + B_{21}\phi_1'' + B_{22}\phi_1 - C_2(\phi_2' - \phi_1') = 0 \end{cases}$$
(3.32)

Since our goal is to examine the natural frequencies, by neglecting the damping terms, equation (3.32) can be further simplified to the form of

$$\begin{cases}
\phi_1'' = -B_{12}/(1 - B_{11}B_{21})\phi_1 + B_{22}B_{11}/(1 - B_{11}B_{21})\phi_2 \\
\phi_2'' = B_{12}B_{21}/(1 - B_{11}B_{21})\phi_1 + -B_{22}/(1 - B_{11}B_{21})\phi_2
\end{cases}, (3.33)$$

and the characteristic matrix of equation (3.33) is

$$A = \begin{pmatrix} 0 & 1 & 0 & 0 \\ -B_{12}/(1 - B_{11}B_{21}) & 0 & B_{22}B_{11}/(1 - B_{11}B_{21}) & 0 \\ 0 & 0 & 0 & 1 \\ B_{12}B_{21}/(1 - B_{11}B_{21}) & 0 & -B_{22}/(1 - B_{11}B_{21}) & 0 \end{pmatrix}.$$
(3.34)

The eigenvalues of matrix A are the natural frequencies of the linearized system in non-dimensional form. The natural frequencies of the identified system were found to be 1.336Hz and 2.904Hz. Through FFT analysis, the natural frequencies obtained by the experiment of free vibration are 1.25Hz and 3.00Hz. Comparison in Table 3.10 shows that the natural frequencies match the FFT result from experiment and the 'true' values calculated by the settings of the double pendulum. It suggests that the identified parameters, excluding the friction terms, are reliable for the purpose of system linearization.

Table 3.10. Natural frequencies.

_	Identified	Experimental	Error × 100%	'true'
$f_{n1}(hz)$	1.336	1.25	6.9%	1.292
$f_{n2}(hz)$	2.904	3.00	3.2%	2.940

3.5 The energy balance method for identification of the damping coefficients

In chapters 2 and 3, the identification results were satisfying except for the small friction coefficients. The inaccuracy of friction coefficients became worse for noisy

experiment data. The reason is due to solution method, i. e. least mean square method, which tends to give more inaccurate solution for smaller parameters, e. g. the small friction coefficients in this study. Also, it showed that the errors in friction terms, since they are much smaller than other parameters, have little influence on other estimated values. Consequently, we apply an energy balance method to estimate the damping coefficients.

Suppose we have a single d. o. f. system with a governing differential equation

$$\ddot{x} = -kx - c\dot{x} - f(x) - f_p(x)p(t) + g(t), \tag{3.35}$$

where k, c, f(x) and $f_p(x)$ are unknown, and c is a small damping coefficient. First, we can apply harmonic balance method to identify the parameters. Multiplying equation (3.35) by $\cos \frac{mt}{T}$ and integrating it over one cycle of a periodic orbit, it can then be expressed as

$$\int_{t}^{t+T} (\ddot{x} + kx) \cos \frac{mt}{T} dt =$$

$$- \int_{t}^{t+T} \{c\dot{x} + f(x)\} \cos \frac{mt}{T} dt - \int_{t}^{t+T} \{f_{p}(x)p(t) + g(t)\} \cos \frac{mt}{T} dt.$$
(3.36)

Similarly, we can also obtain equations for $\sin \frac{mt}{T}$ functions. The unknown functions f(x) and $f_p(x)$ can be approximated by function series with unknown coefficients (see Chapter 1), and the integrals become the corresponding sub-harmonics in the FFT spectrum. Then, the equation (3.36) can be converted to a matrix equation similar to equation (2.15). One of the advantages of the harmonic balance method is that it can identify all the parameters simultaneously. However, smaller parameters are also vulnerable to noise influence from other terms.

To eliminate the noise from other terms, with the parameters partially known from the harmonic balance identification, we can refer to energy balance method [56] for a second-step identification. For some periodic orbit D of (3.35), we want to find

the energy generated or dissipated by each term in the equation over one cycle, and we obtain

$$\oint_D \ddot{x}dx = -k \oint_d xdx - c \oint_D \dot{x}dx - \oint_D f(x)dx - \oint_D f_p(x)p(t)dx + \oint_D g(t)dx. \quad (3.37)$$

The \ddot{x} , kx and f(x) terms represents the conservative terms. Hence, theoretically, the work done by the conservative forces within one cycle is zero. Equation (3.37) then becomes

$$c \oint_{D} \dot{x} dx = -\oint_{D} f_{p}(x)p(t)dx + \oint_{D} g(t)dx, \qquad (3.38)$$

where the left hand side of the equation is the energy dissipated by the damping term, the right hand side is the energy input into the system by force and parametric excitation. The integrals in (3.38) can be calculated. Thus, if we can obtain multiple periodic orbits of the system, we can then solve the damping coefficients by the least mean square method. Since we have obtained the quite accurate estimation of those unknown functions in the harmonic balance identification, the damping coefficient can then be identified more accurately by the energy balance method.

Table 3.11. Identified damping coefficients by the energy balance method.

_	Identified	Experimental	Error × 100%
_	C_{11}	C_{12}	C_2
The identified	-0.0004	0.0045	0.0396
True values	0.000101	0.00366	0.0485
error	_	23%	18%

For the single pendulum system in Chapter 1, the identified damping coefficient is $c_r = 0.0353$, and the corresponding error is 2.1% which is much smaller than result error of the harmonic balance identification. For multi-d. o. f. systems, we can

apply a similar method to each differential equation, and obtain the more accurate estimation of the damping terms. Table 3.11 listed the identified damping terms by energy balance method. Apparently, the second-step identification obtained much better results. But the error is still much larger than 10%. The reasons could be noise contamination in the signals, or inaccurate estimation of the 'true' values which were also estimated by the small amplitude free vibration.

3.6 Concluding remarks

A double pendulum experiment was examined for chaotic system identification. The investigated system was a multi-degree-of-freedom system with strong non-linearity, e. g. mixed ϕ_i , ϕ_i' and ϕ_i' non-linearity with whirling in S^1 space. However, only displacement signals were directly measured. To adapt to these new challenges, some modifications were added to the harmonic balance identification algorithm:

- 1. The identification appeared to be less noise-resistant in this case, mainly due to the strong nonlinear term of $(\phi_i')^2 \sin(\phi_2 \phi_1)$ and $\phi_i'' \cos(\phi_2 \phi_1)$. The high frequency noise contaminated the strong nonlinear terms at lower frequencies without adequate low pass filtering of each component before convolution.
- 2. A digital differentiation algorithm was developed and applied to the experimental data in order to make the identification results more robust even with large recurrence errors in the extracted orbits. It could be of use for limited data sets. However, the digital differentiation algorithm also introduced differentiation error, and thus, did not give accurate values of friction terms.
- 3. Choices of sub-harmonic terms also had influence on the identified parameters. Inappropriate selection of sub-harmonics can generate poor results. To avoid poor results, the key factor was to avoid noise contaminated sub-harmonics. For

the present system, the sub-harmonics of frequencies less than the excitation frequency were selected to avoid noise.

4. Linear regression techniques were applied to quantify the identification error ϵ_i , which reflected the error of the identified parameters by examining the residues and the predicted values. Based upon the identification error, an optimization algorithm was proposed to improve the result. An identification error less than 10% indicated an rather satisfying result. However, optimization is limited by its statistical properties, and can not work for all data to satisfy the rule of thumb.

Friction was a problem in the identification process. For slightly damped systems, since the friction factors were much smaller than other parameters, the identification could not produce accurate values of the friction terms. Noise and recurrence error were the two factors that contributed to this error. However, the harmonic balance algorithm is robust, and the validation process showed that the friction error had little effect on other identified parameters. Based upon the identified non-damping parameters, the damping coefficients were identified again in the second step of the identification—the energy balance method which exploits the energy balance and dissipation of the vibration system. The results were tested to be improved. Meanwhile, the convergence of the identification algorithm was not fully discussed in the experimental study, mainly due to the direct comparison between the identified and the measured parameters. In lien of convergence, the model was verified using residuals, comparisons to known parameters and linearized properties. Through the experiment, it can be concluded that the examined identification method can be applied to systems with chaotic response, strong non-linearity and multiple degrees of freedom. With adequate modification, the identification result could be improved, and the quality of the result can be quantified by the identification error.

CHAPTER 4

Simplification to Frequency

Domain Method

4.1 System identification by frequency method

Pure frequency based parametric identification method has long been limited to non-chaotic systems. The reason is that, generally, frequency domain methods are based upon frequency response functions, or the harmonic balance method. For linear systems, their responses to any kind of dynamical load (which can be expressed as the sum of simple loads, e. g. harmonic loads), by superposition, is equal to the sum of the responses of each simple load acting separately. Thus, for linear systems, the harmonic balance identification is equivalent to using frequency response functions (FRFs) if multiple frequencies of excitation were used. The FRF is perfect for linear system identification, since the FRF can be easily generated by an impact response. For weak nonlinearity, Richard [12] and Kerschen [11] developed the conditional reverse path (CRP) method based upon the FRFs, which seperates the response into linear and nonlinear response parts. In [18, 19, 20, 21, 22], the harmonic balance method was proposed to identify non-chaotic nonlinear systems, because it requires steady state responses, i. e. periodic orbits. Similarly, Plakhtienko [16, 17] and Ghanem [23]

developed respectively the special weight method and the wavelet analysis method. All of the three methods have a common feature: a basis of orthonormal functions. Furthermore, they all require a periodic response, though it is not an obvious requirement in the latter two methods. Discrete signal reconstruction by the orthonormal basis requires periodic orbits. It inspired Yuan and Feeny [24, 25] to extract unstable periodic orbits (UPOs) from data and then apply the harmonic balance method for identification. This method was examined by whirling and experimental systems in previous chapters. It can be regarded as a hybrid time-frequency (HTF) method. The idea comes from the knowledge that hyperbolic chaotic systems, though having no steady state periodic orbits, have chaotic responses with dense sets of unstable periodic orbits inside.

In previous research [24, 29] and previous chapters, the HTF method has been tested successfully on various chaotic systems, either by simulation or by experiment. Although the method is capable of being applied to any chaotic system, the process could be time-consuming since it requires extracting UPOs from the chaotic data. For better results, it requires more accurately extracted UPOs and more orbits. Therefore, the method requires a large amount of the collected data. Furthermore, for large d. o. f. systems, recurrences are less frequent, meaning UPOs of low periodicity are visited less often. These drawbacks make it hard or impossible for fast parametric identification, or real-time identification. Hence, one would like to investigate if it is possible to skip the process of extracting unstable periodic orbits by applying more chaotic properties, such that the harmonic balance method can be more conveniently applied to nonlinear/chaotic systems.

4.2 More chaotic properties and the improved frequency domain method

The UPOs are extracted by satisfying the recurrence error tolerance,

$$||S(k+nT) - S(k)|| < \epsilon, \tag{4.1}$$

where $S(k) = [x(k) \ x(k+T_d) \ \cdots \ x(k+mT_d)]$ is the displacement signal in an m dimensional embedding space [52], T is the excitation period, T_d is the time delay for embedding dimension, and ϵ is the tolerance of recurrence error. Hence, we say a close approximation of the UPO is found when equation (4.1) is satisfied. The extraction method is usually targeted for short term periodic orbits. For long periodic orbits (n large), the extraction can be much simpler.

As we know that the set of unstable periodic orbits is the dense skeleton of the hyperbolic chaotic attractor, it actually implies that for any chaotic orbit (of some hyperbolic chaotic attractor with UPOs inside), a UPO can be found in any neighborhood of the chaotic orbit, and the extracted UPOs can be utilized for chaos investigation [57, 53, 58, 59, 60]. Here, we will use this property and also add a claim that:

Given a bounded hyperbolic chaotic set, assuming unstable periodic orbits inside the attractor, any chaotic orbit within some time interval nT, where n is a large integer, can be 'approximated' to some extent by an unstable periodic orbit with nT periodicity with a similar frequency spectrum. The similarity increases as n gets larger.

The word 'approximate' here generally can not be examined by the rule in (4.1) for extracting UPOs, rather by the frequency spectra: the end-points may have significant error, but the most of the orbit is a close approximation to a period-n orbit.

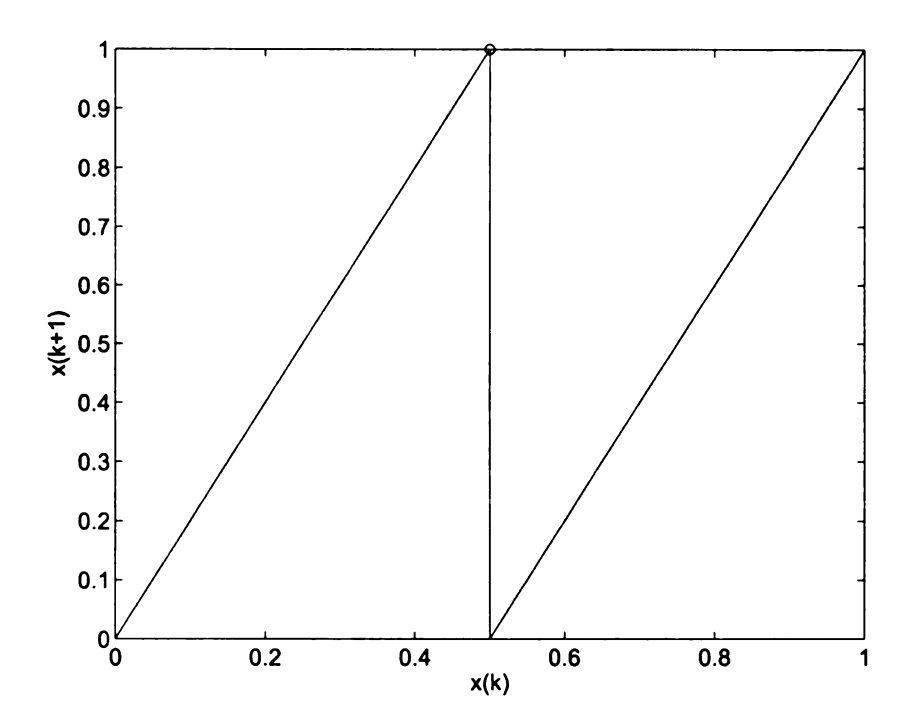


Figure 4.1. The left shift one dimensional map

The claim comes from the fact that every chaotic set can be converted to equivalent symbolic dynamics [52, 61]. With symbolic dynamics, the hidden properties of chaos emerge clearer before our eyes. For instance, we can take a look at a one dimensional map (shown in Figure 4.1) expressed by

$$x(k+1) = \begin{cases} 2x, & 0 \le x < 0.5 \\ 2x - 1, & 0.5 \le x < 1 \end{cases}$$
 (4.2)

This map is conjugate to the left shift operation of binary numbers in the interval [0,1) in symbol dynamics,

$$x(k+1) = x(k) \times [10]_b \mod 1,$$
 (4.3)

where the subscript b represents binary numbers. The uncountable set of irrational numbers in [0,1) forms the chaotic attractor. On the other hand, the countable set of rational numbers in [0,1) form the set of the unstable periodic orbits, and it is dense in [0,1). Since the set of irrational numbers is a set of Lebesgue measure 1, the probability of observing a unstable periodic orbit is zero. However, for any chaotic orbit $x(t;x_0)$ of length n starting from an irrational number x_0 , there is always some periodic orbit $y(t;y_0)$ with periodicity n starting from rational number y_0 , such that $||y_0-x_0|| < 2^{-n}$, which implies the first n binary digits of x_0 and y_0 are identical. Comparing $x(t;x_0)$ and $y(t;y_0)$, we observe that, for the first n points of these two orbits,

$$|x(k;x_0) - y(k;y_0)| < 2^{-(n-k)}, \forall k \le n.$$
 (4.4)

The error between the chaotic orbit and the periodic orbit increases as t increases. For t = n, since $y(t; y_0)$ is a period n orbit, $y(n; y_0) = y_0 \approx x_0$, whereas, $x(n; x_0)$ becomes some number other than x_0 , and thus, forms a 'recurrence' error. For the extraction of short periodic orbits, we can use the rule of (4.1) by choosing chaotic orbits with small recurrence errors. However, the extraction of UPOs is harder for high d. o. f. systems, and can only utilize a small part of the data for identification.

Indeed, it has been observed by Yuan [62] that long chaotic orbits were good for parametric identification by the harmonic balance method, though they did not satisfy the UPO extraction rule. It then raises the question whether the long chaotic orbits are usable for UPO approximation. For any long orbit x, i. e. large n number, given an error level ϵ , according to inequality (4.4), there exists a K, such that for the first K points of that chaotic orbit, the error between the chaotic orbit and some period-n orbit satisfies

$$||x(k; x_0) - y(k; y_0)|| < 2^{-(n-k)} < \epsilon, \forall k \le K < n.$$

It implies that the first K points of a sampled chaotic orbit $x(t; x_0)$ of length n are very close to the corresponding points of some unstable periodic orbit $y(t; y_0)$, and the rest of x may deviate from y. Hence, we can express x(t) by

$$x(t;x_0) = y(t;y_0) + e_1(t) + e_2(t), \tag{4.5}$$

where e_1 and e_2 are error functions, and $e_1(t) = \left\{ \begin{array}{l} x(t;x_0) - y(t;y_0), & t \leq K \\ 0, & t > K \end{array} \right.$

 $e_2(t) = \begin{cases} 0, & t \leq K \\ x(t;x_0) - y(t;y_0), & t > K \end{cases}$. Function e_1 represents the first K points of the chaotic orbit where the approximation error is small and $|e_1(t)| < \epsilon$. Function e_2 represents the tail part of the chaotic orbit where the error to the periodic orbit tends to increase beyond the tolerance of error ϵ , but is still limited $|e_2(t)| < 1$. In the frequency domain, the discrepancy between x and y is

$$\mathcal{F}\{x(t;x_0) - y(t;y_0)\} = \mathcal{F}\{e_1(t)\} + \mathcal{F}\{e_2(t)\}. \tag{4.6}$$

Obviously, if we can manage to reduce the error caused by the tail part, i. e. $(n-K) \ll n$, the majority of the chaotic orbit can be a good representation of some periodic orbit. As for the tail part, in the frequency domain, the recurrence error generated by $e_2(t)$ can also be neglected if $(n-K) \ll n$. Hence, in the frequency domain, the chaotic orbit $x(t;x_0)$ becomes a close approximation to $y(t;y_0)$. The solution to this problem is simply a large n, i. e. a long chaotic orbit. For instance, suppose the tolerance of error $\epsilon=0.01$, and n=100. There are only six tail points out of the length-100 orbit with errors greater than ϵ , and in frequency domain, the amplitude of the recurrence error e_2 is less than 0.02, which is acceptable. Therefore, every long chaotic orbit in the left-shift map is a good approximation of some unstable periodic orbit, and the approximation is better if n is larger.

This simple example based upon the shift map on the unit interval can be generalized since all the chaotic systems are equivalent to some corresponding symbol dynamics. Thus, the claim is supported.

The claim simplifies the investigated systems' identification method, and turns it into a pure frequency method. Assuming a single chaotic data $\{S(k)\}$ was sampled, the chaotic data itself is a very long approximated unstable periodic orbit in the frequency domain, and can be used directly for identification purposes. To acquire more UPOs within the limited data and improve the identification results, we can divide the orbit into pieces by some interval $\tau = nT$. For each piece, we can apply the harmonic balance method and get the same equations as those in (2.15). However, without inequality (4.1) satisfied, the recurrence error can cause jump noise in the frequency spectrum, and thus generate inaccuracy for identification process. This shortcoming can be overcome by choosing nT large enough such that the jump noise influence to the whole power spectrum is reduced to an acceptable level.

It is now clear that a pure frequency method is justified. The pure frequency method for chaos is intimately tied to our understanding of unstable periodic orbits and the hyperbolic chaotic set.

4.3 Calculation examples

We will use two examples here to examine the improved method. The first one is a simulated single pendulum with horizontal base excitation. The second example is a double pendulum experiment. In both of the systems, a linear regression based optimization method was applied to improve the identification results.

4.3.1 Base-excited single pendulum

The simulation was based upon a horizontally excited single pendulum. Its nondimensional differential equation is

$$\ddot{\theta} + 2\xi/r\dot{\theta} + 1/r^2\sin\theta - f\sin t\cos\theta = 0, \tag{4.7}$$

where $t=\omega \tau$, ω is the angular excitation velocity, and τ is the actual time; ξ is the viscous damping coefficient; $r=\omega/\omega_N$, $\omega_N=\sqrt{mge/J}$ is the natural frequency of the linearized system, m is the pendulum mass, e is the the centroid offset from the pendulum hinge, J is the moment of inertia about the hinge point. Meanwhile coefficient f=mea/J, and a is the excitation amplitude. For simplicity, we denote $c_r=2\xi/r$ as the new non-dimensional friction coefficient. The function $f\sin t\cos\theta$ is the nonlinear parametric excitation term, and $1/r^2\sin\theta$ is the autonomous nonlinear part. In the simulated system, $c_r=0.036$, f=1.52 were used. Assuming viscous damping and displacement nonlinearity, the differential equation is

$$c_r \dot{x} + f_{anl}(x) + f_{nnl}(x) \cos t + f_{pnl}(x) \sin t = -\ddot{x},$$
 (4.8)

where f_{anl} is the unknown autonomous part, f_{nnl} and f_{pnl} are the unknown parametric excitation parts. The unknown functions can be approximated by

$$f_{anl} \approx \sum_{i=1}^{N} q_i \phi_i(x), \tag{4.9}$$

$$f_{nnl} \approx \sum_{i=1}^{N} n_i \phi_i(x), \tag{4.10}$$

$$f_{pnl} \approx \sum_{i=1}^{N} p_i \phi_i(x), \tag{4.11}$$

where $\phi_i(x)$ is a linear interpolation function:

$$\phi_k(x) = \begin{cases} \frac{x - (k-1)d}{d}, & (k-1)d < x < kd \\ \frac{(k+1)d - x}{d}, & kd \le x < (k+1)d \\ 0, & otherwise \end{cases}$$

Hence, the differential equation is to be identified in the form of

$$c_{\tau}\dot{x} + kx + \sum_{i=1}^{N} q_{i}\phi_{i}(x) + \sum_{i=1}^{N} n_{i}\phi_{i}(x)\cos t + \sum_{i=1}^{N} p_{i}\phi_{i}(x)\sin t = -\ddot{x}.$$
 (4.12)

Meanwhile, since angular displacement is a S^1 signal, we used $z = \exp(i\theta)$ to solve for $\dot{\theta}$ since it is much easier than the original method (see 2.2). Two sets of data were examined: the noise-free data and the data with 10% random noise which was a noise source with uniform distribution and the amplitude equal to 10% of the amplitude of the signal. Compared to noise with normal distribution, the uniformly distributed noise has more high frequency components and easier for computer generation. The long data was cut into equal-length pieces with $\tau = 60T$. The τ value can be selected randomly as long as the periodicity is large enough for UPO approximation (see previous section for error estimation) such that the recurrence impulse is small enough in the frequency domain. Meanwhile, we should also avoid large τ such that adequate number of UPOs can be obtained for identification purposes. For the noise free data, the identified $c_r = 0.0352$, and the unknown functions were displayed in Figure 4.2. Compared to the HTF method in Chapter 2, the error is even smaller. Figure 4.3 also compares the Poincaré sections of the original system and the identified system. The chaotic property of the two systems is quite similar. For the data with 10% random noise, the identification algorithm shows strong noise-resistance. The estimated c_r is 0.0343, and the identified stiffness functions are displayed in Figure 4.4.

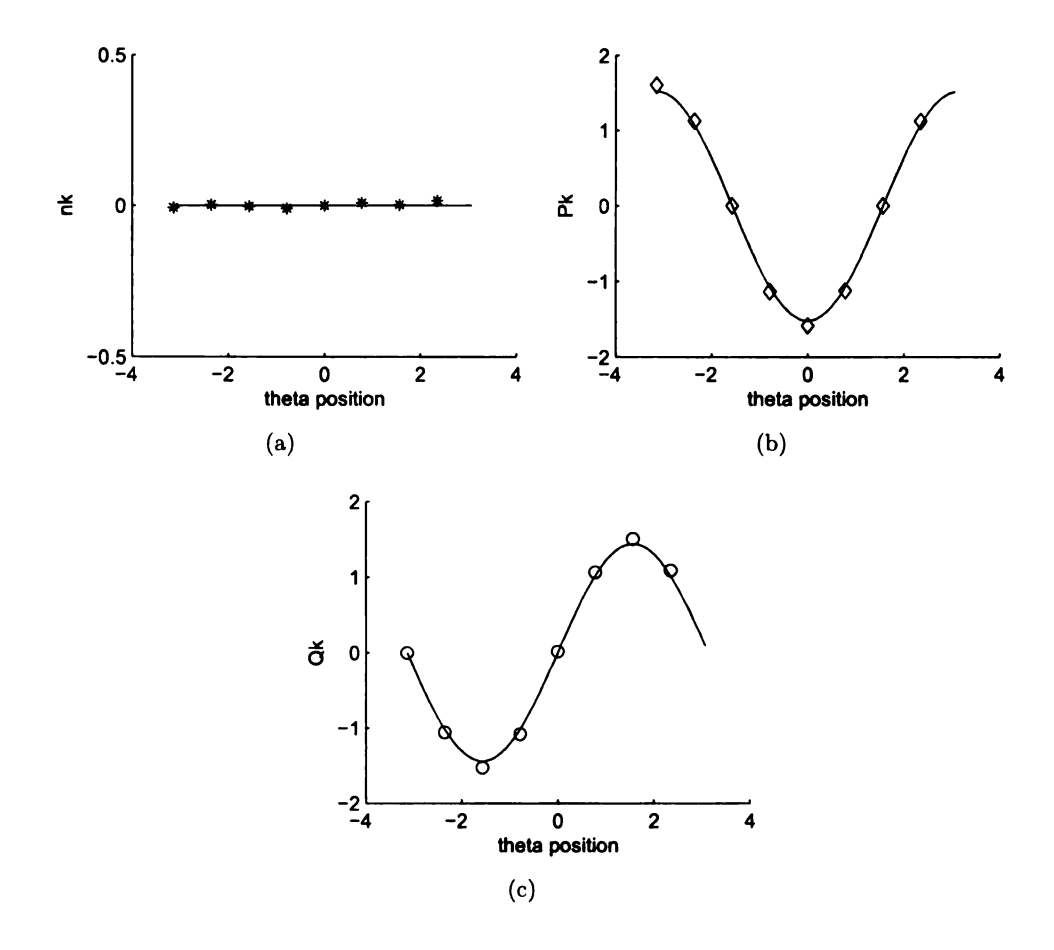


Figure 4.2. Identified functions by interpolation functions on noise-free data, (a) n_k , (b) p_k , (c) q_k .

4.3.2 Experimental double pendulum

The second example is a double pendulum system with vertical base excitation. It is both a whirling and a multi-degree-of-freedom system. A 100T orbit length was selected. During identification process, the high frequency noise was filtered out by a digital filtering technique, and linear-regression-based optimization was applied for a better result. The identified parameters are listed in Table 4.1 in comparison with the 'true' values (the values were measured by other methods, and thus, may not be

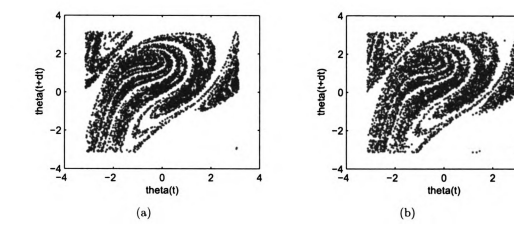


Figure 4.3. Comparison of Poincaré sections, (a) the original system, (b)the identified system

the exact parameter values, see Chapter 3).

Shown in Figure 4.5 is the residual plot of the first matrix equation. It can be seen that the residuals are much less than 10% of the maximum predicted value, implying a good identification result by the 10% rule of thumb. Actually, the small residual values were obtained even without using the optimization process. It supports the claim that any long chaotic orbit is close to some unstable periodic orbit.

4.4 Concluding remarks

In this chapter, we improved and simplified the parametric identification method for chaotic systems [24]. Assuming hyperbolic chaos for the investigated system, due to properties of a chaotic attractor, the set of unstable periodic orbits forms a dense skeleton of the attractor. Also, a long chaotic segment is arbitrarily close to a UPO, except at the tail or head part, and is approximately the same in its frequency spectrum. Thus, balancing harmonics of an arbitrary long segment of

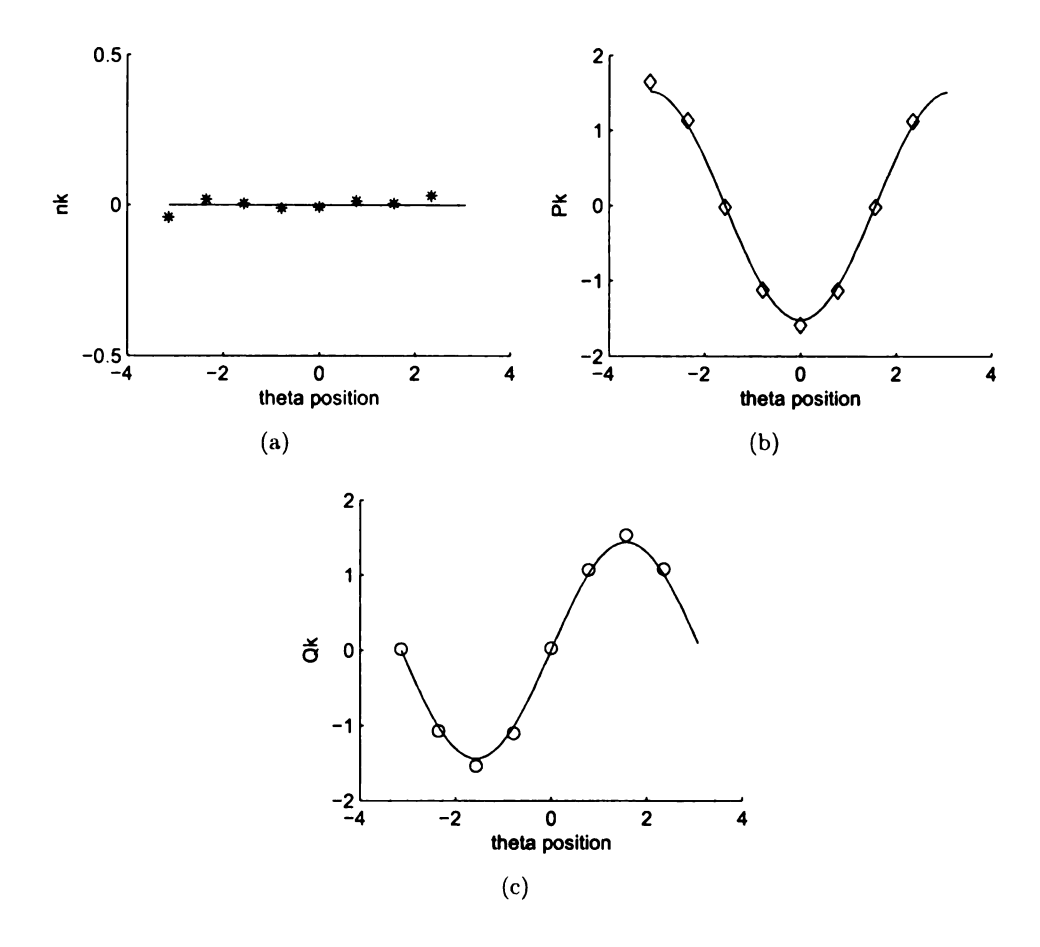


Figure 4.4. Identified functions by interpolation functions on 10% noise contaminated data, (a) n_k , (b) p_k , (c) q_k .

chaotic data simplifies the identification method from a complicated one involving harmonic balance method and extraction of UPOs to a pure frequency method applied to a long chaotic segment. Simulation and experiment were examined to verify this improvement. The method was seen to be quite noise resistant.

With this simplification, previous research on whirling systems, and the optimization of the identification by refining the set of sub-harmonics, the harmonic balance method has been tested to be a very powerful and simple tool for the identification of strongly nonlinear systems. The new discovery also unites the identification pro-

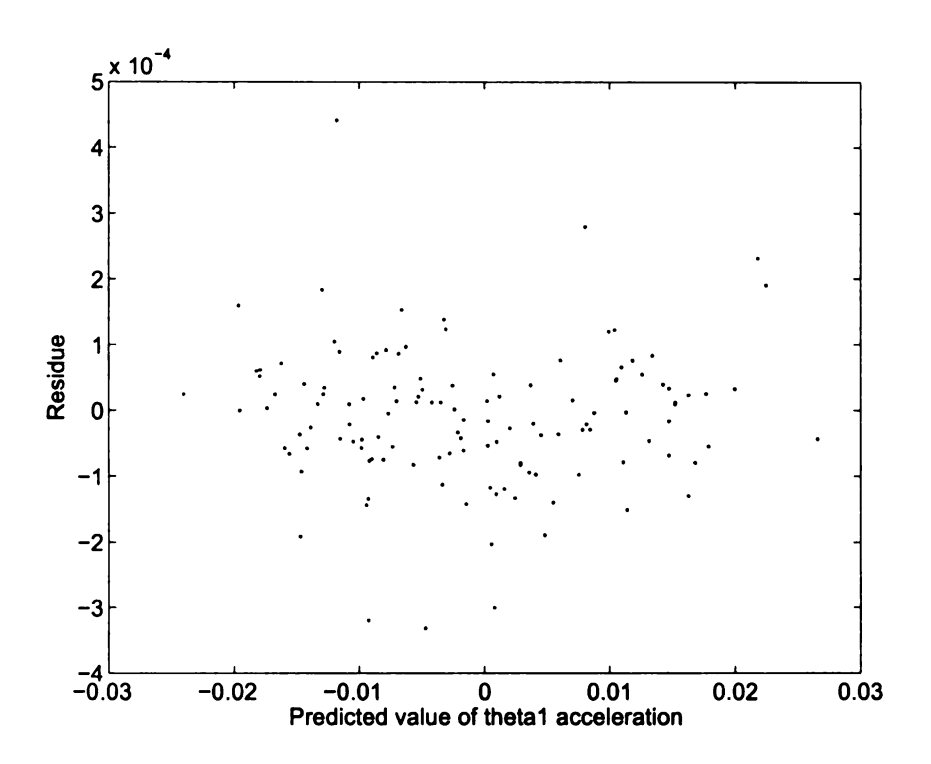


Figure 4.5. The residual plot of the first matrix equation of the double pendulum system

Table 4.1. Comparison of the true values and the identified parameters by new frequency method.

Parameters	Identified values	True values	Error×100%
B_{11}	0.1125	0.1131	7.8%
B_{12}	0.0770	0.0711	8.3%
B_{15}	0.0821	0.0820	0.1%
B_{21}	1.6091	1.6816	4.3%
B_{22}	0.2539	0.2630	4.5%
B_{25}	0.2839	0.2913	3.5%
C_{11}	0.0003	1.02×10^{-3}	_
C_{12}	-0.0010	0.00366	_
C_{2}	0.0077	0.0485	-

cess of periodically excited linear and nonlinear systems under the commonly used frequency domain method, i. e. the harmonic balance method.

Meanwhile, the research prompts a great amount of future work. Compared to some other previous frequency methods of nonlinear systems [12], the present method has no limitations to strongly nonlinear or chaotic systems. However, at present, the harmonic balance method can be applied to nonlinear systems only if under periodic excitation. For linear systems, the present method can be simplified to frequency response functions (FRF) method, and can be applied to free vibration (under impact) and random vibration (under random excitation, e. g. ergodic random signals) cases. For nonlinear systems, identification under impact or random excitation are, at present, still limited to weak nonlinearity, and are not available to the harmonic balance method.

Nevertheless, the requirement of periodic orbits could be changed in the future if we look at the periodic response in the frequency domain. We can say linear systems have stable frequency response functions (FRF) under different excitations, due to the fact that their stable responses are always stable periodic orbits with no change of shape. On the contrary, the nonlinear systems do not have structurally stable FRFs under different excitations. Their FRFs are liable to change for different excitation amplitudes, and are not defined for random excitation. The extreme representation of the instability is chaotic systems, in which the stable responses are no longer stable periodic orbits, but chaos with embedded UPOs. Actually, we assume that a single free vibration after a single impact is not adequate for nonlinar system identification unless we know exactly what type of nonlinearity that the system has. Instead, we would refer to a series of impact vibration signals, e. g. systems under periodic impact excitation. For randomly excited systems, the case is more complicated. We believe that some analogue can be made between chaotic systems under periodic excitation and nonlinear systems under random (ergodic) excitation.

CHAPTER 5

The Reduced Order Models of Nonlinear Systems Based on Proper Orthogonal Modes

5.1 Need for reduced order models

As the degree of freedom increases, the numbers of parameters increases, and the complexity of the analysis and identification is magnified. A good way to overcome these issues is with reduced order models. As such, with increasingly large system order, at some point, reduced order modeling becomes mandatory.

In this chapter, we use proper orthogonal decomposition (POD) as the vehicle for reduced order modeling. The parametric identification is then performed on the reduced order model itself, thus marrying the POD with parametric identification.

In what follows, we review the POD: its strengths and shortcomings. We then propose an enhancement of POD reduced order modeling that allows the identified system to be applied to conditions beyond those for which the POD was performed.

5.2 Proper orthogonal decomposition introduction

Proper orthogonal decomposition, or Karhunen-Loève decomposition, has been widely used tool for empirical modal analysis. As a statistical method utilizing the correlation matrix derived from a set of measurement histories, POD leads to proper orthogonal modes (POMs), which are taken as empirical modes, from the eigenvectors of the correlation matrix, and the corresponding energy level of each mode, known as proper orthogonal values (POVs), from the matrix eigenvalues. For linear systems with evenly distributed mass, POMs actually represent the linear normal modes (LNMs) [26]. Therefore, POD can be used as modal analysis tool [27, 28, 29, 4, 30, 31]. In [31], a weighted POD method was proposed to show the common nature between POMs and LNMs. Meanwhile, since its introduction, POD has been widely used in turbulence as modal reduction tool [3, 32, 33], and recently in structural dynamics [34, 35, 36, 37, 38, 39, 40, 41, 42, 43].

The process of finding POMs is very simple. For a random field $\theta(x,t)$ defined on a spatial domain Ω , the field can be decomposed into two parts by

$$\theta(x,t) = \mu(x) + \vartheta(x,t), \tag{5.1}$$

where $\mu(x)$ is the mean value, and $\vartheta(x,t)$ is the oscillation part. The snapshot of $\vartheta(x,t)$ in time t_k , $k=1, 2, \ldots, N$, is denoted as $\vartheta_k(x)$. The objective is to find a function $\phi(x)$ which is most similar to the set of $\vartheta_k(x)$ on average. It can be obtained by solving the following integral eigenvalue problem:

$$\int_{\Omega} \langle \vartheta_k(x) \vartheta_k(z) \rangle \phi(z) dz = \lambda \phi(x), \tag{5.2}$$

$$\int_{\Omega} \phi^2(x) dx = 1, \tag{5.3}$$

where $\langle \vartheta_k(x)\vartheta_k(z)\rangle$ is the averaged cross correlation function, and the equation (5.3) is an added normalization condition to make the solution unique.

Solving (5.2) and (5.3), we can obtain eigenfunctions $\phi_i(x)$, and corresponding eigenvalues λ_i . The $\phi_i(x)$ is the *i*th proper orthogonal mode, and the corresponding λ_i is the proper orthogonal value of this mode under the collected data set. The mode indices i are ordered by the values of the POVs, from largest to smallest. The POV λ_i also shows how much energy lies in that mode. The total energy is defined by $\sum_{j=1}^{N} \lambda_j$, and the share of energy in each mode is $\lambda_i/\sum_{j=1}^{N} \lambda_j$.

The signal $\vartheta_k(x)$ can now be represented in terms of $\phi_i(x)$ by

$$\vartheta_k(x) \approx \sum_{j=1}^l a_j \phi_j(x), \tag{5.4}$$

where the coefficient $a_j = (\vartheta(x,t), \phi_j(x))$. The number of significant modes l is generally determined by $\sum_{j=1}^{l} \lambda_j$ greater than, for example, 99.9% of the total energy.

In practice, the data is discretised in both time and space. Thus, for m observations of an n dimensional vector \vec{x} , the ensemble of the signal becomes a matrix

$$\mathbf{X} = [\vec{x_1} \dots \vec{x_m}] = \begin{pmatrix} x_{11} \dots x_{1m} \\ \vdots & \ddots & \vdots \\ x_{n1} \dots & x_{nm} \end{pmatrix}. \tag{5.5}$$

If \vec{x} has zero mean (\vec{x} is the varying part of some field variable), then the covariance matrix **S** is defined as

$$\mathbf{S} = \frac{1}{m} \mathbf{X} \mathbf{X}^{\mathbf{T}}.\tag{5.6}$$

The POMs and POVs are now the eigenvectors and eigenvalues of the matrix S. For high dimensional systems like turbulence, the matrix can be huge, and a direct solu-

tion for eigenvectors and eigenvalues is quite difficult. In this case, another method was introduced by Sirovich [63], but the details are not to discuss in this dissertation.

With the POMs as empirical modes, we can then apply them to build reduced order models (ROMs). The dissertation research on POD and parametric identification is quite different from the POD method in fluid turbulence research, the latter of which is mainly a tool for model order reduction from PDEs to ODEs by POMs and the Garlekin method [33]. The investigation in the dissertation is a further step in building reduced order structural models by POD without necessarily requiring knowledge of the continuous system. Assuming no, or partial, knowledge of the governing equations of the systems, we try to reconstruct the systems by building differential equations, based upon the empirical modes, expressed as

$$\mathbf{M}\ddot{\vec{x}} + \mathbf{C}\dot{\vec{x}} + \mathbf{K}\vec{x} + f_{n1}(\vec{x}, \dot{\vec{x}}) + f_{n2}(\vec{x}, \dot{\vec{x}})\vec{y_p}(t) = \vec{y_f}(t),$$
 (5.7)

where all of the coefficients are unknown, functions f_{n1} and f_{n2} are the nonlinear functions, and $\vec{y_f}(t)$ is the external excitation force with known excitation frequency, $\vec{y_p}(t)$ is the parametric excitation. We will then need a parametric identification method to find the best suitable values for the unknown coefficients. For simplicity, the systems investigated here are free vibration systems with no damping. The reason is that this is the initial investigation of a vast issue. The free vibration systems without damping can also display nonlinear normal modes under bounded initial conditions [64, 65, 2], which is a good tool for comparison with POMs. Therefore, equation (5.7) is reduced to

$$\mathbf{M}\ddot{\vec{x}} + \mathbf{K}\vec{x} + f_{n1}(\vec{x}) = 0. \tag{5.8}$$

The linear part of the model involves relatively few problems. However, there are

questions regarding nonlinearity. First, what kind of nonlinearity should be assumed? Even though we know the physical nonlinearity of the original system, it is not clear what form it will have when transmitted into the new modal coordinates. Thus, function series, such as polynomials, are needed to approximate the nonlinearity. Polynomial functions can be functions of displacement or velocity. Generally, it is necessary to know what kind of nonlinearity is involved in the unknown systems. This is why we treat the reconstruction process as a 'graybox'. Second, for the approximation function series, any unnecessary term should be discarded based upon a priori information. The major reason is not for simplicity, but for their influences on the dynamical responses, such as chaos, bifurcation and other nonlinear behaviors sensitive to parameters. Sometimes, the nonlinearity approximation needs guesses and trials, at the present research progress to approximate the dynamical responses of the original system. Third, for the reconstructed reduced order models, one would like to know to what extent it can represent the original system. It is a problem especially for systems with strong nonlinearity. The reduced order models may not work well under different initial conditions. We will discuss these problems later.

Even with many uncertainties and unknowns, POD is popular in modeling and modal analysis because it is simple and empirical. For any system, linear or nonlinear, it gives empirical orthogonal modes of the dynamical behavior, which can be used to set up empirical governing equations, or for detecting the active modes in the vibration data. It is especially useful for analysis of complex structures or fluids. Structural dynamics and fluid turbulence models are continuous and high dimensional. For the turbulence case, the dynamics is also chaotic [66]. Usually, the dynamical governing differential equations of those systems are hard to obtain, or hard to analyze. Thus, one has to refer to approximation methods for analysis, either by discretisation methods like finite element analysis, or by reduced order models, e. g. the POM method. The finite element method is more direct and usually accurate. However, it requires

complex processing, and sometimes, can not give accurate simulation if the systems are complicated, or chaotic. On the other hand, POM reduced order modeling is empirical, as it obtains proper orthogonal modes through experimental data and results in a small number of the governing equations based upon the modal coordinates of the empirical POM. The POM method treats a system like a gray box (known basic dynamical mechanism, unknown global governing equations and parameters), and it gives us functional models that can approximate the dynamical behavior of the unknown systems. We can see that the large scale discretization and ROM methods both have advantages and have different applications. However, in many cases, the reduced order models are not inferior to the other discretisation methods, and those models are much easier to simulate since they are composed of ODEs, instead of PDEs.

5.3 Improving POD for strong nonlinear systems

5.3.1 Limitation of the POD

Proper orthogonal decomposition is basically a linear statistical method. When applied to nonlinear systems, POD has its own limitations. Unlike linear systems, displacement-response configurations of nonlinear normal modes vary with the initial conditions, implying that POMs of nonlinear systems vary with the initial conditions. Therefore, the reduced order model from POM under one data set may only be suitable for initial conditions within a small neighborhood in the phase space of those that generated the sampled data. Beyond this neighborhood, the approximation deteriorates due to nonlinearity. This can be a shortcoming of the POM-based models, especially for systems with strong nonlinearity.

In contrast, NNMs are varying curved surfaces instead of planes in the phase space.

One may consider NNM based reduced order models for more precise prediction of system behavior. The NNM is a useful tool for theoretical modal analysis [64, 65, 2] of nonlinear systems and model order reduction in NNM modal coordinates. However, compared to POM model order reduction, it is complex and time consuming, and requires clear knowledge of the governing equations of systems. For unknown systems with strong nonlinearity, it is then necessary to find a way to improve POM based models for better prediction and applicability under varying initial conditions, which provides robustness of the reconstructed reduced order model. To investigate this, we focused on two nonlinear systems: a two-mass system and a mass-pendulum system, both of which were investigated under the initial conditions exciting only the first nonlinear normal mode, such that single d. o. f. reduced-order models can be built, instead of reconstructing the original two d. o. f. systems. For the former system, the study focused on the limitation of the reduced-order model based only on one POM, and then developing a new modeling method with an added constraint. The purpose of this example is to show whether the added-constraint method can improve the accuracy of the reduced-order model as well as expanding the applicability of the model under more initial conditions. For the latter example, the study focused on how to treat unknown nonlinearity in the new models: nonlinearity approximation with the constraint coordinate included, or nonlinearity with the constraint excluded, which simplifies the nonlinearity approximation since there is only one degree-offreedom involved for this example. By the two examples, the POM-only models and the proposed POM added-constraint models were investigated by low dimensional systems. Investigation on these simple systems will provide a theoretical basis for further study on high dimensional systems.

5.3.2 The example of a two-mass system with nonlinear spring

We consider a two-mass system with the differential equations

$$\begin{cases} \ddot{x}_1 = -2x_1 + x_2 - x_1^3 \\ \ddot{x}_2 = x_1 - 2x_2 \end{cases} , \tag{5.9}$$

where m = 1, and k = 1. In [2], the NNMs and modal differential equations of equation (5.9)were solved for small amplitude vibration.

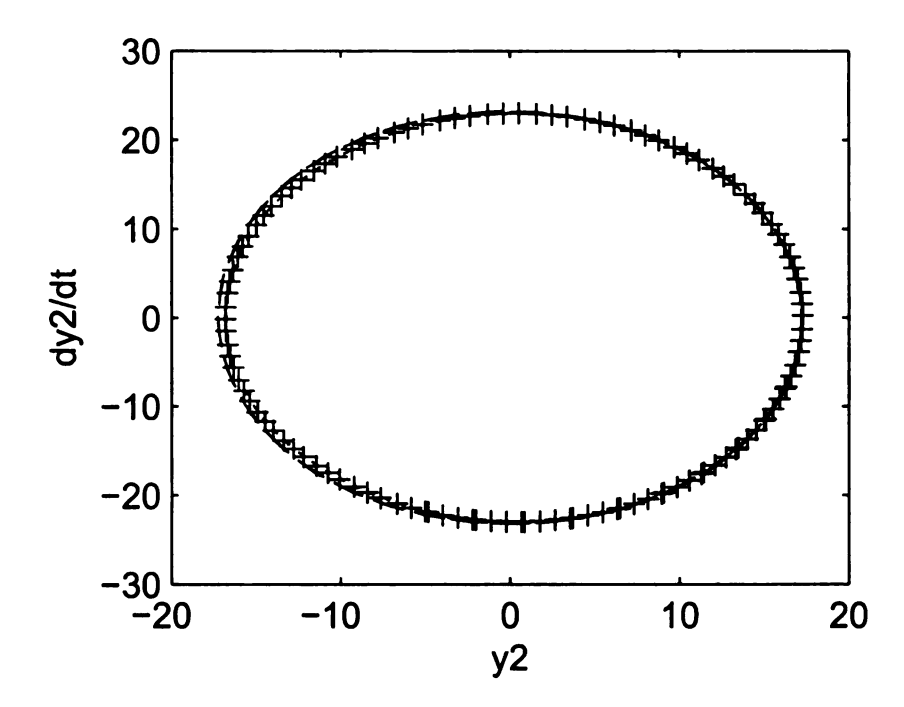


Figure 5.1. Phase portraits of the original system ('+'), the POD only model (the dashed line), and the POD-constraint model (the dotted line) under the 5th initial condition.

To build a reduced-order model for this system, we will only consider the first

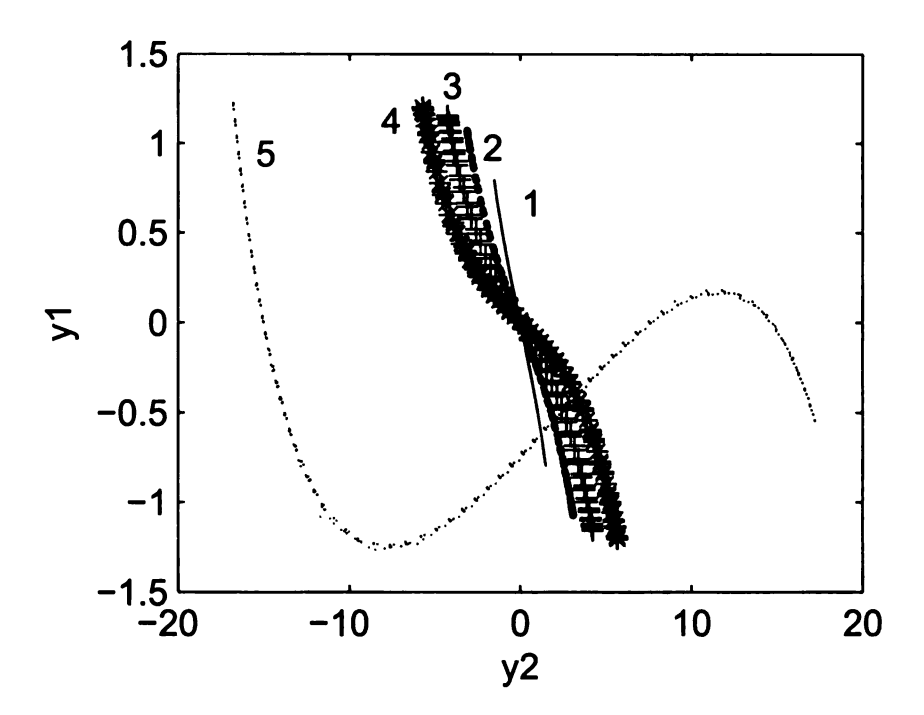


Figure 5.2. First NNM displacement shapes in y_1 , y_2 coordinates, number 1–5 correspond to the five initial conditions.

mode with different initial conditions. Assuming that the system is unknown to us except that it has cubic nonlinearity, the goal is to build a single d.o.f. model for the first mode, and make it applicable for general initial conditions on the first NNM. We used five different initial conditions for the simulation. With zero initial velocities, the five initial displacements were (1, 1.3833), (1.5, 2.9250), (1.75, 4.0365), (2.0, 5.4667), (3.0, 17.0). The reduced order model based on POD was done under the fifth initial condition only.

For the two d. o. f. system, there are two POMs: $\vec{p_1}$ and $\vec{p_2}$. The transformation matrix A can be defined as

$$A = (\vec{p_1} \quad \vec{p_2}).$$

Hence, the modal coordinates can be defined as

$$\vec{y} = A\vec{x},\tag{5.10}$$

or

$$\begin{pmatrix} y_1 \\ y_2 \end{pmatrix} = A^T \begin{pmatrix} x_1 \\ x_2 \end{pmatrix}. \tag{5.11}$$

For the simulated example, we obtained $\vec{p_1} = (-0.990 \ 0.141)$ and $\vec{p_2} = (0.141 \ 0.990)$. The POM $\vec{p_2}$ is the dominant POM, and consists of 99.7% of the total energy. Hence, the matrix $A = \begin{pmatrix} -0.990 \ 0.141 \\ 0.141 \ 0.990 \end{pmatrix}$. The modal coordinates y_1 , y_2 obtained were $y_1 = -.990x_1 + 0.141x_2$ and $y_2 = 0.141x_1 + .990x_2$. We can then use new coordinates to transform the original differential equations into

$$\begin{cases} \ddot{y_1} = g_1(y_1, y_2) \\ \ddot{y_2} = g_2(y_1, y_2) \end{cases}$$
 (5.12)

As y_2 accounts for a greater portion of the total energy, according to the original POD, the y_1 would become significant, and the two d. o. f. system could be reduced a single d. o. f. system in terms of y_2 in equation (5.12). The dynamical behavior of the original two-mass system could be approximated by y_2 only, using

$$\begin{pmatrix} x_1 \\ x_2 \end{pmatrix} = A \begin{pmatrix} 0 \\ y_2 \end{pmatrix}. \tag{5.13}$$

However, if the y_2 mode is not sufficiently dominant, the reduced order model based only on the linear y_2 and equation (5.13) can not predict the system behavior satisfactorily.

Suppose the coefficients of the ODEs, such as equation (5.9), are unknown. Then,

the transformation of the coefficients in equation (5.12) will produce complicated expressions of the original parameters. To bypass this complication, the POM modal projection and the parameter estimation can be coordinated as follows. The form of the dominant equation can be expressed by

$$\ddot{y}_2 = ky_2 + \sum_{j=1}^{3} n_j y_2^j, \tag{5.14}$$

where the parameters are unknown before identification. Assuming displacement signals measured, a parametric identification method can then be applied. For this example, the direct identification method [5] was used, since the simulation signals were noise free and in free vibration. Digital differentiation was applied to obtain velocity and acceleration signals.

Displayed in figure 5.1 are phase portraits of the original two-mass system and the one d.o.f. identified POM model under the fifth initial condition. A discrepancy between the two systems is visible in the behavior of y_2 . On the other hand, under these initial settings, the behavior of the two-mass system is apparently one dimensional. Meanwhile, Figure 5.2 shows the changing modal displacement shapes under these conditions. The displacement mode shape of the fifth condition is the most different among them. Obviously, the modal surface is quite curved, and the POM model (5.14) under the fifth condition can not be applied to other initial settings. This raises the question of how to improve our model without introducing extra dimensions to make the POM model more applicable to other initial conditions.

Traditionally, for systems like this one, POMs have to be re-calculated to reconstruct the model under other conditions. To increase the applicability to a range of initial conditions, the proposed solution is to add a constraint to the modal coordinates. Its inspiration comes from solving for individual NNMs [2]. Basically, the idea is to introduce a constraint coordinate y_1 obtained from the POD. However, unlike

an extra d.o.f., it is a coordinate dependent on modal coordinate y_2 and velocity \dot{y}_2 , and it can be expressed by

$$y_1 = f(y_2, \dot{y}_2) \approx \sum_{j=0}^{M} \sum_{k=0}^{M} a_{j,k} y_2^j \dot{y}_2^k.$$
 (5.15)

The constraint coordinate y_1 increases the accuracy of the POM model in addition to enlarging its applicable domain in the phase space.

In the simulation, a cubic polynomial was used to approximate the constraint surface, and the coefficients $a_{j,k}$ were estimated by the least mean-square method. The model differential equation was also modified by introducing y_1 :

$$\begin{cases} y_1 = \sum_{j=0}^3 \sum_{k=0}^3 a_{j,k} y_2^j \dot{y}_2^k \\ \ddot{y}_2 = k_1 y_1 + k_2 y_2 + n(-0.990 y_1 + 0.141 y_2)^3 \end{cases},$$
 (5.16)

where k_1 and k_2 are unknown coefficients of the linear terms, and n is the coefficient of the known x_1^3 nonlinearity. substituting (5.15) into equation (5.16), we can obtain

$$\ddot{y_2} = h(y_2, \dot{y_2}) = k_1 \sum_{j=0}^{3} \sum_{k=0}^{3} a_{j,k} y_2^j \dot{y_2}^k + k_2 y_2 + n \left(\sum_{j=0}^{3} \sum_{k=0}^{3} a_{j,k} y_2^j \dot{y_2}^k + 0.141 y_2\right)^3,$$
(5.17)

which is a simple single d. o. f. nonlinear oscillator. The new model can be regarded as the added-constraint model.

Table 5.1. Identified parameters of the POM-constraint model (5.16) under the first three conditions

_	k_1	k_2	n
Identified	-0.9932	-1.7069	-0.1607
True values	-0.9532	-1.7212	-0.1412
Errors	4.2%	0.9%	13.8%

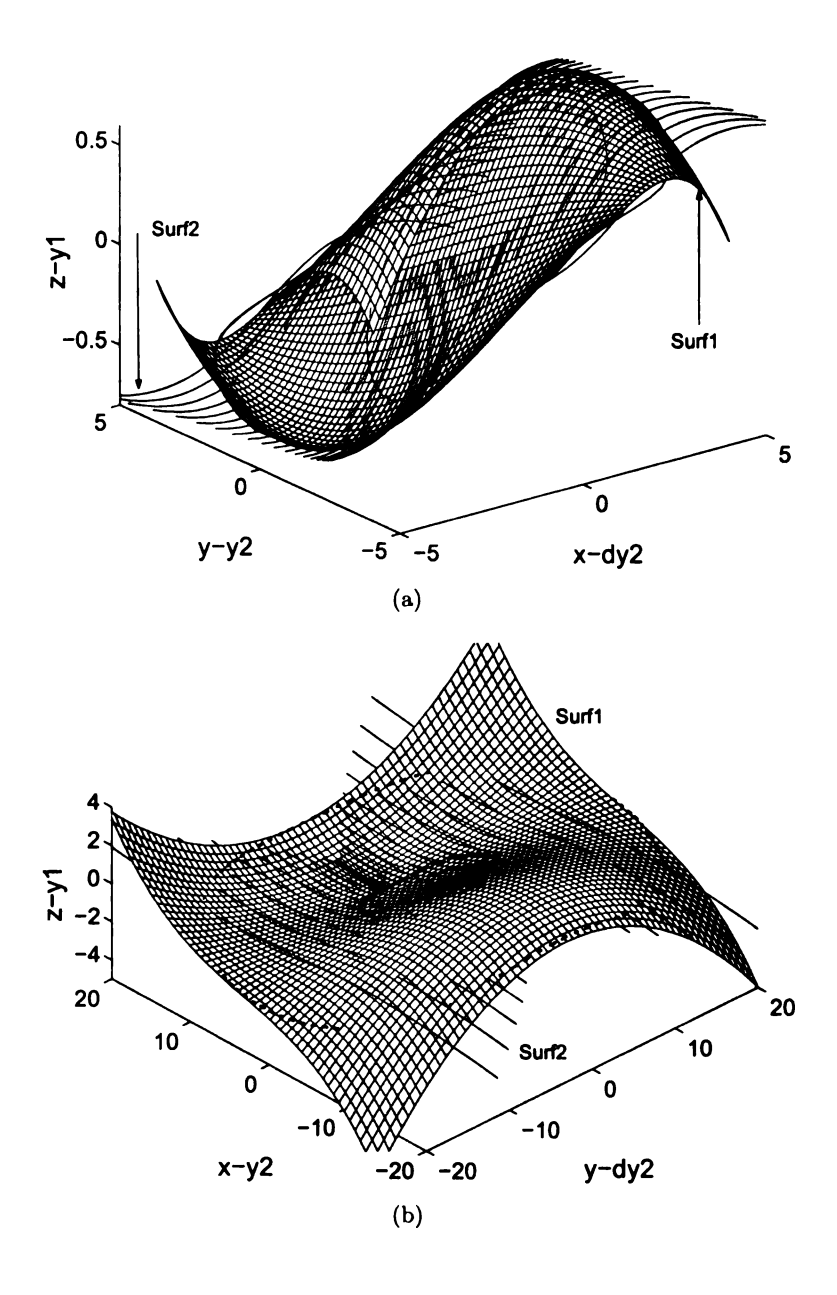


Figure 5.3. Comparison of the invariant manifold: (a) under small amplitude (the first three conditions), (b) under all five conditions; Surf 1 is the empirical surface from POD, Surf 2 is Shaw's surface, the continuous lines are the orbits under five conditions; x axis is y_2 , y axis is y_2 , z axis is y_1 .

First, the coefficients were estimated under the first three conditions. Displayed in Table 5.1 are identified parameters of the y_2 differential equation, and it shows a close match with the true values calculated from the linear transformation of the two-mass equation (5.9) except the nonlinear term. The discrepancy in the coefficient of the nonlinear term may come from the small amplitude vibration where nonlinear effect is not so apparent, and the error from digital differentiation. Upon obtaining the identified equation, Figure 5.3(a) displays the constraint surface (surf 1) fit for the first three initial conditions which are of smaller oscillation amplitude. The continuous lines are the corresponding three orbits (the orbits are partially covered by the surfaces and are hard to sec). Surf 2 is the surface obtained by Shaw's polynomial approximation of NNM, which is a good approximation of the NNM surface under small amplitude vibration. For small amplitude vibration, the two surfaces match well. However, as the vibration amplitude increases, Shaw's surface deviates from the true orbits. Instead, the empirical POM model, which was fit from data that was not 'small' in asymptotic terms, shows a better match for more orbits in the phase space.

Figure 5.3(b) shows the surface fit (Surf 1) for the identified system under all of the five initial conditions. In Figure 5.1, the dynamical orbit under the fifth initial condition is also shown in the phase space (the dotted line), and shows a closer match with the original system compared to the POD-only model. Noticeably, the fifth orbit is much larger than the other four orbits. Shaw's surface shows large discrepancy from the real orbits for large amplitude vibration. On the other hand, noticing that the identified model changed after using a larger data set, the empirical surface changes to fit the fifth orbit, but also shows discrepancy for small amplitude orbits. The discrepancy results from an inadequate polynomial approximation as well as the nature of least mean square method. We can adjust our overall approximation by using a different data set consisting of more records of small amplitude orbits, or a weighted data set which gives more weight to the small orbits, such that the

discrepancy over the whole surface can be more evenly distributed.

Through the analysis above, it is clear that if y_1 is neglected, i. e. neglecting equation (5.15) when the energy in y_1 is negligible comparing to the dominant POM, the ROM becomes a POM-only model (5.14). The constraint model, however, does not neglect y_1 , but incorporates the curvature of the true NNM, to achieve the form of equation (5.15). Effectively, this puts the model into the form of equation (5.17), which is a differential equation with nonlinearity in displacement and velocity. By its construction, it is made to accommodate dynamics of a wide range of initial conditions.

5.3.3 The example of a mass-pendulum system

The differential equation and the nonlinearity

In the previous example, the added-constraint method was successful in enhancing the adaptability of the POM reduced order model for a nonlinear system. Nevertheless, under assumptions of known nonlinearity, the examined system is quite simple. In practice, the nonlinearity is quite often not clear to us. It is necessary to use function series to approximate the nonlinearity.

We tested this problem by examining a more complex system: the mass-pendulum system. Figure 5.4 shows a sketch of this system, where the mass block has a horizontal displacement x, and the arm has an angular displacement θ . The corresponding differential equation is

$$\begin{cases} \ddot{x} + b_{11}x + b_{12}\{\ddot{\theta}\cos\theta - \dot{\theta}^2\sin\theta\} = 0\\ \ddot{\theta} + b_{21}\sin\theta + b_{22}\ddot{x}\cos\theta = 0 \end{cases},$$
 (5.18)

where $b_{11} = k/m_1 + m_2$, $b_{12} = m_2 e/\{(m_1 + m_2)l\}$, $b_{21} = m_2 gel/J_{o2}$, $b_{22} = m_2 e/J_{o2}$, m_1 and m_2 are the masses of the block and the pendulum (the mass of the

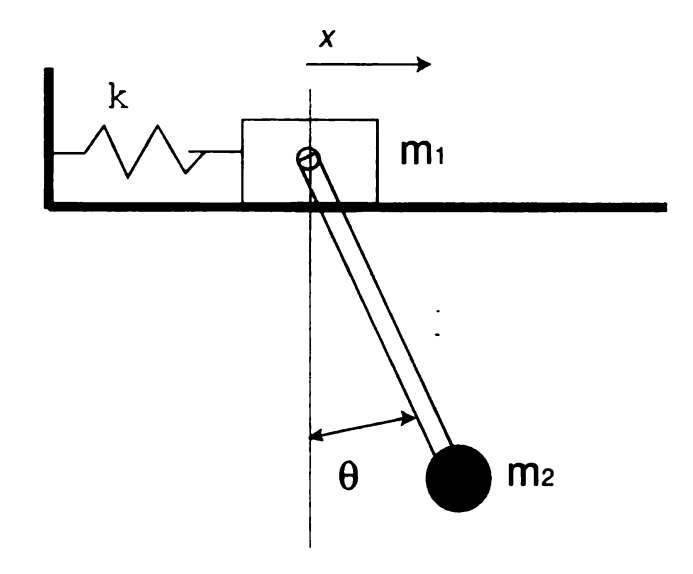


Figure 5.4. A sketch of the mass-pendulum system.

bar included), J_{o2} is the mass moment of inertia of the pendulum with respect to the pendulum joint, e is the distance of the pendulum centroid to the joint, and $\hat{x} = x/l$ is the non-dimensional displacement. For convenience, we drop the hat of the non-dimensional displacement \hat{x} . The nonlinear terms are strong, including interaction terms of the mass and the pendulum, mixed nonlinear terms involving displacement, velocity and acceleration, and trigonometric functions. As a result, it is hard to determine what kind of nonlinear format will show in the POM reconstructed reduced order model. In the simulation, the initial conditions were chosen to excite only the first NNM of the system. The POM extraction and the model identification process were similar to the previous example. However, the two NNMs of the mass-pendulum system were found only in the absence of whirling.

Now, we denote z_1 as the major POM which consists of most of the energy of the data, and z_2 as the minor POM which is orthogonal to z_1 . The added-constraint model will be composed of z_1 and z_2 . Two types of the added constraint models were

tested. The first one is

$$\begin{cases} z_2 = f_c(z_1, \dot{z_1}) \\ \ddot{z_1} + k_{z1}z_1 + p(z_1) = 0 \end{cases}, \tag{5.19}$$

where the differential equation of z_1 consists of only z_1 . On the contrary, the second model, considering z_2 as a dependent variable of z_1 , can be expressed as

$$\begin{cases} z_2 = f_c(z_1, \dot{z_1}) \\ \ddot{z_1} + k_{z1}z_1 + k_{z2}z_2 + p(z_1, z_2) = 0 \end{cases}$$
 (5.20)

In both of the models, the constraint equations are functions of z_1 and z_1 . But, in the first model, the POM differential equation has only one independent variable z_1 , and the nonlinearity is approximated by a polynomial of z_1 . In contrast, the POM differential equation of the second model has both z_1 and z_2 , and the nonlinearity is approximated by a polynomial of z_1 , z_2 . The second model appears to be a better approximation model to the system dynamics, because, much like the previous example, the z_2 , as a function of z_1 and z_1 , is also introduced in the differential equation and is generally closer to the actual nonlinearity. It also brings more complexity in the nonlinearity identification, and the problem may be worse for high d. o. f. systems. Besides, extra terms in the nonlinearity approximation may unstable dynamical behavior. For this simulation study, the unknown parameters of equation (5.19) and (5.20) were identified by the harmonic balance method discussed in the previous three chapters of the dissertation.

Table 5.2. Physical parameters used in the simulation

$m_1 \text{ (kg)}$	0.1	$m_2 ext{ (kg)}$	0.1
k (N/m)	100	l (m)	.04

Simulation setting and the POD

The parameter values used in the simulation are listed in Table 5.2, and the mass of the pendulum bar was neglected. Five initial conditions were tested, in which the initial velocities were zero, and the initial displacements for x and θ , from small to large amplitude, were: (0.125, 0.385), (0.250, 0.733), (0.375, 1.10), (0.500, 1.54), (0.575, 1.892). The resulting dynamical behavior corresponded the first NNM of this system, under five different initial conditions on that NNM.

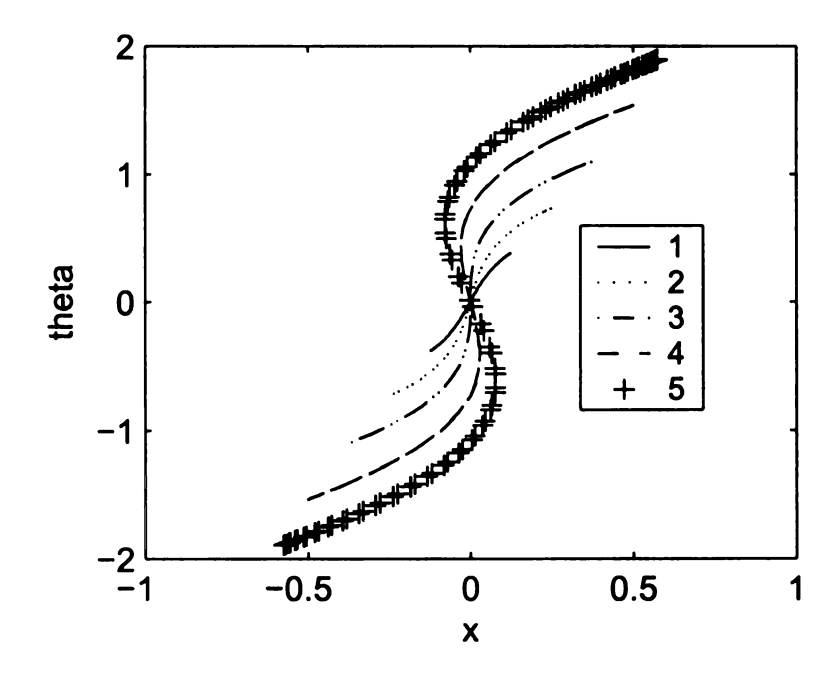


Figure 5.5. The shapes of the 1st NNM of the mass-pendulum system under 5 i. c.: 1. (0.125, 0.385), 2. (0.250, 0.733), 3. (0.375, 1.10), 4. (0.500, 1.54), 5. (0.575, 1.892)

The dominant POM obtained under the first initial condition was $\vec{z_1} = [0.2838 \ 0.9589]^T$, which consists of 99.93% of the total energy. The minor POM was $\vec{z_2} = [-0.95890.2838]^T$. Figure 5.5 shows the five displacement shapes of the

first NNM under these non-whirling conditions. It is clear that for large amplitude vibration (curves 4, 5) the normal mode is quite twisted. If a POM based reduced order model is built on z_1 , it is accurate for the first initial condition. However, the reduced order model under $\vec{z_1}$ is not applicable to the other initial conditions listed here. Therefore, one would like to test if the added-constraint model can adapt to those initial conditions.

Table 5.3. Estimated polynomial coefficients of the constraint equation

a_1	0.00132	a_2	5.96×10^{-3}	a_3	-0.0105
a_4	-0.00327	a_5	1.21×10^{-4}	a_6	2.49

The added constraint and the weighted least mean square solution

In the study, the added constraint was estimated by a cubic polynomial:

$$z_2 = a_1 z_1 + a_2 \dot{z_1} + a_3 z_1^3 + a_4 \dot{z_1}^3 + a_5 z_1^2 \dot{z_1} + a_6 z_1 \dot{z_1}^2, \tag{5.21}$$

where a_i are the unknown coefficients. For better approximation of the small amplitude oscillation, the coefficients were solved by the weighted least mean square method based on the data of all five initial conditions.

We can denote the following equation as the unweighted least mean square matrix equation:

$$\mathbf{A}\vec{x} = \vec{q},\tag{5.22}$$

where \vec{x} is the vector of the unknown coefficients, \vec{q} is some known terms without

unknown coefficients,

$$\mathbf{A} = \left(\begin{array}{c} \mathbf{A_1} \\ \vdots \\ \mathbf{A_5} \end{array} \right),$$

and the small matrices A_i are data matrices from free responses to different initial conditions. Vector \vec{x} can be solved by this unweighted least mean square method. Then, we can transform the matrix A to a weighted matrix

$$\mathbf{A}_w = \left(egin{array}{c} w_1 \mathbf{A}_1 \ dots \ w_5 \mathbf{A}_5 \end{array}
ight),$$

where w_i is the weight. Correspondingly, we also denote

$$ec{q}_w = \left(egin{array}{c} w_1 ec{q}_1 \ dots \ w_5 ec{q}_5 \end{array}
ight).$$

Replacing \mathbf{A} , \vec{q} by \mathbf{A}_{w} , \vec{q}_{w} , equation (5.22) becomes

$$\mathbf{A}_{w}\vec{x} = \vec{q}_{w},\tag{5.23}$$

which is the weighted least means square method. The advantage of the weighted solution method is that we can adjust the approximated solution \vec{x} by giving different weights to subsets. We can give large weights to some subsets of the data if we want the approximated solution to have small discrepancy with the corresponding subsets. In the case of the NNM approximation, larger weights were given to the data sets from smaller oscillations such that the approximated constraint surface can have an evenly distributed error over all vibration amplitudes. Thus, the result is better

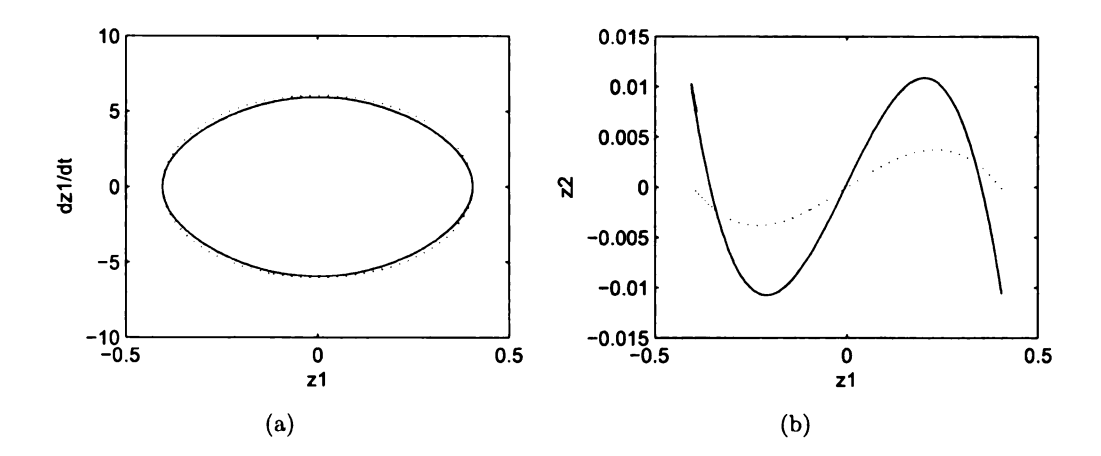


Figure 5.6. Comparison of Model I (the dotted lines) to the original mass-pendulum system (the continuous lines) simulated under 1st initial condition, (a) phase plane, (b) mode shape.

than the estimation from the unweighted least mean square method which tends to accommodate more with the large amplitude orbits.

To the investigated system, the estimated values of the coefficients are listed in Table 5.3. The constraint were shared by both of the reduced order models.

Model of type I

Substituting a cubic polynomial into model-1 (5.19), we obtain

$$\begin{cases}
z_2 = \sum_{j=0}^3 \sum_{k=0}^3 a_{j,k} z_1^j \dot{z_1}^k \\
\ddot{z_1} + k_{z_1} z_1 + a_{nl} z_1^3 = 0
\end{cases} ,$$
(5.24)

where $k_{z1} = 0.0571$, $a_{nl} = -0.00468$ in the investigation. The nonlinear term is represented by only a cubic polynomial, and is simple for estimation.

Displayed in figures 5.6, 5.7, 5.8, are the dynamical behaviors of the original system and the approximated model of the first type. The approximated model was built on the data from five initial conditions. It shows that the approximated model

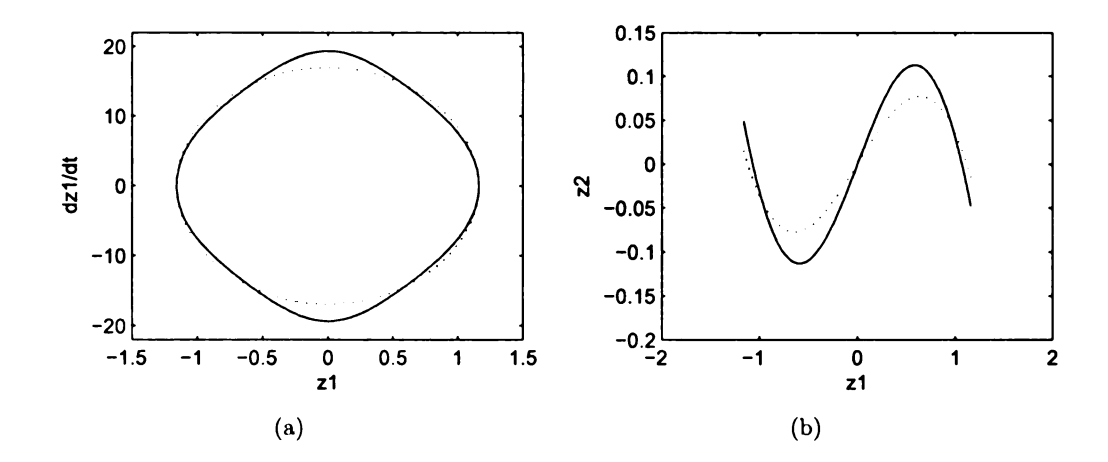


Figure 5.7. Comparison of Model I (the dotted lines) to the original mass-pendulum system (the continuous lines) simulated under 3rd initial condition, (a) phase plane, (b) mode shape.

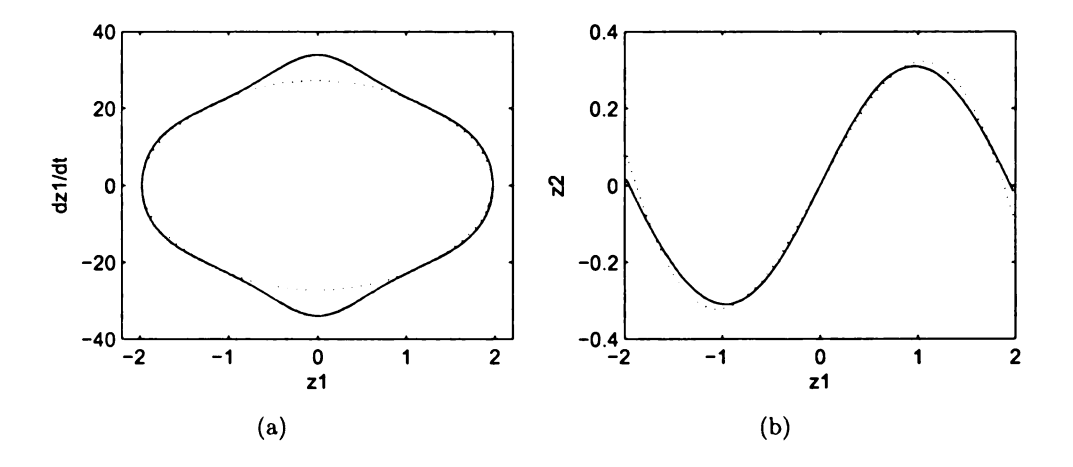


Figure 5.8. Comparison of Model I (the dotted lines) to the original mass-pendulum system (the continuous lines) simulated under 5th initial condition, (a) phase plane, (b) mode shape.

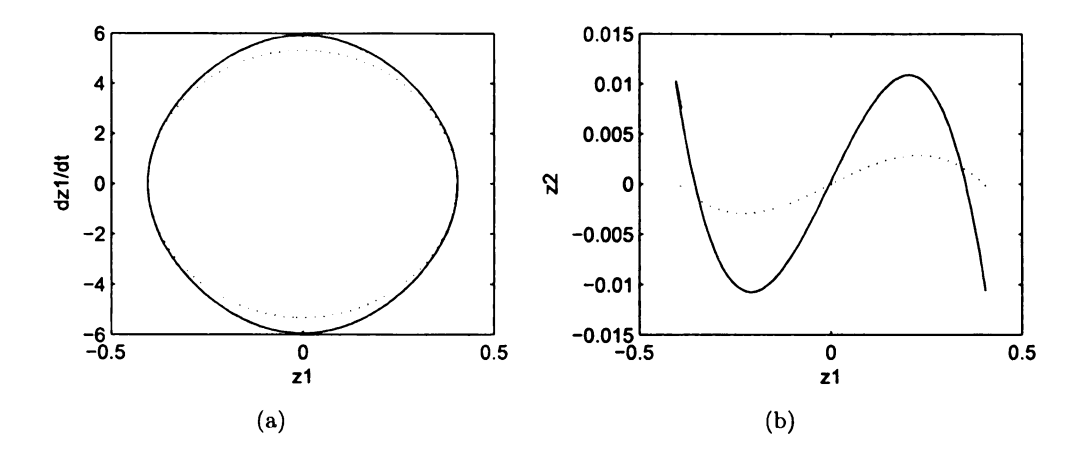


Figure 5.9. Comparison of Model II (the dotted lines) to the original mass-pendulum system (the continuous lines) simulated under 1st initial condition, (a) phase plane, (b) mode shape.

is a good representation of the original system. The approximation is better for the small amplitude vibration conditions, e. g. the first initial condition. As the vibration amplitude increases, the phase plane curves show increasing difference between the full and reduced order models. Part of the reason could be that the cubic nonlinearity of z_1 is inadequate to represent the nonlinearity of the original system. Meanwhile, by mode shape comparison in figures 5.6, 5.7, 5.8, the vibration mode shapes of the identified model are close to the real NNM shapes, and the minor displacement z_2 is properly approximated. Noticeably, the energy in z_2 coordinate increases as the oscillation amplitude increases. This model has the same differential equation of z_1 as the POM-only model, implying same dynamic behavior of z_1 . The only difference is that the POM-only model consider $z_2 = 0$, whereas, in the present mode, z_2 is a curve which can accommodate the change of initial conditions. Obviously, comparing to the POM-only model, the added-constraint made the response of the ROM closer to the actual first NNM of the original system, and thus improved the approximation of the dynamic behavior of the original system.

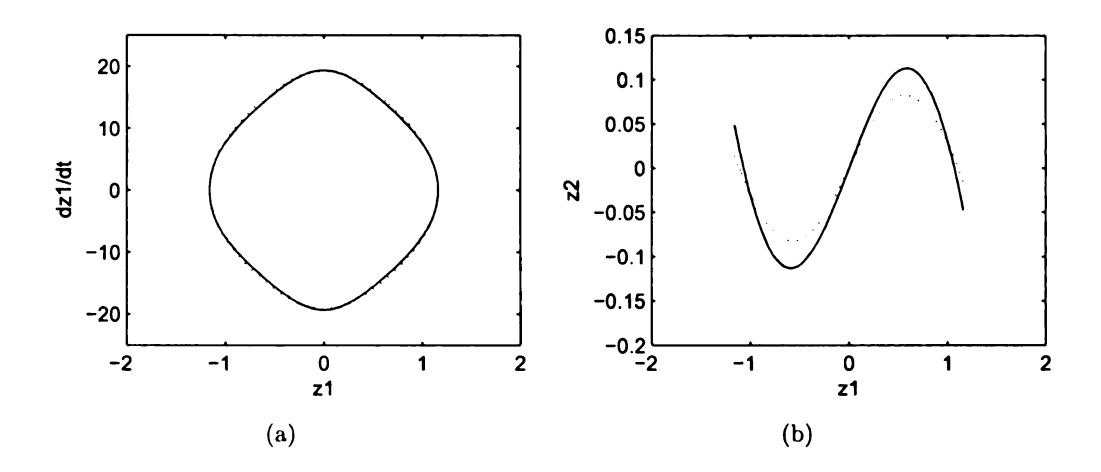


Figure 5.10. Comparison of Model II (the dotted lines) to the original mass-pendulum system (the continuous lines) simulated under 3rd initial condition, (a) phase plane, (b) mode shape.

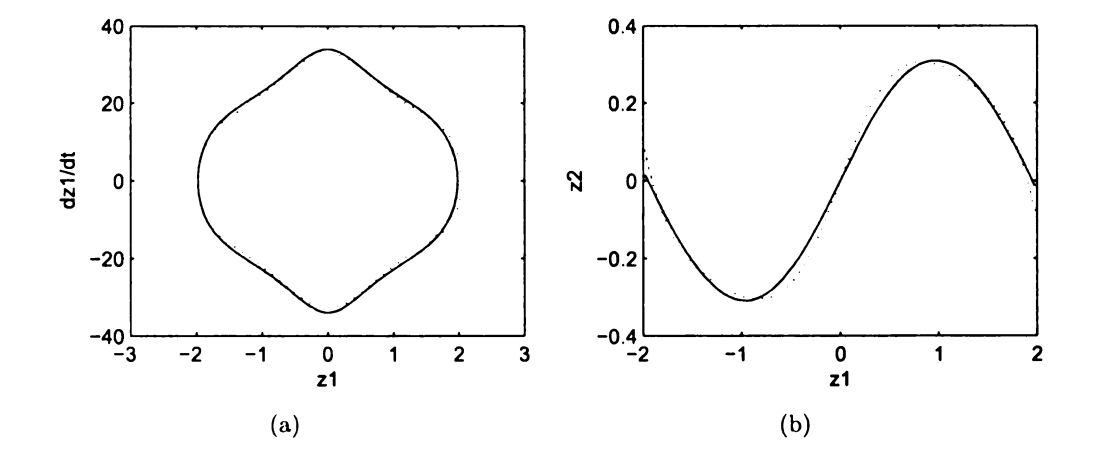


Figure 5.11. Comparison of Model II (the dotted lines) to the original mass-pendulum system (the continuous lines) simulated under 5th initial condition, (a) phase plane, (b) mode shape.

Model of type II

A more complex polynomial was used to estimate the nonlinearity in model-2 (5.20), and it was

$$z_{2} = \sum_{j=0}^{3} \sum_{k=0}^{3} a_{j,k} z_{1}^{j} \dot{z}_{1}^{k}$$

$$\ddot{z}_{1} + k_{z1} z_{1} + k_{z2} z_{2} + d_{1} z_{1}^{3} + d_{2} z_{1}^{2} z_{2} + d_{3} z_{1} z_{2}^{2} = 0$$
(5.25)

where the identified values are $k_{z1} = 0.0403$, $k_{z2} = 0.383$, $d_1 = 0.00218$, $d_2 = -0.146$, and $d_3 = -0.453$ for the mass-pendulum system. The nonlinear terms are up to the cubic order of z_1 and z_2 . Theoretically, the nonlinearity approximation is better than that of the model-I.

Noticeably, the z_2^3 term was not included in the z_1 differential equation of (5.25). It was found that there was unstable behavior of the identified system if z_2^3 nonlinearity was included, and the corresponding response tended to be quasi-periodic. It looks like a trial and error process, but it is not. Actually, the original systems also showed the bifurcation to quasi-periodic response as the initial offset increases. The z_2 ³ term made the response of the reduced-order model quasi-periodic at a smaller initial offset. The identification process is performed on state values during responses, and not on stability characteristics. Therefore, in sensitive systems, while a model is identified for response values, it may be close to a bifurcation set, and may not have the right stability. Thus, the model of equation (5.25) was selected for better approximation of the original system. It shows that the nonlinear terms in the identification model can bring unexpected results in the simulation. To the added constraint model, since another dependent variable z_2 is included, the problem becomes more complicated. For this example, the 'full' set of nonlinear terms actually deteriorated the system dynamics of the second model. However, the dilemma is that one does not know in advance what terms are unnecessary, or undesired. The problem has to be solved by reducing the higher order terms of the approximation functions, which increases the difficulty of system identification.

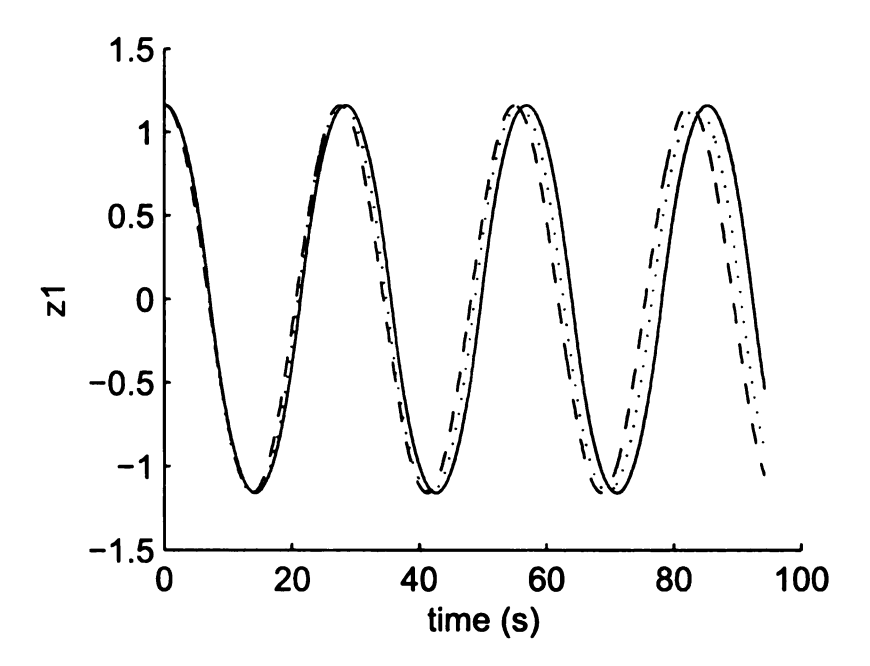


Figure 5.12. A time domain comparison between the original system (continuous line), the Model-I (dashed line), the Model-II (dotted line) under the 3rd initial condition.

Figures 5.9, 5.10, 5.11 show the comparison between model type II (5.25) and original system by phase planes and vibration mode shapes. Due to the effect of more nonlinear terms, by comparing the phase plane orbits, this model better approximates to the original system in large amplitude vibration (Fig. 5.10, 5.11) than the first model. On the other hand, the approximation of the small amplitude vibration is not so satisfying comparing to the model of the first type. Possible reason can be the influence of the nonlinear terms of z_2 .

Displayed in Figure 5.12 is a time domain signal comparison between the original system and the two models. The time domain responses of the three systems are very similar. But, the vibration frequencies are lightly different. In Figure 5.13, the variation of the natural frequencies is compared among the three systems. It shows that the reduced order model can also display inaccuracy in frequency domain. The

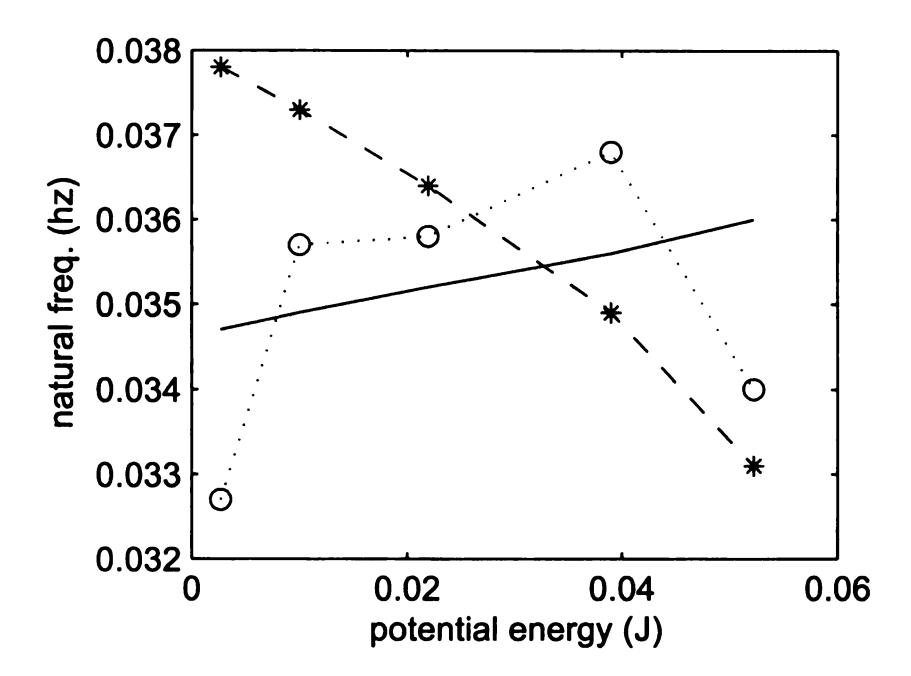


Figure 5.13. Natural frequency comparison under different initial conditions (represented by the maximum potential energy) between the original system (continuous line), the Model–I (dashed line), the Model–II (dotted line); the '*' and 'o' mark the five initial conditions for Model-I and Model-II.

natural frequency change of the original system is a hardening curve as the vibration amplitude (maximum potential energy) increased. Whereas, the curve of model-I is a softening curve which resulted from the negative identified value of a_{nl} in (5.24), and the corresponding frequency discrepancy is large. The model of the second type is somewhat a better approximation of the original system in the natural frequency comparison.

5.4 Concluding remarks

In this chapter, the POM reduced order models of nonlinear systems was investigated. Unlike the model order reduction techniques in turbulence [3, 32, 33], the complete process of the proposed idea is to reconstruct and identify the governing differential equations based upon proper orthogonal modes. The advantages of the method are the abilities to simplify and identify an unknown complex system simultaneously. But, it also brings the difficulty of identifying correctly the nonlinearity of the original systems. Moreover, for systems with strong nonlinearity, the POM based reduced order model can not give accurate prediction of the dynamics in conditions other than the given initial conditions upon which the proper orthogonal modes were extracted. Hence, the dissertation study generalized the POM based method by introducing an added-constraint such that the reduced order model can be more accurate in prediction of system dynamics as well as applicable to different initial conditions.

Two examples were examined: a two-mass system with a hardening spring and a mass-pendulum system. Both of the two examples show success of the added-constraint model, in which, due to the strong nonlinearity, the basic POM models are not adequate in simulating system behaviors under different initial conditions. Meanwhile, in the simulation study of the mass-pendulum system, two types of added-constraint models were investigated: one with only the POM coordinates and the

other one with POM coordinates and added-constraint coordinates involved. The former one was found to be more suitable for small amplitude vibration. In this example, however, the latter one was shown to be more accurate in predicting large amplitude vibration.

The study was successful in the two examples of low-dimensional systems, which are under free vibration with no damping. However, more experimental and simulation studies are needed for forced vibration systems, high-dimensional complex systems, and chaotic systems. The questions involve what POMs are needed for reduced order modeling, how to identify nonlinear terms in multi-degree-of-freedom systems, how to apply the added-constraint method to improve the accuracy and applicability of the POM model, and determining which type of models are best for the investigated systems. If all of the obstacles can be solved, the added-constraint POM model can be very powerful in system identification and simulation.

CHAPTER 6

Conclusions and Future Work

6.1 Main contributions

The purpose of this dissertation was to provide a handy and useful tool for parametric identification of nonlinear/chaotic systems, and also to reconstruct reduced order models of complex systems based upon proper orthogonal modes and parametric identification methods.

The parametric identification method is based upon harmonic balance method [24], and focused on chaotic systems. Due to the nature of chaos—no stable steady state behavior—the identification process first refers to the extraction of the unstable periodic orbits, which form a dense set existing within the chaotic set. Then the harmonic balance method can be applied upon the UPOs to identify the unknown parameters. The dissertation study did a thorough investigation on the application of this method: simulation and experimental study, multi-degree-of-freedom systems, and whirling systems. The major achievements include

 The method was examined successfully on whirling systems, e. g. singlependulum and double-pendulum systems. In both of the cases, only angular displacement signals were supposed to be known, consistent with the limitations of practical experiments. The special feature of whirling systems was

- that the angular displacements were not continuous signals, but signals in S^1 space $[-\pi,\pi)$. Thus, special modifications were made in the process of UPO extraction and the approximation of velocity and acceleration signals.
- 2. Noise reduction techniques were applied in the experimental investigation of multi-degree-of-freedom systems, e. g. the double pendulum system with base excitation. There were three reasons for applying noise reduction: the noise contamination in the signals, the recurrence error of the extracted UPO, and the strong nonlinearity which magnified the noise influence and propagated it from high to low frequencies. The noise reduction techniques include low-pass-filtering, digital differentiation, and choice of sub-harmonics by which the less noise-contaminated sub-harmonics of the UPOs were selected for harmonic balance identification.
- 3. Based upon the understanding of the least mean square method, an error quantification method was proposed to examine the accuracy of the estimated parameters. The quantification ideas were based upon linear regression and statistical methods. Also, by the error quantification process, an optimization process was established to improve the identification results by an optimized selection of sub-harmonics. The indicators of a good identification were small identification error value, and an even and random distribution of the estimation errors.
- 4. With more understanding of the chaotic set and the unstable periodic orbits, under the assumption of hyperbolic chaotic attractor and unstable periodic orbits contained within, the identification process which originally involved the extraction of UPOs and the harmonic balance method was simplified to a nearly pure frequency method simple harmonic balance identification. The simplification was due to the fact that any chaotic orbit, if long enough, is an approximation of some UPO. The longer the chaotic orbit, the better the approximation. This

property was justified with simple symbol dynamics. The calculation examples showed that the simplification could identify the parameters with satisfying results. The meaning of this simplification should not be under-estimated. The most direct result is to make the identification process fast and requires relatively small data set, i. e. it is more efficient. Hence, it is possible to apply this method to cases of real-time identification. Meanwhile, the simplification also makes the identification of all nonlinear systems possible by only one method – the harmonic balance identification.

With the progress in identification techniques, the focus of the dissertation then switched to the reduced order models by means of proper orthogonal modes, e. g. the reduced order models for systems with strong nonlinearity. The POMs are experimental optimized orthogonal modes. They have been useful for model order reduction. The dissertation study goes further in the direction of model order reduction, i. e. reconstruction of reduced order models for unknown systems. Two simple examples were given to test the method of added-constraint models. The special feature of the added-constraint method is that extra constraint equations are added to minor mode such that the constraint and the differential equation of the dominant POM together form the new reduced order models. Through two example systems, it revealed:

- 1. In both the studies, the nonlinear added-constraint method showed better approximation of the systems' dynamics than the POM-only reduced order models. Also, the method made the reduced order models applicable to more general initial conditions. Compared to the nonlinear normal modes, the added-constraint method is empirical and able to adjust the approximation model by different data, i. e. different initial conditions.
- 2. The identification of the nonlinear terms was more difficult if little knowledge was known for the nonlinearity of the original systems. Two types of nonlin-

ear models were examined in the mass-pendulum model: the model with no constraint modal coordinates in the governing differential equations and the one with constraint modal coordinates in the differential equations. The first model was simpler, and more accurate for small amplitude oscillation. On the contrary, the second model was more feasible for large amplitude oscillation, and showed the difficulty in finding appropriate nonlinear terms in the model to represent the nonlinearity of the original systems.

6.2 Directions for future work

There were achievements through this study on both parametric identification method and the added-constraint POM reduced order models. However, many questions still remain:

• In the experimental study, the identification of friction coefficients were erroneous. The reason was due to the small values of those parameters. It indicates that the small parameters are more vulnerable to noise contamination, and thus, hard to identify. Therefore, the energy balance method was applied to identify the friction parameters. For non-damping small terms, e. g. small geometric terms, similar procedure can also be developed. Suppose we have a single d. o. f. vibration system expressed as

$$\ddot{x} + kx + c\dot{x} + a_n x^3 = f(t), \tag{6.1}$$

where f(t) is a periodic excitation, and a_n is a small nonlinear coefficient compared to linear coefficient k and c. Like the identification to small damping terms in previous examples, the estimation of a_n will be hard in harmonic identification process, due to the influence of other large terms. To reduce the noise

from other terms, multiplying (6.1) and integrating over one cycle of a periodic orbit, we obtain

$$\int_{t}^{t+T} \ddot{x}xdt + \int_{t}^{t+T} kx^{2}dt + \int_{t}^{t+T} c\dot{x}xdt + a_{n} \int_{t}^{t+T} x^{4}dt = \int_{t}^{t+T} f(t)xdt.$$
(6.2)

Noticeably, the integration of the velocity term over one cycle of a periodic orbit is zero. Hence, equation (6.2) can be transformed to

$$a_n \int_t^{t+T} x^4 dt = \int_t^{t+T} \dot{x}^2 dt - \int_t^{t+T} kx^2 dt + \int_t^{t+T} f(t)x dt.$$
 (6.3)

The a_n can be solved by least mean square method if there are more than one periodic orbit. The advantage of equation (6.3) is that there are fewer, and only displacement and velocity terms. If the displacement signal is directly measured, it is believed to be quite accurate. On the other hand, the velocity and acceleration signals are to be obtained by the Fourier series method or digital differentiation, which have been proved to have more high-frequency noise. The high frequency noise is the worst for the acceleration signal. Hence, we are quite confident that the estimation of a_n by (6.3) is more accurate than the harmonic balance identification. For multi-degree-of-freedom systems, similar methods are expected to be developed and improve the accuracy of nonlinearity identification.

• The simplification of the harmonic balance identification method makes it possible for real-time identification of chaotic systems. As we know that every chaotic orbit can be an approximated orbit of some UPO, real-time identification can be possible if the length of the UPO can be properly chosen. The goal is to identify relatively slowly varying parameters of the governing equation, or to assess damage of systems. Meanwhile, due to the similarity between the

harmonic balance method and the wavelet analysis, the real-time identification of chaotic systems can also be done by wavelet analysis. The questions are how fast can the process be and the issue of noise-resistance.

- It is also possible that the identification method can be applied to nonlinear/chaotic systems under random or impulse excitation. The idea lies in the analogue between the random excitation and the impulse excitation. The basic root of this idea still comes from re-thinking of the unstable periodic orbits and chaotic set. But it should be considered more in the frequency domain, instead of the time domain.
- The POD process for whirling systems requires study. The whirling signals, i. e. the angular displacements, are not applicable to the traditional definition of the proper orthogonal decomposition, since these signals are in a spherical space. Hence, the reduced order models are hard to apply to whirling systems. The possible solution can be to use the complex variables, instead of real variables, to represent the whirling signals.
- Nonlinear reduced order modeling is difficult. The approximation method can
 be troublesome since unnecessary nonlinear terms can bring undesired dynamical behavior for strongly nonlinear systems. The problem will become more
 difficult for complex structures where the nonlinearity is not clear. An idea
 might be to incorporate stability measures into identification process [67].
- The added-constraint model, though successfully explained in the two examples,
 is still in development, and needs to be examined by complex, high-dimensional
 structures. The problems involve the determination of POM coordinates and
 the constraint constraints, and how far can the method improve the performance
 of the reduced order models.

BIBLIOGRAPHY

- [1] K. T. Alligood and et al. CHAOS An Introduction to Dynamical Systems. New York: Springer-Verlag, 1997.
- [2] S. W. Shaw and C. Pierre, "Normal modes for non-linear vibratory systems," *Journal of Sound and Vibration*, vol. 164, no. 1, pp. 85-124, 1993.
- [3] J. L. Lumley, Stochastic Tools in Turbulence. New York: Academic Press, 1970.
- [4] S. Han and B. F. Feeny, "Enhanced proper orthogonal decomposition for the modal analysis of homogeneous structures," *Journal of Vibration and Control*, vol. 8, pp. 19–40, 2002.
- [5] K. S. Mohammad and et al., "Direct parameter estimation for linear and non-linear structures," *Journal of Sound and Vibration*, vol. 153, no. 3, pp. 471–499, 1992.
- [6] M. R. Hajj, J. Fung, and et al., "Parametric identification of nonlinear dynamic systems," Computers & Structures, vol. 20, no. 3, pp. 487-493, 1985.
- [7] Q. Chen and G. R. Tomlinson, "Parametric identification of systems with dry friction and nonlinear stiffness a time series model," *Journal of Vibration and Acoustics*, vol. 118, no. 2, pp. 252-263, 1996.
- [8] R. K. Kapania and S. Park, "Parametric identification of nonlinear structural dynamic systems using time finite element method," *AIAA Journal*, vol. 35, no. 4, pp. 719–726, 1997.
- [9] G. Verbeek, A. Dekraker, and D. H. Vancampen, "Nonlinear parametric identification using periodic equilibrium states application to an aircraft landing gear damper," *Nonlinear Dynamics*, vol. 7, no. 4, pp. 499-515, 1995.
- [10] M. R. Hajj, J. Fung, and et al., "Damping identification using perturbation techniques and higher order spectra," *Nonlinear Dynamics*, vol. 23, no. 2, pp. 189–203, 1986.
- [11] G. Kerschen, V. Lenaerts, and et al., "Identification of a continuous structure with a geometrical non-linearity part i: Conditioned reverse path method," *Journal of Sound and Vibration*, vol. 262, no. 4, pp. 889-906, 2003.

- [12] C. M. Richard and R. Singh, "Identification of multi-degree-of-freedom non-linear systems under random excitations by the reverse-path spectral method," *Journal of Sound and Vibration*, vol. 213, no. 4, pp. 673-708, 1998.
- [13] O. Gottlieb and M. Feldman, "Application of a hilbert-transform based algorithm for parameter estimation of a nonlinear ocean system roll model," *Journal of Offshore Mechanics and Arctic Engineering*, vol. 119, pp. 239-243, 1997.
- [14] M. Feldman, "Non-linear free vibration identification via the hilbert transform," Journal of Sound and Vibration, vol. 208, no. 3, pp. 475-489, 1997.
- [15] M. Feldman, "Non-linear system vibration analysis using hilbert transform-i. free vibration analysis method 'freevib'," *Mechanical Systems and Signal Processing*, vol. 8, no. 2, pp. 119-127, 1994.
- [16] N. P. Plakhtienko, "Methods of identification of nonlinear mechanical vibrating systems," *International Applied Mechanics*, vol. 36, no. 12, pp. 1565–1594, 2000.
- [17] N. P. Plakhtienko, "A method of special weight-functions in the problem of parametric identification of mechanical systems," DOPOV AKAD NAUK A, vol. 8, pp. 31-35, 1983.
- [18] K. Yasuda, S. Kawamura, and et al., "Identification of nonlinear multi-degree-of-freedom systems (presentation of a technique)," JSME International Journal, Series III, vol. 31, pp. 8-14, 1988.
- [19] K. Yasuda and S. Kawamura, "A nonparametric identification technique for non-linear vibratory systems (proposition of a technique)," *JSME International Journal, Series III*, vol. 31, pp. 365-372, 1989.
- [20] K. Yasuda and K. Kamiya, "Identification of a nonlinear beam (proposition of an identification technique)," JSME International Journal, Series III, vol. 33, pp. 535-540, 1990.
- [21] K. Yasuda and K. Kamiya, "Experimental identification technique of nonlinear beams in time domain," *Nonlinear Dynamics*, vol. 18, pp. 185–202, 1997.
- [22] M. Thothadri and et al., "Nonlinear system identification of multi-degree-of-freedom systems," *Nonlinear Dynamics*, vol. 32, pp. 307-322, 2003.
- [23] R. Ghanem and F. Romeo, "A wavelet-based approach for model and parameter identification of nonlinear systems," *International Journal of Non-linear Mechanics*, vol. 36, pp. 835-959, 2001.
- [24] C. M. Yuan and B. F. Feeny, "Parametric identification of chaotic systems," Journal of Vibration and Control, vol. 4, no. 4, pp. 405-426, 1998.
- [25] B. F. Feeny, C. M. Yuan, and et al., "Parametric identification of an experimental magneto-elastic oscillator," *Journal of Sound and Vibration*, vol. 247, no. 5, pp. 785-806, 2001.

- [26] B. F. Feeny and R. Kappagantu, "On the physical interpretation of proper orthogonal modes in vibrations," *Journal of Sound and Vibration*, vol. 214, no. 4, pp. 607-616, 1998.
- [27] B. F. Feeny, "On the proper orthogonal modes and normal modes of continuous vibration systems," *Journal of Vibration and Acoustics*, vol. 124, no. 1, pp. 157– 160, 2002.
- [28] B. F. Feeny, "On proper orthogonal coordinates as indicators of modal activity," *Journal of Sound and Vibration*, vol. 255, no. 5, pp. 805-817, 2002.
- [29] B. F. Feeny and Y. Liang, "Interpreting proper orthogonal modes of randomly excited vibration systems," *Journal of Sound and Vibration*, vol. 265, no. 5, pp. 953-966, 2003.
- [30] G. Kerschen and J. C. Golinval, "Physical interpretation of the proper orthogonal modes using the singular value decomposition," *Journal of Sound and Vibration*, vol. 249, no. 5, pp. 849–865, 2002.
- [31] S. Han and B. Feeny, "Application of proper orthogonal decomposition to structural vibration analysis," *Mechanical Systems and Signal Processing*, vol. 17, no. 5, pp. 989-1001, 2002.
- [32] J. L. Lumley, "The structure of inhomogeneous turbulent flow," *Atmospheric Turbulence and Radio Wave Program*, pp. 166–178, 1967. (A. M. Yaglom and V. I. Tatarski, editors) Moscow: Nauka.
- [33] G. Berkooz and et al., "The proper orthogonal decomposition in the analysis of turbulent flows," Annual Review of Fluid Mechanics, vol. 25, pp. 539-575, 1993.
- [34] W. Z. Lin and et al., "Proper orthogonal decomposition and component mode synthesis in macromodel generation for the dynamic simulation of a complex mems device," *Journal of Micromechanics and Microengineering*, vol. 13, pp. 646-654, 2003.
- [35] M. S. Riaz and B. F. Feeny, "Proper orthogonal modes of a beam sensed with strain gages," *Journal of Vibration and Acoustics*, vol. 125, pp. 129-131, 2003.
- [36] A. Sarkar and M. P. Paidoussis, "A cantilever conveying fluid: coherent modes versus beam modes," *International Journal of Non-linear Mechanics*, vol. 39, pp. 467-481, 2004.
- [37] J. P. Cusumano and B. Y. Bai, "Period-infinity periodic motions, chaos, and spatial coherence in a 10-degree-of-freedom impact oscillator," *Chaos, Solutions, and Fractals*, vol. 3, pp. 515-535, 1993.
- [38] J. P. Cusumano and et al., "Spatial coherence measurements of a chaotic flexible-beam impact oscillator," Aerospace Structures: Nonlinear Dynamics and System Response, ASME-AD, vol. 33, pp. 13-22, 1993.

- [39] V. Lenaerts and et al., "Proper orthogonal decomposition for model updating of non-linear mechanical systems," *Mechanical Systems and Signal Processing*, vol. 15, no. 1, pp. 31-43, 2000.
- [40] I. T. Georgiou and I. B. Schwartz, "Dynamics of large scale coupled structural/mechanical systems: a singular perturbation/proper orthogonal decomposition approach," *Journal of Applied Mathematics*, vol. 59, no. 4, pp. 1178–1207, 1999.
- [41] R. Kappagantu and B. F. Feeny, "An 'optimal' modal reduction of a system with frictional excitation," *Journal of Sound and Vibration*, vol. 224, no. 5, pp. 863–877, 1999.
- [42] R. V. Kappagantu and B. F. Feeny, "Part1: dynamical characterization of a frictionally excited beam," *Nonlinear Dynamics*, vol. 22, pp. 317-333, 2000.
- [43] R. V. Kappagantu and B. F. Feeny, "Part2: proper orthogonal modal modeling of a frictionally excited beam," *Nonlinear Dynamics*, vol. 23, pp. 1-11, 2000.
- [44] G. Kerschen, B. F. Feeny, and et al., "On the exploitation of chaos to build reduced-order models," Computer Methods in Applied Mechanics and Engineering, vol. 192, no. 13-14, pp. 1785-1795, 2003.
- [45] W. V. de Water and M. Hoppenbrouwers, "Unstable periodic orbits in the parametrically excited pendulum," *Physical Review A*, vol. 44, no. 10, pp. 6388-6397, 1991.
- [46] J. Jeong and S.-Y. Kim, "Bifurcations in a horizontally driven pendulum," *Journal of Korean Physical Society*, vol. 35, no. 5, pp. 393-398, 1999.
- [47] S. R. Biship and M. J. Clifford, "Zones of chaotic behavior in the parameterically excited pendulum," *Journal of Sound and Vibration*, vol. 189, pp. 142-147, 1996.
- [48] R. V. Dooren, "Chaos in a pendulum with forced horizontal support motion: a tutorial," *Chaos, Solutions and Fractals*, vol. 7, no. 1, pp. 77-90, 1996.
- [49] V. B. Raybov, "Using lyapunov exponents to predict the onset of chaos in non-linear oscillators," *Physical Review E*, vol. 66(1), no. 016214, 2002.
- [50] W. Szemplinska-Stupnicka and E. Tyrkiel, "The oscillation-rotation attractors in the forced pendulum and their peculiar properties," *International Journal of Bifurcation and Chaos*, vol. 12, no. 1, pp. 159–168, 2002.
- [51] M. Clerc, P. Coullet, and E. Tirapegui, "The stationary instability in quasireversible systems and the lorenz pendulum," *International Journal of Bifurca*tion and Chaos, vol. 11, no. 3, pp. 591-603, 2002.
- [52] H. D. Abarbanel, R. Brown, and et al., "The analysis of observed chaotic data in physical systems," *Reviews of Modern Physics*, vol. 65, pp. 1331–1392, 1993.

- [53] D. Auerbach and et al., "Exploring chaotic motion through periodic orbits," *Physical Review Letters*, vol. 58, pp. 2387-2389, 1987.
- [54] D. P. Lathrop and E. J. Kostelich, "characterization of an experimental strange attractor by periodic orbits," *Physical Review A*, vol. 40, pp. 4028-4031, 1989.
- [55] Z. Al-Zamel and B. F. Feeny, "Improved estimations of unstable periodic orbits extracted from chaotic sets," 2001 ASME Design Engineering Technical Conferences, Proceedings of Det'01, 2001.
- [56] J. W. Liang and B. F. Feeny, "Identifying damping in forced oscillators using a harmonic energy balance," *IMECE-2002*, 11 2002. New Orleans, IMECE2002 CD-ROM.
- [57] J. P. Eckmann and D. Ruelle, "Ergodic theory of chaos and strange attractors," Reviews of Modern Physics, vol. 57, no. 3, pp. 617-656, 1985.
- [58] O. Biham and W. Wenzel, "Characterization of unstable periodic orbits in chaotic attractors and repellers," *Physical Review Letters*, vol. 63, no. 8, pp. 819– 822, 1987.
- [59] P. Cvitanović, "Invariant measurement of strange sets in terms of cycles," *Physical Review Letters*, vol. 61, no. 24, pp. 2729-2732, 1987.
- [60] G. H. Gunaratne and I. Procaccia, "Organization of chaos," Physical Review Letters, vol. 59, no. 13, pp. 1377-1380, 1987.
- [61] K. Mischaikow and et al., "Construction of symbolic dynamics from experimental time series," *Physical Review Letters*, vol. 82, no. 6, pp. 1144-1147, 1999.
- [62] C. M. Yuan, Parametric identification of chaotic systems, PHD dissertation. East Lansing, MI 48824: Michigan State University, 1995.
- [63] L. Sirovich, "Turbulence and the dynamics of coherent structures, part i: Coherent structures," Quarterly of Applied Mathematics, vol. 45, pp. 561-571, 1987.
- [64] I. T. Georgiou and I. B. Schwartz, "Invariant manifolds, nonclassical normal modes, and proper orthogonal modes in the dynamics of the flexible spherical pendulum," Nonlinear Dynamics, vol. 25, pp. 3-31, 2001.
- [65] E. Pesheck and et al., "Nonlinear modal analysis of structural systems using multi-mode invariant manifolds," *Nonlinear Dynamics*, vol. 25, pp. 183-205, 2001.
- [66] D. Ruelle and F. Takens, "On the nature of turbulence," Communications in Mathematical Physics, vol. 20, pp. 167-192, 1971.
- [67] M. Thothadri and F. C. Moon, "Nonlinear system identification of systems with periodic limit-cycle response," *Nonlinear Dynamics*, vol. 39, no. 1-2, pp. 63-77, 2005.